

TRANSPORT PROPERTIES OF LITHIUM DIFFUSED EVAPORATED
AMORPHOUS GERMANIUM AND GLOW DISCHARGE DEPOSITED
AMORPHOUS SILICON ($a\text{-Si:H}$) AND THE STUDY OF LIGHT
INDUCED CHANGES IN $a\text{-Si:H}$ BY SURFACE PHOTOVOLTAGE

by

SHAILENDRA KUMAR

PHY

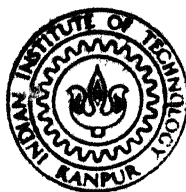
1984

D

KUM

TARA

TH
PHY/1984/D
K 966



DEPARTMENT OF PHYSICS
INDIAN INSTITUTE OF TECHNOLOGY, KANPUR
MAY, 1984

**TRANSPORT PROPERTIES OF LITHIUM DIFFUSED EVAPORATED
AMORPHOUS GERMANIUM AND GLOW DISCHARGE DEPOSITED
AMORPHOUS SILICON ($a\text{-Si} : \text{H}$) AND THE STUDY OF LIGHT
INDUCED CHANGES IN $a\text{-Si} : \text{H}$ BY SURFACE PHOTOVOLTAGE**

A Thesis Submitted
in Partial Fulfilment of the Requirements
for the Degree of

DOCTOR OF PHILOSOPHY

by

SHAILENDRA KUMAR

to the

**DEPARTMENT OF PHYSICS
INDIAN INSTITUTE OF TECHNOLOGY, KANPUR
MAY, 1984**

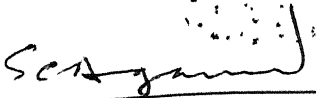
87520

PHY-1984-D-KUM-TRA

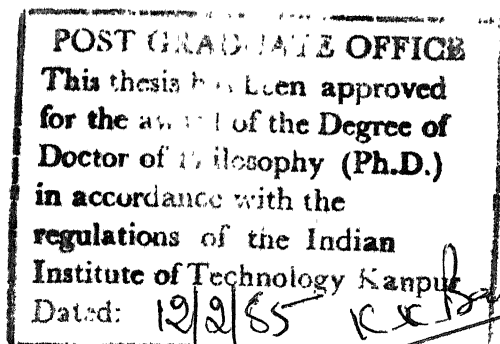
CERTIFICATE

This is to certify that the work presented in this thesis entitled, 'TRANSPORT PROPERTIES OF LITHIUM DIFFUSED EVAPORATED AMORPHOUS GERMANIUM AND GLOW DISCHARGE DEPOSITED AMORPHOUS SILICON (a-Si:H) AND THE STUDY OF LIGHT INDUCED CHANGES IN a-Si:H BY SURFACE PHOTOVOLTAGE' by Shailendra Kumar has been carried out under my supervision and it has not been submitted elsewhere for a degree.

May, 1984.



(S.C. Agarwal)
Department of Physics
Indian Institute of Technology
Kanpur, India



ACKNOWLEDGEMENTS

It is a great pleasure to express my gratitude to Dr.S.C.Agarwal for introducing the field of amorphous semiconductors to me and noble guidance throughout the course of this work.

My sincere thanks are due to Professors H.Fritzsche, R.Sharan, T.M.Srinivasan, R.K.Ray, A.Mookerjee, S.Guha, W.Paul, A.Man Singh for various helpful discussions at different stages of this work.

I am also thankful to Professor R.M.Singru, Head, Physics Department, IIT-Kanpur and Dr.S.C.Sen for encouraging me and taking a keen interest in the progress of my research work.

It is also a great pleasure to thank Drs.P.N.Dixit, Ashok Kumar, V.A.Singh, K.Shahi, Rakesh Lal and V.Bhaumik for various helpful discussions and suggestions at different stages of this work. I also thank my colleague Mr.D.S.Misra for a nice company throughout the work.

My sincere thanks are due to my friends Drs.A.K.Sinha, Mukul Misra, B.P.Singh, Gyanesh Chandra, Mohd.Rafat, M.Pal and Messrs R.C.Srivastava, Manu Mathur and many others who helped me in more than one ways and made my stay at IIT-Kanpur a memorable pleasure.

I am thankful to Mr.J.S.Sharma and his associates in Physics Workshop, Mr.J.N.Sharma and his associates in Glass Blowing Shop, Mr.R.L.Arora and his associates of Electronic Shop, Mr.S.D.Sharma and his associates in Low Temperature Laboratory and Mr.Beni Prasad of my laboratory.

I thank Mr.U.S.Misra for his excellent meticulous and patientful typing, Mr.B.K.Jain for tracing the figures and Mr.Hrushikes Panda and L.S.Rathaur for cyclostyling.

The work carried out here would not have been possible without the emotional support and constant encouragement from my father, I wish to express my profound regards to my parents, uncles, brothers and sisters.

-Shailendra Kumar

CONTENTS

	<u>Page</u>
LIST OF TABLES	
LIST OF FIGURES	
SYNOPSIS	
CHAPTER 1	
INTRODUCTION	1
References	16
CHAPTER 2	
LITHIUM DIFFUSED AND HYDROGENATED AMORPHOUS GERMANIUM	20
2.1 Introduction	20
2.2 Theory of Conductivity and Thermopower	21
2.2a Kubo-Greenwood Formulae	21
2.2b Transport Processes	23
i) Conduction in Extended States	23
ii) Conduction in Localized States	24
2.2c Small Polaron Model and Phonon Drag Effect	27
2.2d Combination of Transport Processes	28
2.2e Temperature Dependence of the Fermi Level and Mobility Edges on Transport	29
2.3 Experimental	31
2.3.1 Preparation	31
2.3.2 Characterization	32
a. Structure	32
b. Electrical	33

2.3.3	Measurement of Conductivity and Thermopower	33
2.4	Results	37
2.5	Discussion and Conclusions	40
	References	49
CHAPTER 3	UNDOPED AND LITHIUM DOPED a-Si:H	51
3A	Conductivity and Thermopower	51
3A.1	Introduction	51
3A.2	Preparation and Characterization	52
3A.3	Experimental Results	57
	a) Effect of Hydrogenation	57
	b) Effect of Light Soaking on σ and S in the Doped and Li doped a-Si:H	61
3A.4	Discussion	68
	i) Variation σ_o with E_o	69
	ii) Variation of E_μ by Doping	74
	iii) Variation of E_μ by Light Soaking	76
	iv) Deviation of $Q(T)$ versus $1/T$ Curves from Linearity	77
3B	Gradient Doping	81
3B.1	Introduction	81
3B.2	Experiment	82
3B.3	Results and Discussion	84
	References	95

	<u>Page</u>
CHAPTER 4	
SURFACE PHOTOVOLTAGE IN a-Si:H	98
4.1 Introduction	98
4.2 Theory of Surface Photovoltage	101
i) Solution of Poisson's Equation in Dark and Light	101
ii) Graphical Analysis of SPV	108
4.3 Experimental	114
4.4 Experimental Results	120
a. Frequency Dependence	121
b. Dependence upon Intensity and Energy of Light	121
c. Effect of Etching, Aging and Ambients	124
d. Temperature Dependence	126
4.5 Interpretation	128
a. Frequency Dependence	129
b. Intensity Dependence	130
c. Change in Surface Conditions	130
d. Temperature Dependence	133
4.6 Light Soaking and SPV	137
4.6a Experimental Results	137
4.6b Discussion	144
References	148
CHAPTER 5	
SUMMARY AND CONCLUSIONS	150
References	155

LIST OF TABLES

<u>Table</u>	<u>Title</u>	<u>Page</u>
3.1	V_{oc} and J_{sc} in configurations 'a' and 'b'	93
4.1	Specifications of I8007 AC FET INPUT Operational Amplifier	118

LIST OF FIGURES

<u>Figure</u>	<u>Title</u>	<u>Page</u>
2.1	Decay of I_d at 300K for various polarizing electric fields	34
2.2A	Geometry of the sample used to measure conductivity and thermopower	35
2.2B	Geometry of the cryostat used to measure conductivity and thermopower	35
2.3a	Conductivity (σ) versus $10^3/T$, Curve 1 (evaporated a-Ge, $T_s = 150^\circ\text{C}$), Curve 2 (evaporated a-Ge:Li, $T_s = 150^\circ\text{C}$), Curve 3 (evaporated a-Ge:H, $T_s = 150^\circ\text{C}$), Curve 4 (sputtered a-Ge:H, $T_A = 250^\circ\text{C}$, ref.15), and Curve 5 (glow-discharge a-Ge:H, $T_s = 230^\circ\text{C}$, ref.26)	39
2.3b	Thermopower (S) versus $10^3/T$ for samples shown in Fig.2.3a	39
2.4	Conductivity (σ) versus $T^{-1/4}$, Curve 1 (evaporated a-Ge), Curve 2 (evaporated a-Ge:Li) and Curve 3 (evaporated a-Ge:H)	45
3.1	d.c. glow-discharge system, 1. High tension feed through, 2. Pyrex anode shield, 3. Anode, 4.Ceramic post, 5.Aluminium screen (cathode), 6. Steel plate containing heater, 7. Substrates, 8. Thermocouple gauge, 9. Electrical feed through	53
3.2	Electron diffraction micrograph of a-Si:H deposited at $T_s = 580\text{K}$	55
3.3	I-R spectra of a-Si:H, a : sample deposited at $T_s = 300\text{K}$, b: sample deposited at $T_s=580\text{K}$	56

<u>Figure</u>	<u>Title</u>	<u>Page</u>
3.4a	Conductivity (σ) versus $1/T$, (3.4b) Thermopower (S) versus $1/T$, Curve 1. Undoped a-Si:H ($T_S = 300^\circ\text{C}$), Curve 2. Evaporated a-Si ($T_A = 290^\circ\text{C}$), Curve 3. Evaporated a-Si ($T_A = 310^\circ\text{C}$). Curves 2 and 3 are from ref.4	58
3.5	Conductivity (σ) versus $1/T$ for undoped a-Si:H in the heat-dried state (A) and in light soaked state (B)	
3.6a	Conductivity (σ) versus $1/T$ and (3.6b) Thermopower (S) versus $1/T$ in the heat-dried state (A) and light soaked state (B). Curve U. Undoped a-Si:H, Curve 1. Lightly Li doped a-Si:H, Curve 2. Heavily Li doped a-Si:H Curves 3 and 4 are for Li diffused and Li implanted a-Si:H respectively (ref.8)	65
3.7	Conductivity prefactor (σ_0) versus conductivity activation energy (E), open circles are for heat-dried state and closed circles for light soaked stated. Triangles are for a-Si:H (Li) samples from ref.16. Open, low temperature range and closed, high temperature range	70
3.8	$Q(T)$ versus $1/T$, $E_d = E_\sigma - E_s$, Q_0 is the intercept of $Q(T)$ versus $1/T$ curve at $1/T_0$	73
3.9	Lithium diffusion in presence of the electric field	83
3.10	Current (I) versus voltage (V) for a gradient doped a-Si:H (Li) in dark and light (flux = 100 mW/cm^2)	85

<u>Figure</u>	<u>Title</u>	<u>Page</u>
3.11	Current (I) versus voltage (V) for an a-Si:H (Li) samples without gradient in dark and light (flux = 100 mW/cm ²)	86
3.12	Annealing in presence of an electric field reverse polarity of the photovoltage	88
3.13a	Geometry of the sample to measure potential profile (3.13b) Photovoltage (V _{oc}) versus distance (x)	89
3.14	Schottky barrier with the neutral bulk (configuration a) and with a built in potential in the bulk (configuration b)	91
4.1	Energy band-diagram for a-Si:H with an accumulated surface in light. E _o and E _v are mobility edges, E _f is the Fermi level in dark. E _{fn} and E _{fp} are quasi Fermi levels for trapped carriers. Potential V is positive and energy level E in bulk in shifted to E-eV _s at the surface	102
4.2A	Space-charge density Q _{sc} versus surface potential v _s for a-Si:H with negative space charge region in dark (1) and light (2 : n _b = 5x10 ¹⁰ cm ⁻³ and 3: n _b = 5x10 ¹² cm ⁻³)	109
4.2B	Space-charge density Q _{sc} versus surface potential v _s for c-Si (intrinsic) with negative space-charge region in dark (1) and light (2 : n _b = 10 ¹⁰ cm ⁻³ ; 3 : n _b = 10 ¹¹ cm ⁻³ ; 4 : n _b = 10 ¹² cm ⁻³)	110

<u>Figure</u>	<u>Title</u>	<u>Page</u>
4.3A	Arrangement for the measurement of SPV. 3 is a semitransparent electrode. Electrodes 1 and 2 are for measurement of G and are grounded for SPV measurements. 4 is a FET input operational amplifier	115
4.3B	Geometry used to measure SPV at the back surface	115
4.3C	Geometry used to measure SPV at the front surface, keeping separation between electrode 3 and the sample same as in (B)	115
4.4	System to measure SPV at different temperatures in vacuum. 1 and 2. NiCr electrodes, 3. semitransport electrode, 4. aluminium substrate holder, 5. heater, 6. another aluminium plate, 7. FET input amplifier, 8. ceramic stand, 9. base plate having a vacuum line, 10. brass cylinder, 11. quartz window, 12. heat shield, 13. feed throughs	116
4.5A	SPV as a function of repetition frequency (f) of pulsed light on the front surface of a-Si:H sample	122
4.5B	SPV as a function of intensity (I) of the pulsed light for optical gap light E_1 and high energy light E_2	122

<u>Figure</u>	<u>Title</u>	<u>Page</u>
4.6	Conductance (G) and SPV after different surface treatments of an a-Si:H sample. A (non-etched, heat-dried measured in vacuum), B (etched, measured in air), C (state B measured in vacuum, 10^{-5} Torr), D ₁ (after heat-drying C, measured in vacuum, E (heat-dried after 15 days of D ₁ , measured in vacuum), F (heat dried E after 30 days of D ₁ , measured in vacuum D ₂ (after etching and heat drying F, measured in vacuum)	125
4.7	SPV as a function of T for an a-Si:H sample. Curve 1 (non-etched and heat-dried front surface), Curve 2 (etched and heat-dried front surface), and Curve 3 (heat-dried back surface)	127
4.8	Energy band diagram with upward band bending (A) at the surface ($V_s = 0.1V$) and with downward band bending (B) at the surface ($V_s = 0.1V$)	132
4.9	Conductance (G) in different states of the cycle experiment for an a-Si:H sample. A (heat-dried state), B (light soaked state), F (state B in presence of moisture), C (state A in presence of moisture), F' (state C after light soaking)	138
4.10	G and SPV in different states of the cycle experiment. G is in upper half of the figure and SPV in the lower half. SPV curve 1 is for high energy light $E = 3.0$ eV and Curve 2 is for optical gap light $E = 1.8$ eV	140

<u>Figure</u>	<u>Title</u>	<u>Page</u>
4.11	G and SPV for an undoped a-Si:H sample and lightly Li doped a-Si:H (Li) sample in different states of the cycle experiment SPV is for optical gap light $E_1 = 1.8$ eV	141
4.12	G and SPV for an etched-a-Si:H sample in different states of the cycle experiment. A' (non-etched, heat-dried state), B' (non-etched, light soaked state) A to F' states are same in the cycle experiment	142

SYNOPSIS

Transport Properties of Lithium Diffused Evaporated
Amorphous Germanium and Glow Discharge Deposited
Amorphous Silicon (a-Si:H) and the Study of
Light Induced Changes in a-Si:H by Surface
Photovoltage

SHAILENDRA KUMAR

Ph.D.

Department of Physics
Indian Institute of Technology, Kanpur
May 1984

Amorphous germanium and amorphous silicon prepared by evaporation have structural defects consisting of regions of missing atoms (called voids) with unsaturated dangling bonds at the internal surfaces of these voids. There is a continuous distribution of localized states in the mobility gap of a-Ge and a-Si, with density of states at the Fermi level, $g(E_F)$, of the order of $10^{20} \text{ cm}^{-3} \text{ eV}^{-1}$. This high density of localized states pins the Fermi level and doping in these films is ineffective. These films are not photoconducting, show little field effect and are not much interesting from the technological point of view. It is also difficult to do fundamental physics on them.

Hydrogenated a-Ge (a-Ge:H) and a-Si(a-Si:H) thin films prepared by glow-discharge of germane and silane gases respectively have a low density of states at the Fermi

level. For a-Ge:H, $g(E_f) \cdot 10^{18} = 5 \times 10^{18} \text{ cm}^{-3} \text{ eV}^{-1}$ and for a-Si:H $g(E_f) \cdot 10^{16} = 10^{17} \text{ cm}^{-3} \text{ eV}^{-1}$. It is found that the hydrogen, present at the time of deposition, saturates dangling bonds and reduces strains in the lattice of these films. Thus, it reduces the density of states and modifies the mobility gap. a-Si:H is photoconducting and can be doped n-type or p-type efficiently. However, doping in a-Ge:H is not efficient. The possibility of doping increases the importance of a-Si:H films from the physics as well as the device point of view.

With the hope that lithium, having one bonding electron, may saturate dangling bonds in evaporated a-Ge, lithium diffused a-Ge films (a-Ge:Li) have been studied (Chapter 2). For comparison, a-Ge:H films have also been prepared by evaporating Ge in a partial pressure of hydrogen. However, it is found that although Li saturates the dangling bonds, a-Ge:Li films are also not photoconducting and cannot be doped. a-Ge:Li films having lithium concentration more than 5 at % get polarized upon application of an electric field and take several hours to get depolarized even at room temperature. The measurements of conductivity (σ) and thermopower (S) on a-Ge:H, a-Ge:Li are described and compared with those of evaporated a-Ge.

In crystalline semiconductors, the study of electronic transport properties can be used to get information

about their electronic structure. However, in amorphous semiconductors the electronic transport mechanism is not well understood. The theoretical models for amorphous semiconductors, which have been proposed so far, ignore the heterogeneities and are not able to explain fully the experimentally observed results. The potential fluctuations caused by the heterogeneities are known to be present in most of the amorphous semiconductors. The structure and a random distribution of defects are expected to play an important part in the transport properties of amorphous semiconductors.

The observed behaviour of $\sigma(T)$ and $S(T)$ in a-Ge:Li, a-Ge:H can be qualitatively explained using the existing models. It is concluded that for a more detailed explanation, a model which takes into account quantitatively the heterogeneities present in this material is needed, which at present does not exist.

Chapter 3 (part A) discusses the conductivity and thermopower measurements on undoped a-Si:H and lithium diffused a-Si:H. Lithium acts as an interstitial donor in a-Si:H. a-Si:H films prepared by d.c. glow discharge of 3% silane in argon are doped with Li by thermal diffusion. An increase in σ of a-Si:H films by a factor of 10^5 to 10^6 is obtained by doping. The dark and photo transport properties of undoped and doped a-Si:H films get changed |

upon light soaking of a few hours (Staebler-Wronski effect). Annealing at 150° - 200°C for 2 hours in vacuum brings back the original state. However, there is a considerable debate as to whether it is a bulk or a surface effect and its origin is not yet clear. The effect of light soaking on transport properties (σ and S) is also given in this chapter. An attempt is made to understand qualitatively the effect of doping and light soaking on σ and S , considering various proposed transport mechanisms. However, for a quantitative explanation, one must take into account the effect of potential fluctuations caused by heterogeneities and charged defects in these films.

In a-Si:H, a gradient of Li^{+} ions along the length of the sample is achieved by diffusing Li at high temperatures in the presence of an electric field. A small photovoltage arising from the gradient doping is observed (Chapter 3, part B). The potential distribution along the length of gradient doped samples is studied, and its possible use to increase the efficiency of a-Si:H solar cells is discussed.

a-Si:H films are prepared in thin film geometry and the presence of space-charge regions at the front surface and the film substrate interface affects transport properties of these films. Several attempts to measure surface potential in a-Si:H have been made by making surface

photovoltage (SPV) measurements. However, in contrast to the usual behaviour in c-semiconductors, the saturated value of SPV in a-Si:H does not give surface potential. In Chapter 4, by solving the Poisson's equation, for a continuous distribution of states in the mobility gap, a relation is obtained between the space charge density and the surface potential for a-Si:H in dark as well as in light. It is shown that SPV, in a-Si:H depends upon the properties of surface states and therefore may not give surface potential. Experimentally observed SPV and conductance in different surface conditions support this view. The frequency and temperature dependence of SPV are studied and can be explained using the theory presented. The effect of light soaking and adsorbates on SPV is also studied. SPV is found to be positive in the heat-dried (annealed at 150°C for 2 hrs), light soaked states and in the presence of humidity. Light soaking increases SPV on the non-etched surface, but decreases it on the etched surface. SPV is measured on a heat-dried sample after exposing it to a sequence of light soaking and humidity and in the reverse sequence. From this experiment it is concluded that light soaking changes the surface as well as bulk of a-Si:H.

Finally, Chapter 5 consists of the summary of results and the conclusions.

CHAPTER 1

INTRODUCTION

Considerable exploratory work on amorphous and liquid semiconductors was done by the Leningrad School since the early fifties. But the wide spread interest in amorphous semiconductors was provoked in the late 60's by the fabrication of switching and memory devices from amorphous chalcogenide alloys¹. The understanding of switching and memory processes from the physics point of view became a great challenge and a large amount of work has since been going on to study amorphous semiconductors. The basic difference between the crystalline and amorphous semiconductors is the atomic arrangement. In the crystalline state, there is a regular arrangement of atoms, resulting in a long range order (LRO), while in the amorphous state, there is no LRO.

Ioffe² (1951) pointed out that the basic nature of a solid depends upon the short-range order (SRO) and more explicitly, on the number of first neighbours of an atom (the first coordination number). Further, the basic electronic properties of a solid are determined primarily by the SRO, rather than by the LRO. It is the SRO, which is maintained in the amorphous state of the material. Based on Anderson's theory³, Mott⁴ has argued that the spatial fluctuations in

the potential caused by the configurational disorder in amorphous materials may lead to the formation of localized states, which do not occupy all the different states in the band, but form a tail above and below the normal band. There is a continuous distribution of localized states in the forbidden energy gap of amorphous semiconductors⁵. Their number and energy spread increases with the degree of randomness and the strength of scattering. In addition, deviations from the ideal random network, such as vacancies (voids) dangling bonds and chain ends contribute localized states within the forbidden energy gap⁶. Since the SRO is determined by the nature of bonding in the solid, it is clear that a classification of amorphous semiconductors along these lines is most appropriate. Thus depending upon the bonding, one has different kinds (e.g. ionic, covalent etc.) of amorphous semiconductors⁶. Following the work of Kastner⁷, it was recognized that the covalently bonded amorphous semiconductors consist of two categories;

(i) the tetrahedrally bonded amorphous semiconductors, e.g., amorphous germanium (a-Ge) and amorphous silicon (a-Si); and (ii) the lone pair semiconductors, e.g. Se, As, As₂S₃, and multicomponent chalcogenide glasses. Compound amorphous materials present a complex system to study as they have structural as well as compositional disorder. Therefore, in an attempt to understand basic properties of amorphous semiconductors much interest has been shown towards elemental

amorphous semiconductors i.e. amorphous germanium (a-Ge) and silicon (a-Si). However, even after more than a decade of work, these materials are not yet fully understood⁸.

a-Ge and a-Si films prepared by evaporation (or sputtering) have structural defects consisting regions of missing atoms (called voids)^{9,10}, with unsaturated (dangling) bonds at the internal surfaces of these voids. These films are porous¹¹. Electron spin resonance (ESR) study have shown density of spins of the order of 10^{20} cm^{-3} , and reduces upon annealing¹². This high density of spins was found to be a true bulk property^{10,13}. The states derived from the randomness of potential and from the electrons on the void surfaces are primarily responsible for the mobility gap properties¹⁴. The high density of localized states pin the Fermi level and addition of impurities does not normally have much effect on the position of the Fermi level. In fact, addition of impurities in large quantity modifies the structure of the material, and the controlled variation of electrical properties of pure a-Ge and a-Si is not possible⁶. Heat treatments of evaporated films, i.e. by raising substrate temperature (T_s) or annealing upto a temperature (T_A) just below the crystallization temperatures of respective materials reduce voids, and associated strain and dangling bonds¹⁵ and reduce the density of states to about $10^{19} \text{ cm}^{-3} \text{ eV}^{-1}$ ¹⁶. This density of states is still large

enough to pin the Fermi level. Emphasis has now been given to other techniques of preparation of a-Ge and a-Si in order to get a better material with less density of gap states.

Hydrogenated amorphous germanium (a-Ge:H) and hydrogenated amorphous silicon (a-Si:H) by the glow-discharge of GeH_4 and SiH_4 gases^{17,18} and by sputtering in an argon atmosphere mixed with hydrogen^{19,20}, are found to have a smaller density of localized states than the pure films. Among them only a-Si:H proved to be a promising amorphous semiconductor. It has a low density of localized states (10^{16} to $10^{17} \text{ cm}^{-3} \text{ eV}^{-1}$) at the Fermi level and can be doped n-type or p-type¹⁸. The presence of hydrogen of the order of 5 to 30 at% in a-Si:H films²¹ not only saturates dangling bonds but also reduces strains in the structure of the material. However, a-Ge:H has a density of localized states of the order of $10^{18} \text{ cm}^{-3} \text{ eV}^{-1}$ at the Fermi level²². The reason for this is not quite clear. Doping of a-Ge:H films is less efficient because it still has a large number of density of states.

a-Si:H has attracted the attention of many workers to this field, especially after the announcement of successful fabrication of solar cells²³. a-Si:H films were first prepared by Chittick et.al. by the glow-discharge of silane gas²⁴. The study of the structure, electronic density of states and transport properties have been

conducted, and information obtained has been utilized to improve the a-Si:H devices.

The properties of a-Si:H films are strongly sensitive to preparation conditions²⁵ (such as substrate temperature, T_s , power used to decompose gases, flow rate, partial pressure of gases and other factors which might affect the plasma conditions). Although all the parameters, which give good quality films (i.e. small density of states at the Fermi level) are not yet known fully, such films are usually prepared at high substrate temperature ($T_s = 300^\circ\text{C}$), low power density and high flow rate.

The presence of hydrogen and its bonding is detected by studying the infrared absorption. NMR results have indicated that the distribution of hydrogen in a-Si:H is strongly inhomogeneous²⁷. These films are also not isotropic along the thickness of the sample²⁸. In the beginning of the deposition, atoms see the substrate and during the first minutes of film growth various impurities desorbed or sputtered from the walls of the deposition chamber may become incorporated in the growing film²⁸. The presence of an oxide layer and adsorbates at the top layer, give space-charge region at the front surface. The top layers may be enriched or partially depleted of hydrogen depending on out diffusion and the hydrogen equilibrium process. Such vertical heterogeneities were detected by

various depth-probing analytical techniques²⁹.

In contrast to crystalline semiconductors our knowledge about the electronic transport in amorphous semiconductors is rather limited. In amorphous semiconductors one deals not only with a single processes, but with a combination of transport processes, such as hopping transport in the localized states and conduction in the extended states⁶. In case of a-Si:H the interpretation of experimental data is severely impeded by the fact that we are dealing with an alloy system of silicon and hydrogen, and that this material can be prepared in the form of thin films only²⁸. In addition, the temperature range accessible to transport experiments is usually rather limited. At low temperatures, the material becomes a good insulator, while at higher temperatures, the films change their properties due to structural annealing and effusion of hydrogen²¹. In addition the role of potential fluctuations due to heterogeneities and random distribution of defects in transport properties is not known²¹.

A phenomena which is of fundamental as well as applied interest is the changes in a-Si:H films caused by light soaking. In 1977, Staebler and Wronski³⁰ reported that the dark and photo conductance of these films reduced by several orders of magnitude after prolonged light

exposure. The changes are reversible upon annealing to 150-200°C for a few hours. The light soaking is now known to modify many of the electronic properties of a-Si:H, and in particular it is associated with the slow degradation of solar cells³¹. There is a considerable debate in the literature about the origin of the changes upon light-soaking.

For example there has been a controversy over whether it is a bulk or a surface effect³². Different experiments, such as field effect³³, capacitance-voltage³⁴, diffusion length³⁵, absorption coefficient in the near infrared³⁶, and electron spin resonance³⁷ show an increase in gap states upon light soaking. It has been suggested that these new gap states are probably dangling bonds, which act as recombination centers³⁷.

Experiments with forward and reversed biased junction diodes indicate that recombination is the main cause for creation of these defects. Since this process does not occur under strong reverse bias and takes place under forward bias even without light exposure³⁹. Alternatively, Adler⁴⁰ suggested that no defects are created by light, but recombination of photogenerated carriers induces excess neutral dangling bonds. These metastable centers are responsible for the increase in the density of spins, change

of the Fermi level and most of the other experimental results.

Recently it is reported that light soaking increases metastable negative charge in the surface oxide layer on a-Si:H films⁴¹. In contrast to the Staebler-Wronski effect, which normally causes a decrease in dark conductance, the new metastable state reported yields a large increase in conductance of p-type a-Si:H films. Surface photovoltage⁴² studies have shown that light soaking changes surface as well as the bulk. Changes on the surface depend upon the presence of an oxide layer and adsorbates. Thermopower and conductivity measurements⁴³ have indicated that light soaking increases random distribution of charged defects in the bulk.

In the present work, the effect of lithium diffusion on transport properties of evaporated a-Ge films have been studied (Chapter 2). Lithium has one bonding electron and its thermal diffusion in a-Ge⁴⁴ is possible. With a hope that Li will diffuse to voids in evaporated a-Ge and may saturate dangling bonds at the internal surfaces, lithium diffused evaporated a-Ge films have been prepared. Although Li saturates dangling bonds, a-Ge:Li is not photoconducting and is not suitable for doping. For a comparative study of lithium diffusion with hydrogenation, a-Ge:H films have been also prepared by evaporating Ge in a

partial pressure of hydrogen. Transport studies are also done on a-Si:H films before and after lithium diffusion (Chapter 3).

In contrast to a-Ge, lithium acts as an interstitial donor in a-Si:H⁴⁵. In a-Si:H prepared by d.c. glow-discharge of 3% silane in argon, lithium doping is achieved by thermal diffusion at high $T = 200^{\circ}\text{C}$. In Chapter 3(A), transport properties of undoped and Li doped a-Si:H are studied. Li in a-Si:H increases conductivity and decreases activation energy. The temperature dependence of σ for lithium doped a-Si:H (a-Si:H(Li)), is in agreement with that reported by Beyer and Fischer⁴⁵. Thermopower (S) is negative. The temperature dependence of S for a-Si:H(Li) is similar to that reported at low temperatures, but different at high temperatures.

Conductivity (σ) and thermopower (S) have been measured in the temperature range (200K to 450K) to study the effect of lithium diffusion and hydrogenation. S for a-Ge below $T = 280\text{K}$, is almost constant and negative. Hydrogenation decreases conductivity and increases negative thermopower at all temperatures. These results are similar to those reported⁴⁶. Lithium diffusion also reduces conductivity of a-Ge films (a similar action as of hydrogenation). But in these films the positive component of thermopower is more, at all temperatures. Qualitative interpretation of

10

these results have been given with the help of theoretical models developed by Beyer and Stuke⁴⁶, Lewis⁴⁷ and Jones et.al.⁴⁸. It is concluded that for a more detailed explanation, a model which takes into account quantitatively the heterogeneities present in this material is needed, which at present does not exist.

The effect of light soaking on transport properties has been studied on doped and undoped a-Si:H samples. Light soaking decreases conductivity and the magnitude of thermopower of lightly Li doped samples. It does not change conductivity of highly doped samples, but reduces the magnitude of thermopower. These are compared with the results obtained by Hauschildt et.al.⁴³ who have studied the effect of light soaking on σ and S of phosphorus doped a-Si:H. They find a decrease in σ in agreement with the present results, but reported an increase in the magnitude of negative thermopower upon light soaking. Recently Mell and Beyer⁵⁰ have reported the effect of light soaking on compensated a-Si:H samples. In these samples, an increase in conductivity and a decrease in the magnitude of negative thermopower is observed upon light soaking. At present, there are no quantitative explanation of the effect of light soaking on the transport properties. Probably, light soaking increases the charged defect centers and their effect may depend upon the position of the Fermi level⁴³.

For a quantitative explanation, one must take into account the effect of potential fluctuations caused by heterogeneities and charged defects in these films. Transport results analysed qualitatively with the help of existing theoretical models.

A gradient of concentration of impurities in c-semiconductors has been observed to give rise to a potential gradient within the sample⁵⁰. In lithium doped a-Si:H, a gradient of Li^+ ions has been obtained by diffusing Li in presence of an electric field at a high temperature ($T = 200^\circ\text{C}$) (Chapter 3B). In a gap cell geometry of a-Si:H (Li), having a potential gradient, an open-circuit voltage (V_{oc}) ≥ 100 mV and a short-circuit current (J_{sc}) $\approx 10^{-3} \text{ A/cm}^2$ have been observed upon shining light. Use of this linear potential gradient to increase the efficiency of Schottky barrier device (sandwich geometry) has been suggested by fabricating a series combination of a Schottky barrier and a gradient doped a-Si:H. However, the attempts have not been successful so far. Possible causes are discussed.

Since a-Si:H samples are prepared in thin film geometry. Surface effects are important. a-Si:H is in electronic equilibrium not only with its surface and interface states but also with its substrate, its surface oxide layers and various chemisorbed species. All these

effects produce a nonzero surface potential, which may change with temperature and light exposure and affect the electronic properties of a-Si:H films²⁸. The interpretation of conductivity and thermopower and other basic properties, without knowing the behaviour of space-charge layers at surfaces is difficult. Therefore, for a consistent and correct interpretation of experimental results, the study of surface properties in detail is important.

Various experimental techniques developed to study the surface properties for crystalline semiconductors, have been applied to a-Si:H. One of these is the measurement of change in dark conductance (G) upon exposing the surface of the sample to different ambients⁵¹. Large changes in G upon adsorption of polar gases (NH_3 , H_2O , $\text{C}_2\text{H}_6\text{O}$ etc) on thin films of a-Si:H have been reported by Tanielian⁵¹. LeComber et.al.⁵² and Street et.al.⁵³ observed effects of gate voltage on dark and photoconductance measured in a-Si:H FETs. The results have been interpreted in term of the presence of a surface potential. Solomon³² studied the effect of white bias light illumination on the luminescence from a-Si:H due to band gap light and high energy light. No effect of bias light was observed on the band gap light luminescence, but luminescence at high energy light increased. The observed increase in the luminescence intensity indicated the presence of a space charge layer at

the surface. Surface photovoltage (SPV, change in surface potential upon shining light) have been used to measure surface potential in c-semiconductors⁵⁴. A change in the surface potential upon shining light is possible (i) by a charge redistribution between the surface states and the space-charge region and or (ii) by a redistribution of charge within the space charge region. It has been generally believed that light tends to flatten the bands and the SPV measured at high intensities directly gives the surface potential (band bending) at the surface⁵⁴. Although, this can be shown to hold good for process (ii)⁵⁵, it may not always be the case for process (i)⁵⁶. It has been shown that when SPV is dominated by the surface states its sign and magnitude is determined by the surface state parameters and it may not give the band bending⁵⁶.

However, in the hope of finding the direction and the magnitude of band bending on the surface of a-Si:H SPV experiments have been carried out in different laboratories. Goldstein and Szostak⁵⁷ estimated the band bending at the surface of a-Si:H by measuring SPV assuming the ansatz to be true. But they were unable to correlate their SPV results with the photoconductivity measurements and concluded that under illumination charge in surface states changes. Whenever, there is an exchange of charge between the space-charge and surface states, it is difficult to obtain band

bending from the SPV data⁵⁶. As such the band bending obtained by Goldstein et.al. may not be correct. Aker et.al.⁵⁷ find that they are unable to explain the measured conductance in the heat dried and light soaked states of a-Si:H, if they assume that the measured SPV in these states directly gives the band bending. We⁴² have also found that it is not possible to explain the changes in the conductivity of a-Si:H upon exposure to moisture vis-a-vis our SPV measurements, if the assumption that the SPV gives band bending were to hold for a-Si:H.

There is, thus, sufficient evidence to suggest that in a-Si:H, which has a continuous distribution of localized states, SPV is affected by the exchange of charges between the surface and the space-charge states and that it is not possible to correlate SPV with band bending, contrary to the general belief.

In Chapter 4, Poisson's equation is solved for surface potential, in a-Si:H, in the presence of light and in dark. A relation between the space-charge density (Q_{sc}) and the surface potential is derived. It is shown that in a-Si:H, SPV is zero for process (ii) and a change in Q_{sc} is necessary to observe SPV (process (i)). It is therefore concluded that SPV in a-Si:H, may not give band bending at the surface.

Experimentally, SPV has been measured using pulsed (chopped) light⁵⁴. Conductance of the sample has also been monitored. It is shown, by measuring SPV and conductance in different surface conditions, that SPV gives neither the magnitude nor the direction of surface potential, in support of the theoretical arguments. Temperature dependence of SPV at the front surface and the back surface (film substrate interface) is found to be different. In contrast to c-Si, SPV in a-Si:H does not become zero at high temperatures, but changes sign. Effect of light-soaking on SPV has also been studied.

Effect of light soaking on SPV depends upon the surface conditions. Measurement of SPV and conductance on a heat-dried sample exposed to a sequence of light soaking and humidity show that the final value of SPV obtained at the end of the cycle depends on the order in which the two are performed. However, the final value of G is almost the same, regardless of the order in which the light soaking and humidity exposure are performed⁵⁰. It is concluded that light soaking changes the surface as well as the bulk of a-Si:H.

Finally, Chapter 5 gives the summary of the results obtained and the conclusions.

REFERENCES

1. S.R.Ovshinsky, Electronics, 32, 76 (1959).
2. A.F.Ioffe, Bull. Acad. Sci. (USSR), 15, 477 (1951).
3. P.W.Anderson, Phys. Rev. 109, 1492 (1958).
4. N.F.Mott, Adv. Phys., 16, 49 (1976).
5. M.H.Cohen, H.Fritzsche, and S.R.Ovshinsky, Phys. Rev. Lett. 22, 1065 (1969).
6. H.Fritzsche in Amorphous and Liquid Semiconductors, edited by J.Tauc (Plenum Press, N.Y., 1974).
7. M.Kastner, Phys. Rev. Lett., 28, 355 (1972).
8. H.Fritzsche, Summary and Closing Remarks, 10th ICALS Tokyo, J.Non Cryst. Solids, 59 & 60, 1289 (1983).
9. S.C.Moss and J.F.Graczyk, Phys. Rev. Lett. 23, 1167 (1969).
10. M.H.Brodsky and R.S.Title, Phys. Rev. Lett. 23, 581 (1969).
11. M.Kastner and H.Fritzsche, Mat. Res. Bull., 5, 631 (1970).
12. S.C.Agarwal, Phys. Rev. B7, 685 (1973).
13. D.Haneman, Phys. Rev. 170, 705 (1968).
14. A.J.Lewis, G.A.N.Connell, W.Pawlik and J.R.Tempkin in Tetrahedrally Bonded Amorphous Semiconductors, edited by M.H.Brodsky, S. Kirkpatrick and D.Weaire (A.I.P. 1974), p.27.
15. M.A.Paesler, S.C.Agarwal, S.J.Hudgens and H.Fritzsche in Proc. of Int.Conf. on Tetrahedrally Bonded Amorphous Semiconductors; Yorktown Heights (1974), A.I.P. Conference No.20, p.37.
16. M.H.Brodsky, D.M.Kaplan and J.F.Ziegler in Proc. 11th Int. Conf. on the Physics of Semiconductors, Warsaw, (P.W.N.Polish Scientific Publishers Warsaw, 1972), p. 529.

17. D.I.Jones, W.E.Spear, and P.G.LeComber, J. Non. Cryst. Solids., 20, 259 (1976).
18. P.G.LeComber and W.E.Spear, Phys. Rev. Lett., 25, 509 (1970).
19. M.H.Brodsky, R.S.Title, K.Weiser and G.D.Pettit, Phys. Rev. B1, 2632 (1970).
20. W.Paul, A.J.Lewis, G.A.N.Connell and T.D.Moustakas, Solid State Comm. 20, 969 (1976).
21. H.Fritzsche, Solar Energy, Mat., 3, 447 (1980).
22. W.Paul in Fundamental Physics of Amorphous Semiconductors, edited by F.Yonezawa (Springer Verlag, N.Y., 1976).
23. D.E.Carlson and C.R.Wronski, Appl. Phys. Lett., 29, 602 (1976).
24. R.C.Chittick, J. Non. Cryst. Solids, 3, 255 (1970).
25. P.G.LeComber, A.Madan and W.E.Spear, J. Non. Cryst. Solids, 11, 219 (1972).
26. M.H.Brodsky, M.Cardona and J.J.Cuomo, Phys. Rev. B16, 3556 (1977).
27. J.A.Reimer, R.W.Vaughan and J.C.Knights, Phys. Rev. Lett., 44, 193 (1980).
28. H.Fritzsche in Electronic and Transport Properties of Hydrogenated Amorphous Silicon, edited by J.I.Pankove (Academic Press, N.Y. 1984).
29. D.E.Carlson, C.W.Magee, and A.R.Triono, J. Electrochem. Soc., 126, 688 (1979).
30. D.L.Staebler and C.R.Wronski, Appl. Phys. Lett., 31, 292 (1977).
31. R.S.Crandall and D.L.Staebler, Solar Cells, 9, 63 (1983), and other articles in this volume.
32. I.Solomon in Fundamental Physics of Amorphous Semiconductors, edited by F.Yonezawa (Springer Verlag, N.Y., 1981).

33. M.H.Tanielian, N.B.Goodman and H.Fritzsche, J. Phys. (Paris), 42, Suppl. C4-375 (1981).
34. D.Jousse, R.Basset and S.Delionibus, Appl. Phys. Lett., 37, 208 (1980).
35. J.Dresner, D.J.Szostak and B.Goldstein, Appl. Phys. Lett., 38, 998 (1981).
36. A.Skuminich, N.M.Amer and W.B.Jackson, Bull. Am. Phys. Soc. 27, 146 (1982).
37. H.Dersch, J.Stuke and J.Beichler, J. Appl. Phys. Lett., 38, 456 (1981).
38. J.I.Pankove, and J.E.Berkeyheiser, Appl. Phys. Lett., 37, 705 (1980).
39. S.Guha, J.Yang, W.Czubatyj, S.J.Hudgens and M.Hack, Appl. Phys. Lett. 42, 588 (1983).
40. D.Adler, Solar Cells, 9, 133 (1983).
41. B.Aker and H.Fritzsche, J. Appl. Phys., (1983), to appear.
42. S.Kumar and S.C.Agarwal, Phil. Mag. (1984), to appear.
43. D.Hauschildt, W.Fuhs and H.Mell., Phys. Stat. Solidi, b 111, 171 (1982).
44. S.Kumar and S.C.Agarwal, in Proc. of Symp. on Non. Cryst. Solids, edited by S.C.Agarwal, (I.I.T. Kanpur, 1980).
45. W.Beyer and R.Fischer, Appl. Phys. Lett., 31, 850 (1977).
46. W.Beyer and J.Stuke, in Proc. 5th Int. Conf. on Amorphous and Liquid Semiconductors, edited by J.Stuke and W.Brenig (Taylor and Francis, London, 1974), p.251.
47. A.J.Lewis, Phys. Rev. B14, 658 (1976).

48. D.I.Jones, P.G.LeComber and W.E.Spear, Phil. Mag. B36, 541 (1977).
49. H.Mell and W.Beyer, J. Non.Cryst. Solids, 59&60, 405 (1983).
50. Z.Trousil, Czech. J. Phys. 6, 96 (1956).
51. M.Tanilian, Phil. Mag. B45, 435 (1982).
52. P.G.LeComber, W.E.Spear, R.A.Gibson, H.Mannspurger and T.Djamdjii, J. Non. Cryst. Solids, 59&60, 505 (1983).
53. R.A.Street, Phys. Rev. B27, 4924 (1983).
54. A.Many, Y.Goldstein and N.B.Grover, Semiconductor Surfaces (North-Holland, Amsterdam, 1965).
55. E.O.Johnson, Phys. Rev. 111, 153 (1958).
56. D.R.Frankl and E.A.Ulmer, Surface Sci., 6, 115 (1966).
57. B.Goldstein and D.J.Szostak, Surface Sci., 99, 235 (1980).
58. B.Aker, S.Q.Peng, S.Y.Cai and H.Fritzsche, J.Non.Cryst.Solids, 59&60, 509 (1983).

CHAPTER 2

LITHIUM DIFFUSED AND HYDROGENATED AMORPHOUS GERMANIUM

2.1 Introduction

Hydrogen reduces density of localized states by saturating dangling bonds at the internal surfaces of voids in a-Ge¹. Lithium has single valence electron and it's thermal diffusion in a-Ge is possible². In a hope to achieve less density of states in the mobility gap of a-Ge by saturating dangling bonds with Li, Li diffused a-Ge films have been prepared. For comparison with hydrogenated a-Ge, conductivity and thermopower measurements have been done. The temperature dependence of conductivity of a-Ge:Li and a-Ge:H samples is similar indicating that Li is saturating dangling bonds, but thermopower results are different. a-Ge:H as well as a-Ge:Li samples are not photoconducting. In section 2.2, a review of theoretical models used to interpret the conductivity and thermopower results of covalent a-semiconductors is given. In section 2.3, preparation methods of a-Ge:Li and a-Ge:H, and measurement methods of conductivity and thermopower are described. In the last section results and their interpretation is given.

2.2 Theory of Conductivity and Thermopower

Amorphous semiconductors have conduction and valence bands of extended states and an optical energy gap³. Absence of periodicity (long range order) reduces sharpness of localized states at the band edges³. In addition one expects that deviations from the ideal covalent random network, such as vacancies, and dangling bonds contribute localized states in certain energy ranges. Mott⁴ suggested that the character of wavefunctions changes at critical energies E_c and E_v which separate the extended and localized states. Here the electron and hole mobilities drop sharply from a low mobility band transport with a finite mobility at $T=0$ to a thermally activated hopping between localized gap states which disappears at $T=0$. These so-called mobility edges define a mobility gap ($E_c - E_v$) which contains only localized states.

2.2a Kubo-Greenwood Formulae

The general expression for conductivity (σ), assuming a single particle picture and neglecting correlation effect is^{3,5}

$$\begin{aligned}\sigma(E, T) &= \int \sigma(E) dE \\ &= |q|^2 \int \mu(E) g(E) f(E, T) [1 - f(E, T)] dE\end{aligned}\quad (1)$$

where $\sigma(E)$ is the conductivity of electrons with energy E , $g(E)$ is the distribution of density of states, $\mu(E)$ the mobility and $f(E)$ is the Fermi distribution function. The thermopower S , at temperature T , is related to the Peltier coefficient π as⁶

$$S = \pi/T \quad (2)$$

where π is the measure of total energy carried by the charge carriers per unit charge and is given by⁵

$$\pi = - \frac{1}{e} \int \frac{(E - E_f) \sigma(E)}{\sigma} dE \quad (3)$$

From equations (2) and (3), one gets

$$S = \frac{k}{e} \int \frac{(E - E_f)}{kT} \frac{\sigma(E)}{\sigma} dE \quad (4)$$

Equations (1) and (4) can be easily simplified for various possible mechanisms of charge transport, using energy band model for a-semiconductors. One of the basic assumptions made in deriving Eq.(1) and (4) is that the material is homogeneous. However, compositional and structural inhomogeneities are known to play an important role in the properties of amorphous solids⁷. Further, Eq.(1) is derived for a one particle system, neglecting correlation effects. In reality, electronic motion is affected by correlation effects and is sensitive to potential fluctuations. Charge motion involves exchange

of energy with the lattice, hence treating conduction in each energy level separately may not be justified⁷.

However, theoretical models for a homogeneous sample have been used to give a qualitative explanation of experimental results.

2.2b Transport Processes

Total conductivity of a material is⁶

$$\sigma = \sum \sigma_i \quad (5)$$

and thermopower⁶

$$S = \frac{\sum \sigma_i S_i}{\sum \sigma_i} \quad (6)$$

where σ_i and S_i represent conductivity and thermopower of various possible charge conduction processes. These are (i) conduction of free carriers (electrons and holes) in the extended states and (ii) hopping conduction in the localized states.

i) Conduction in Extended States

For a nondegenerate semiconductor having mobile electrons above the mobility edge E_c (for holes below E_v) Boltzmann's statistics can be used to describe the occupation of states. The conductivity and thermopower are given by⁷

$$\sigma(E_c, T) = \sigma_-(T) \exp\left(-\frac{E_c - E_f}{kT}\right) \quad (7)$$

and

$$S(E_t, T) = \frac{|E_t - E_f|}{qT} + \frac{k}{q} A(T) \quad (8)$$

where k is the Boltzmann's constant, E_f denotes the Fermi level and q ($q = -|e|$ for electrons and $+|e|$ for holes) is the carrier charge. E_t is the energy of charge carriers, $E_t = E_c$ for electrons and E_v for holes. The conductivity prefactor σ_0 depends upon the carrier mobility and on the density of states at the energy E_c and above. The 'heat of transport' term A of the thermopower is related to the kinetic energy of the charge carriers and is determined by the carrier scattering process⁷.

ii) Conduction in Localized States

a) Phonon Assisted Nearest Neighbour Hopping:

Electrons in localized states can contribute to the conductivity by hopping. An electron moves from one localized state to another with an exchange of energy with a phonon. The jump probability from an occupied to an empty site, being separated by R in space and by $\Delta E > 0$ in energy is given by⁸

$$p = \nu_{ph} \exp\left(-\frac{2R}{a} - \frac{\Delta E}{kT}\right) \quad (9)$$

where ν_{ph} is a characteristic phonon frequency.

If hopping is always to the nearest neighbour in space

(nearest neighbour hopping, NNH) at an energy E_{tn} , the corresponding conductivity (σ_N) and thermopower (S_N) can be shown to be⁷

$$\sigma_N = \sigma_{ON} \exp -(E_{tn} - E_f + W)/kT \quad (10)$$

and

$$\frac{q}{k} S_N = |E_{tn} - E_f| /kT + A_N \quad (11)$$

where W is a typical energy difference between nearest neighbour states. It should be noted that the hopping activation energy W does not appear in the expression of thermopower. The reason is that in eq.(4), mobility term appears in $\sigma(E)$ as well as in σ and cancels out since μ is taken to be independent of E . This therefore predicts the slope of $\ln \sigma$ vs $1/T$ curve to be larger by an amount W , as compared to the $\frac{q}{k} S$ vs $1/T$ slope for hopping conduction.

b) Variable Range Hopping:

At low temperatures, the number and energy of phonons available for absorption decreases so that the hopping is not restricted to nearest neighbour but which instead lie energetically closer (within the range kT). This variable range hopping (VRH) first proposed by Mott⁹ leads for hopping via states near the Fermi level to the

characteristic $T^{-1/4}$ law

$$\sigma_H = \sigma_{OH} \exp(-T_0/T)^{-1/4} \quad (12)$$

where the prefactor σ_{OH} and the constant T_0 have been derived by many workers⁷. Various treatments differ in terms of assumptions involved and derived values differ only by a small numerical factor. σ_{OH} is given by¹⁰

$$\sigma_{OH} = \frac{e}{2(8\pi)^{1/2}} v_{ph} \left[\frac{g(E_f)}{kT} \right]^{1/2} \quad (13)$$

and T_0 is given by¹¹

$$T_0 = 16 \alpha^3 / k g(E_f) \quad (14)$$

where α is the coefficient of the exponential decay of the localized wave functions and is assumed to be independent of E .

In VRH, only states near E_f contribute to the current and it is convenient to write $f(1-f) = -kT \partial f / \partial E$ in Eq.(1). Expanding $g(E)\mu(E)$ in a Taylor series at $E=E_f$. One gets for the nonvanishing term in Eq.(4)^{5,12}

$$S = - \frac{\pi^2}{3} \frac{k}{e} kT \left[d \ln(g) / dE \right]_{E_f} \quad (15)$$

Eq.(15) has been used by many workers⁹ to obtain explicit expressions of S for various distributions of $g(E)$

near E_f . Recently Nagels¹³ et.al. (1983) derived an expression for thermopower. S exhibits a simple temperature dependence of the form

$$\frac{S}{T} \propto \frac{1}{T^{1/n+1}} \quad (16)$$

where n is the dimensionality of the system. For a three dimensional system, in case of VRH, one expects $\frac{S}{T}$ be proportional to $T^{-1/4}$.

2.2 Small Polaron Model and Phonon Drag Effect

Emin¹⁴ has considered the small polaron model for charge transport in amorphous semiconductors. The temperature dependence of conductivity and thermopower in small polaron model and for NNH is similar, hence it is difficult to differentiate between the two processes¹⁵. As such, most of the experimental results in tetrahedral amorphous semiconductors are explained assuming conduction in extended states and hopping conduction in localized states.

Thermopower may have a contribution originating from the directed phonon flow from the hotend to the cold end of the sample⁵. The thermopower, S , is the sum of the usual charge conduction term S_c resulting from spontaneous tendency of charge carriers to diffuse from hot to cold, and a phonon term S_{ph} , resulting from the drag on the

charge carriers exerted by the phonons streaming from hot to cold and in thermal conduction. In amorphous semiconductors, this phonon drag component can be neglected^{16,17}. Because of their negligible mean free path, the carriers lose their extra momentum immediately.

2.2 Combination of Transport Processes

In reality, one or more of the above processes take place simultaneously. Let the contributions of electrons, holes and hopping to conductivity and thermopower be represented by σ_n , σ_p and σ_H and S_n , S_p and S_H respectively.

From Eq.(5) and (6), the total conductivity and averaged thermopower will be given by

$$\sigma = \sigma_n + \sigma_p + \sigma_H \quad (17)$$

and

$$S = \frac{\sigma_n}{\sigma} \left(+ \frac{E_c - E_f}{qT} + \frac{kA_n}{q} \right) + \frac{\sigma_p}{\sigma} \left(- \frac{E_v - E_f}{qT} + \frac{kA_p}{q} \right) + \frac{\sigma_H}{\sigma} S_H \quad (18)$$

If for a monopolar sample, transport is in extended states at high temperatures and NNH in tail states (or in the impurity band) at the lower temperatures, then the conductivity and the thermopower, for an n-type sample will be¹⁸ (e.g. a-Si:H),

$$\sigma = \sigma_n + \sigma_N$$

$$= \sigma_{on} \exp(-|E_c - E_f|/kT) + \sigma_{ON} \exp(-|E_{tN} - E_f| + W)/kT \quad (19)$$

and

$$S = \frac{\sigma_n}{\sigma} \left(+ \frac{|E_c + E_f|}{qT} \right) + \frac{kA_n}{q} + \frac{\sigma_N}{\sigma} \left(- \frac{|E_{tN} - E_f|}{qT} + \frac{kA_N}{q} \right) \quad (20)$$

The subscripts n and N stand for electron conduction in the extended states and for NNH in the localized states respectively.

2.2 .e Temperature Dependence of the Fermi Level and Mobility Edges on Transport

The mobility gap and the relative position of the Fermi level with respect to the mobility edge, are temperature dependent¹⁹. The relative position of E_f may change because of the non-symmetric distribution of states below and above E_f (statistical shift)²¹ and on account of the temperature dependence of the mobility gap¹⁹. To a first order in T, one can write

$$E_c - E_f = (E_c - E_f)_0 - \delta T \quad (21)$$

where δ is the temperature coefficient of $(E_c - E_f)$.

Conductivity σ can be written as

$$\sigma = \sigma_o \exp \left[- \frac{|E_c - E_f|_o}{kT} + \frac{\delta}{k} \right]$$

$$\sigma = \sigma_o \exp \left(\frac{\delta}{k} \right) \exp \left[- \frac{|E_c - E_f|_o}{kT} \right] \quad (22)$$

The coefficient δ is usually approximated from the temperature dependence of the optical absorption edge¹⁹.

Beyer and Overhof^{20,21} considered a quantity, $Q(T)$, which is independent of the positions of the reference energy levels and is given by

$$Q(T) = \ln \sigma + \left| \frac{qS}{k} \right| \quad (23)$$

and with

$$\sigma = \sigma_o \exp (- E_\sigma / kT)$$

and,

$$\frac{qS}{k} = \frac{E_s}{kT} + A$$

one gets,

$$Q(T) = C - E_\mu / kT \quad (24)$$

where,

$$C = \ln \sigma_o + A \text{ and } E_\mu = E_\sigma - E_s$$

Equation (24) holds good for unipolar conduction. The quantity $Q(T)$ is independent of the position of the Fermi level and mobility edges. Consequently it is only determined

by the current path at the mobility edge. Any difference between E_G and E_S will show up as a nonzero slope of Q when this quantity is plotted versus reciprocal temperature. Q vs $1/T$ curve will deviate from a straight line behaviour in case of the bipolar conduction, hopping conduction and in presence of conducting space charge layers at the surface.

2.3 Experimental

2.3.1 Preparation:

Amorphous germanium (a-Ge), lithium diffused a-Ge (a-Ge:Li) and hydrogenated a-Ge (a-Ge:H) have been prepared by evaporation in a standard vacuum coating unit. An oil diffusion pump with a liquid nitrogen trap is used to create a vacuum of better than 10^{-6} Torr. Properties of a-Ge films depend upon many parameters, such as, the rate and angle of deposition, the substrate temperature and the source to substrate distance³. For a comparative study, a-Ge, a-Ge:Li and a-Ge:H films have been prepared under similar conditions on 7059 glass substrates. Source to substrate distance is 18 cm. Substrate temperature T_s is 450K and the rate of deposition is $r = 5 \text{ \AA}/\text{S}$. a-Ge:Li films have been prepared using two sources of evaporation, one for Ge and another for Li. While using one source, another is covered with a shutter. Since Li is highly

reactive, it is kept under trichloroethylene in the evaporation boat. Upon evacuation trichloroethylene having a high vapour pressure evaporates. A lithium layer ($50\text{--}100\text{\AA}$ thick) is sandwiched between two thick layers of a-Ge (each of thickness about 2500\AA). Knowing the thickness of the lithium layer allows to roughly estimate the amount of lithium. After deposition, samples are annealed at $T_s = 150^\circ\text{C}$ for two hours to get an uniform distribution of lithium. a-Ge:H films have been prepared by evaporating Ge at a partial pressure of 5×10^{-5} Torr of purified hydrogen^{22,23}. The thickness of the films is measured by a quartz crystal monitor (Edwards, FTM 3) as well as by the optical interference method²⁴.

2.3.2 Characterization

a. Structural

The a-Ge:Li and a-Ge:H films were found amorphous by X-ray and electron diffraction. I-R spectroscopy on a-Ge:Li samples deposited on KBr pallets showed absorption peaks at 1400 cm^{-1} , 1020 cm^{-1} and 860 cm^{-1} . The position of the peak for Ge-H vibrational mode³ is known to be $\approx 1900\text{ cm}^{-1}$. Taking into account the mass difference between hydrogen and lithium, this peak is expected to shift to $\approx 860\text{ cm}^{-1}$ for Ge-Li. The peaks at 1020 cm^{-1} and 1400 cm^{-1} can be attributed to Ge-Li and Ge-Li-O

complexes²⁵.

b) Electrical

The a-Ge:H films are found ohmic upto the measured field of 10^3 V/cm at 300K. a-Ge:Li films are ohmic, if Li concentration is less than about 5 at%. For higher concentration of Li a polarization occurs, which is probably because of a drift of Li ions in the film. The I-V characteristics are not symmetric with respect to the direction of the applied field, as the films get polarized even during the measurement². The polarization is studied as a function of the polarizing field and the duration of polarization². The decay currents (I_d) observed for different polarizing fields are shown in Fig.(2.1) at room temperature. Depolarization takes several hours to decay at room temperature².

2.3.3 Measurement of Conductivity and Thermopower

The geometry of samples used to measure conductivity and thermopower is shown in Fig.(2.2A). Films of thickness about 0.5 μ m are deposited on 7059 glass substrates. Two NiCr electrodes, each of width 1 mm and length 0.8 cm are deposited at the top of the film with a gap of 1.8 cm. The cryostat used for measuring conductivity and thermopower is shown in Fig.(2.2B). A square

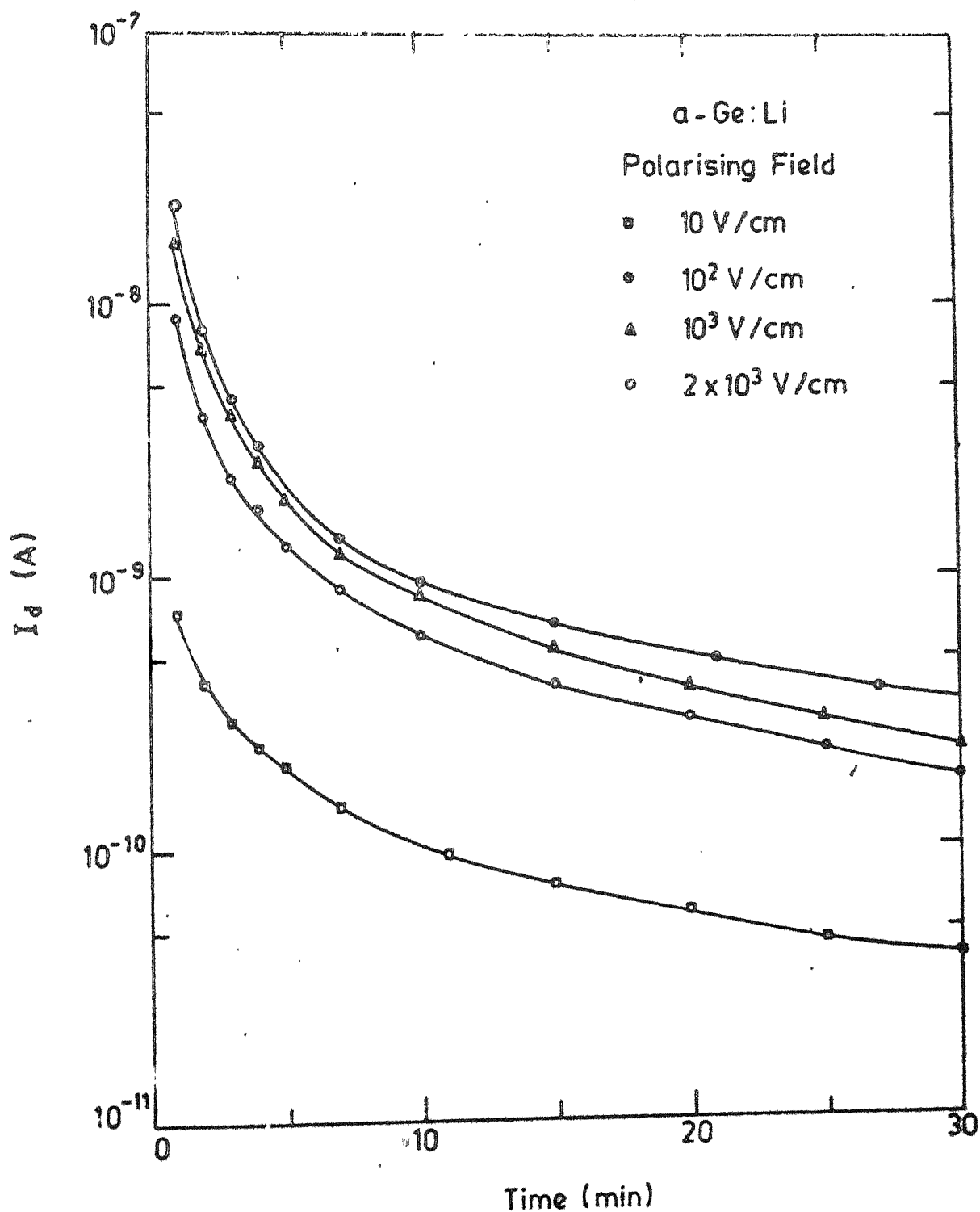


Fig.2.1 : Decay of I_d at 300K for various polarising electric fields.

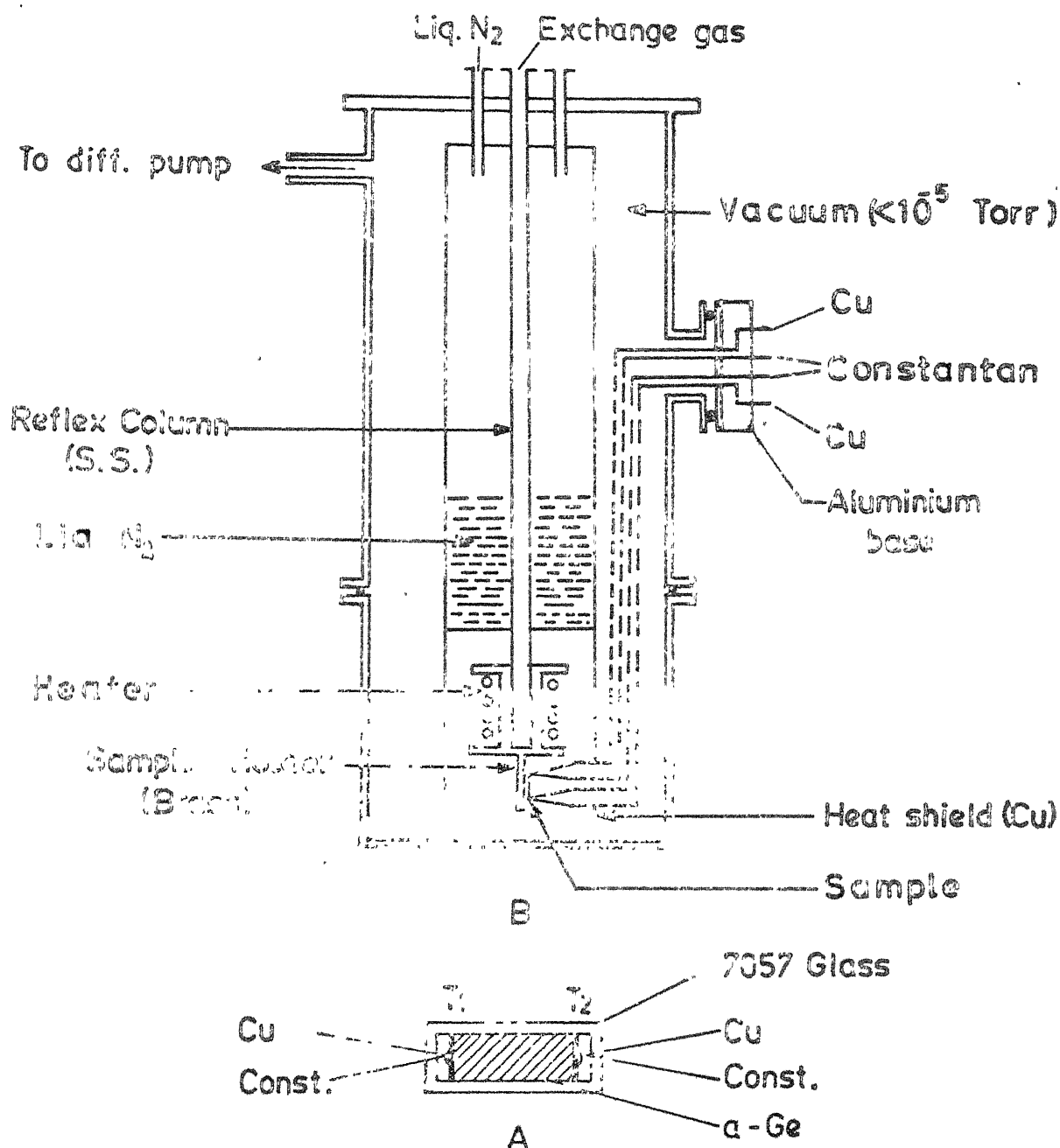


Fig. 2.2A : Geometry of the sample used to measure conductivity and thermopower

B : Geometry of the cryostat used to measure conductivity and thermopower

brass plate is used as a sample holder. One end of the plate is attached to the reflex coloumn, which is made of stainless steel. The reflex coloumn has at its lower end a heater, wound around a copper block as shown. The reflex column passes through the liquid N_2 chamber. The separation of the liquid N_2 chamber from the heater is 2 cm and from the substrate holder, it is 6 cm. The liq. N_2 chamber is supported by two stainless steel tubes and the reflex column, which are brazed in a stainless steel flange. The heater and the sample holder are surrounded by a removable heat shield made of copper. The whole system (liq. N_2 chamber with sample holder and heat shield) is kept in a cylinder, whose lower portion can be removed for loading the sample. The upper portion of the cylinder has the electrical feed throughs and can be connected to a vacuum pump.

Copper constantan thermocouples (wire thickness 0.1 mm) are used to measure the temperature at the two ends of the sample. Thermocouples are attached to the nichrome (NiCr) electrodes with indium solder. Thermocouple wires are insulated with each other and from the system by teflon tape. The thermocouple wires are taken out of the cryostat, without breaking, using hollow teflon insulated feed throughs. The feed throughs outside the cryostat are covered with an aluminium box having UHF connectors, for

electrostatic shielding. The thermocouple voltage is measured with a digital voltmeter (Hewlett packard model No. 3455A). To measure resistance and thermopower the two copper wires are used. V_{oc} is measured with a Keithley 602 electrometer amplifier, using shielded cables.

With liq.N₂ in the liquid N₂ container and using a exchange gas (Nitrogen) in the reflex column, low temperature upto 135K at the sample, loaded in the center of the sample holder, can be achieved. By varying the pressure of the exchange gas different equilibrium points can be achieved. Using different currents in heater and with liq.N₂ in the container different equilibrium points below room temperature can be obtained. A gradient of temperature, $4K < \Delta T < 10K$ is obtained along the length of the sample because of the design geometry. Using different currents in the heater, temperature above room temperature upto 460K can be obtained. The mean temperature $T = (T_1 + T_2)/2$ is taken as a variable temperature parameter for both conductivity and thermopower.

2.4 Results

Lithium diffusion reduces the conductivity (σ) of a-Ge films. The magnitude of decrease depends upon the Li concentration. σ (300K) of a-Ge:Li samples having about 5 at% Li is less than that of a-Ge by a factor of about 50.

It has been observed that a-Ge:Li samples having more than about 5 at% of lithium concentration get electrically polarized upon application of an electric field as small as 10V/cm (sec. 2.32b)². For transport study a-Ge:Li samples having about 1-2 at% Li are therefore chosen. Polarization effect is negligible in these films.

Figs.(2.3a) and (2.3b) show behaviour of conductivity (σ) and thermopower(S) respectively as a function of $1/T$ for a-Ge (curve 1), a-Ge:Li (curve 2) and a-Ge:H (curve 3). For comparison, results obtained on hydrogenated sputtered a-Ge (curve 4, Lewis 1976)¹⁵ on a sample produced by glow discharge of germane^(curve 5)²⁶ are also shown. Curve 4 is for a sample deposited at $T_s = 25^\circ\text{C}$ and annealed at temperature $T_A = 250^\circ\text{C}$. Curve 5 is for a sample deposited at $T_s = 230^\circ\text{C}$.

σ vs $1/T$ curves (1,2 and 3) are straight lines above $T > 320\text{K}$ with slopes 0.2 eV, 0.38 eV and 0.4 eV respectively. Slope of the curve (1) decreases continuously below $T = 320\text{K}$. Slopes of curves (2 and 3) decreases below $T = 280\text{K}$. Curves 4 and 5 deviate from linearity below temperatures $T = 150\text{K}$ ¹⁵ and $T = 200\text{K}$ ²⁶ (not shown in the figure).

Thermopower(S) for a-Ge (curve 1, in Fig.(2.3b)) is negative at room temperature. Its magnitude decreases at low temperatures and becomes constant for $T < 280\text{K}$. Above $T=280\text{K}$, its magnitude increases to a maximum at $T=380\text{K}$ and then decreases with continuously changing slope and

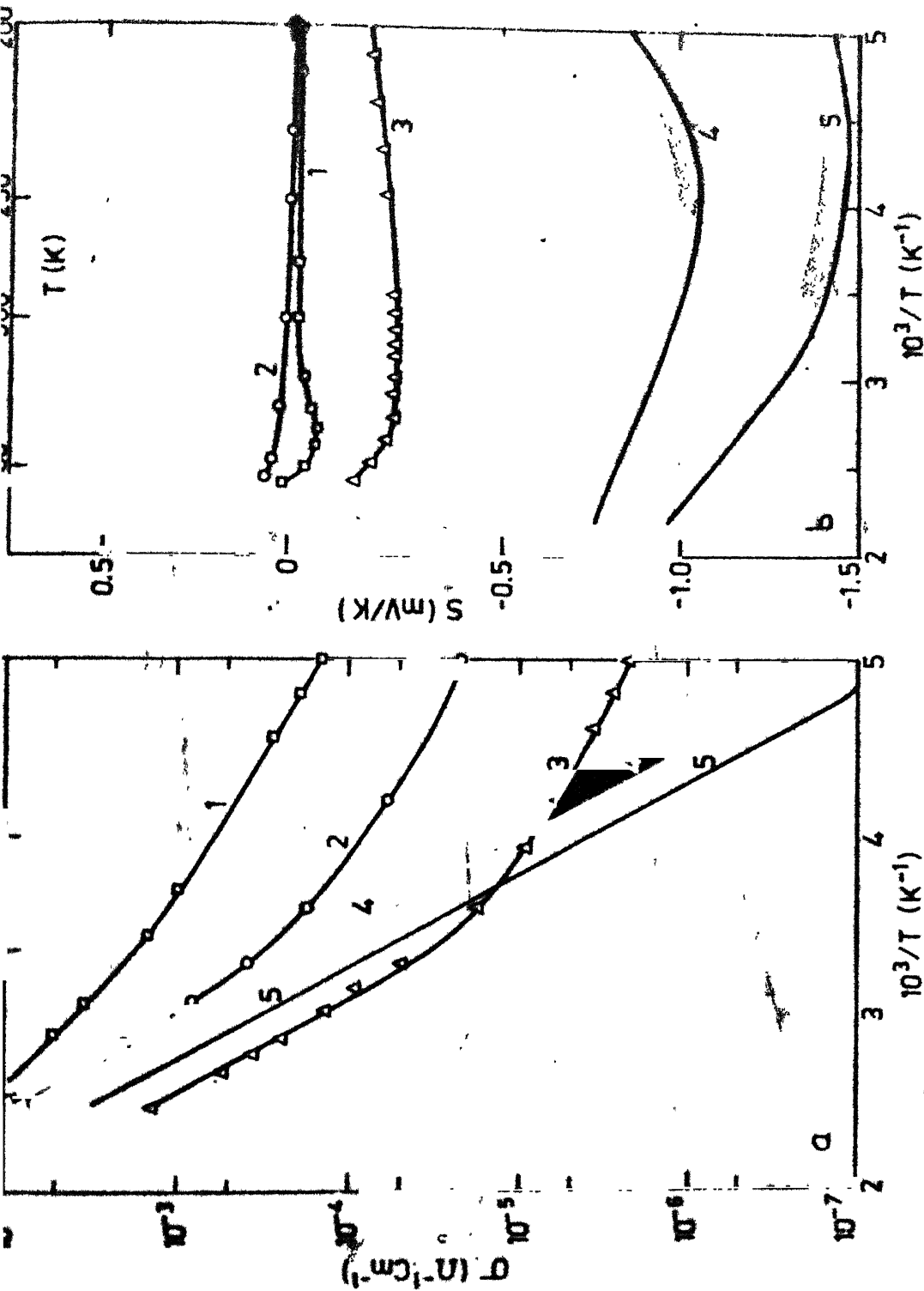


Fig.2.3a : Conductivity (σ) versus $10^3/T$, Curve 1 (evaporated a-Ge, $T_g = 150^\circ\text{C}$), Curve 2 (evaporated a-Ge:Li, $T_g = 150^\circ\text{C}$), Curve 3 (evaporated a-Ge:H, $T_g = 150^\circ\text{C}$), Curve 4 (sputtered a-Ge:H, $T_A = 250^\circ\text{C}$, ref.15), and Curve 5 (glow-discharge a-Ge:H, $T_g = 230^\circ\text{C}$, ref.26).

b : Thermopower (S) versus $10^3/T$ for samples shown in Fig.2.3a.

finally becomes positive at $T=415\text{K}$. This type of behaviour is also observed by others² for slowly evaporated and annealed films of a-Ge. S of a-Ge:H (curve 3 in Fig.(2.2b) is more negative than a-Ge. It is almost constant between temperatures $360\text{K} > T > 290\text{K}$. It shows a negative slope at high temperatures and a positive slope at low temperatures. S for a-Ge:Li (curve 2) is negligible at $T = 300\text{K}$, it is positive for $T > 300\text{K}$ and approaches a small negative value which is equal to that of pure a-Ge at low temperatures.

2.5 Discussion and Conclusions

The electrical conductivity of a-Ge:H is lower by about two orders of magnitude than that of a-Ge and the behaviour of $\sigma(T)$ for the curve 3 is similar to curves 4 and 5 above room temperature. This can be explained by saying that hydrogen saturates dangling bonds in samples evaporated in a partial pressure of hydrogen, just as it does in those sputtered in a partial pressure of hydrogen (curve 4)¹⁵ or made by the glow discharge of germane (curve 5)²⁶. Similarly, the lower value of σ for a-Ge:Li (as compared to evaporated a-Ge) suggests that lithium, having one valence electron, also saturates dangling bonds, just as the hydrogen does.

Increase in negative thermopower upon hydrogenation indicates that the separation between the energy of the conductivity carriers and the Fermi level is more in

a-Ge:H samples than in a-Ge. The behaviour of S for a-Ge:H in high temperature range is similar to that reported by Lewis in sputtered a-Ge:H samples annealed at low temperatures and can be explained in a similar fashion¹⁵. Beyer and Stuke observed similar behaviour in slowly evaporated, and annealed at high temperature ($T_A \sim 400^\circ\text{C}$) a-Ge films²⁷. In all these cases, in the high temperature region, the S vs $1/T$ slope continuously increases as T increases and eventually becomes larger than E_G . It is concluded that the activated conduction is bipolar^{15,27} with the electron contribution dominating the hole contribution in the temperature range studied.

Surprisingly the behaviour of S for a-Ge:Li (curve 2 in Fig.2.3b) is not like that of a-Ge:H. From the conductivity results, one would expect that the curve 2 for S should be in between the curves 1 and 3 in Fig.(2.3b). In a-Ge:Li conduction from positive charges (i.e. holes or Li ions) seems to dominate over electrons at high temperatures. This behaviour of T dependence of S is observed in all samples of a-Ge:Li.

Contribution to σ and S from ionic conduction of Li^+ ions can be shown to be small. It can be calculated approximately from the density of the conducting ions and their average mobility. Though, mobility of Li^+ ions in amorphous lattice will be smaller than in the crystalline lattice, one can take its value in the crystalline lattice

to calculate the maximum possible ionic contribution to conductivity and thermopower. Taking $\mu(\text{Li}^+) \approx 5 \times 10^{-8} \text{ cm}^2/\text{Vs}$ at $T=400\text{K}$, and assuming the density of Li^+ ions of the order of $n \approx 10^{20} \text{ cm}^{-3}$, conductivity due to Li^+ ions $\sigma(\text{Li}^+) = n e \mu \approx 10^{-6} \Omega^{-1} \text{ cm}^{-1}$. Thus at $T = 400\text{K}$, $\sigma_{\text{Li}} / \sigma_e \approx 10^{-3}$. This shows clearly that the contribution of ionic conductivity to the observed σ for a-Ge:Li is negligible. The contribution to S is also negligible. From Eq.(6), the measured thermopower

$$S = \frac{S_e \sigma_e + S_{\text{Li}} \sigma_{\text{Li}}}{\sigma_e + \sigma_{\text{Li}}} \approx S_e + 10^{-3} S_{\text{Li}} \quad (\text{at } 400\text{K})$$

Since the thermopower in ionic conductors is reported to be of the order of a few mV^{29} , the first term dominates. Thus the ionic conduction can not explain the differences in the behaviour of S between a-Ge:Li and a-Ge:H.

The role of hydrogen and lithium complexes in changing the structure of a-Ge lattice may be different. Since Li and hydrogen are present in large amounts (a few at%), instead of ppm in the case of doping etc.), they are expected to change the structure of a-Ge significantly. Li is a larger atom than hydrogen and therefore it is not unreasonable to expect a difference between the structures of a-Ge:H and a-Ge:Li. This may result in a difference in the electronic density of localized states,

and different positions of the Fermi level. This may provide the basis for explaining the observed unexpected behaviour of $S(T)$. A qualitative explanation of the observed behaviour of thermopower near and above the inversion temperature is possible by considering a suitable weighted average of different contributions due to conduction by holes and electrons in the extended states and by hopping in the localised states, given by Eq.(17) and (18). Beyer and Stuke²⁷ have explained their results on as deposited and annealed a-Ge and a-Si films using Eq.(17) and (18). In this analysis S_H is taken from the experimentally observed constant value of S at low temperatures. σ_H is taken to be the value of σ in the temperature region where $T^{-1/4}$ law is observed and is taken equal to the extrapolated $T^{-1/4}$ behaviour at other temperatures. Contribution of holes and electrons to conductivity ($\sigma_n + \sigma_p$) is separated by fitting the thermopower curves. A good fit to their observed data is obtained by treating constants A_n and A_p in Eq.(18) as adjustable parameters. However, the required values of the various parameters involved are not unique and are different for films of the same material, deposited with varying deposition parameters. This uncertainty makes the analysis somewhat less satisfying and prevents one to draw any quantitative conclusions.

The straight line behaviour of σ vs $1/T$ for sputtered and glow-discharge produced a-Ge:H sample is

attributable to the conduction via extended states. For the sputtered sample, $E_{\sigma} = 0.39$ eV and $E_s = 0.18$ eV. Lewis¹⁵ assigned this difference in E_{σ} and E_s to the small polaron hopping. According to him this process rather than conduction by hopping in the localized states in the band tails is more likely resulting in a thermally activated mobility ($E_{\mu} = E_{\sigma} - E_s \simeq 0.2$ eV) in sputtered a-Ge:H. For the glow-discharge sample, the activation energy of the conductivity is equal to the gradient of the thermopower versus $1/T$ graph above $T = 300$ K. From this, Jones et.al.²⁶ concluded that the transport above 300K takes place in the extended electron states (Eq.(19) and (20)). They explained the low temperature data by NNH in the localized states lying about 0.25 eV below E_c (Eq.10)²⁶.

To explain the constant value of S for a-Ge at low temperatures, various interpretations have been given. For VRH near the Fermi level, the magnitude and sign of S will depend upon the shape of $g(E)$. S is expected to be zero or very small for symmetrical distribution of density of states in the mobility gap. For an assymetrical density of states curve with respect to the Fermi level, the sign of S depends on the sign of $\frac{\partial g(E)}{\partial E}$ and is negative when $g(E)$ decreases with energy. Expected behaviour of S , for VRH should be temperature dependent, see Eq.(16), but S is constant, as also observed by many other workers³⁰. For VRH σ is proportional to $1/T^{1/4}$ (Eq.12). Fig.(24) shows σ versus

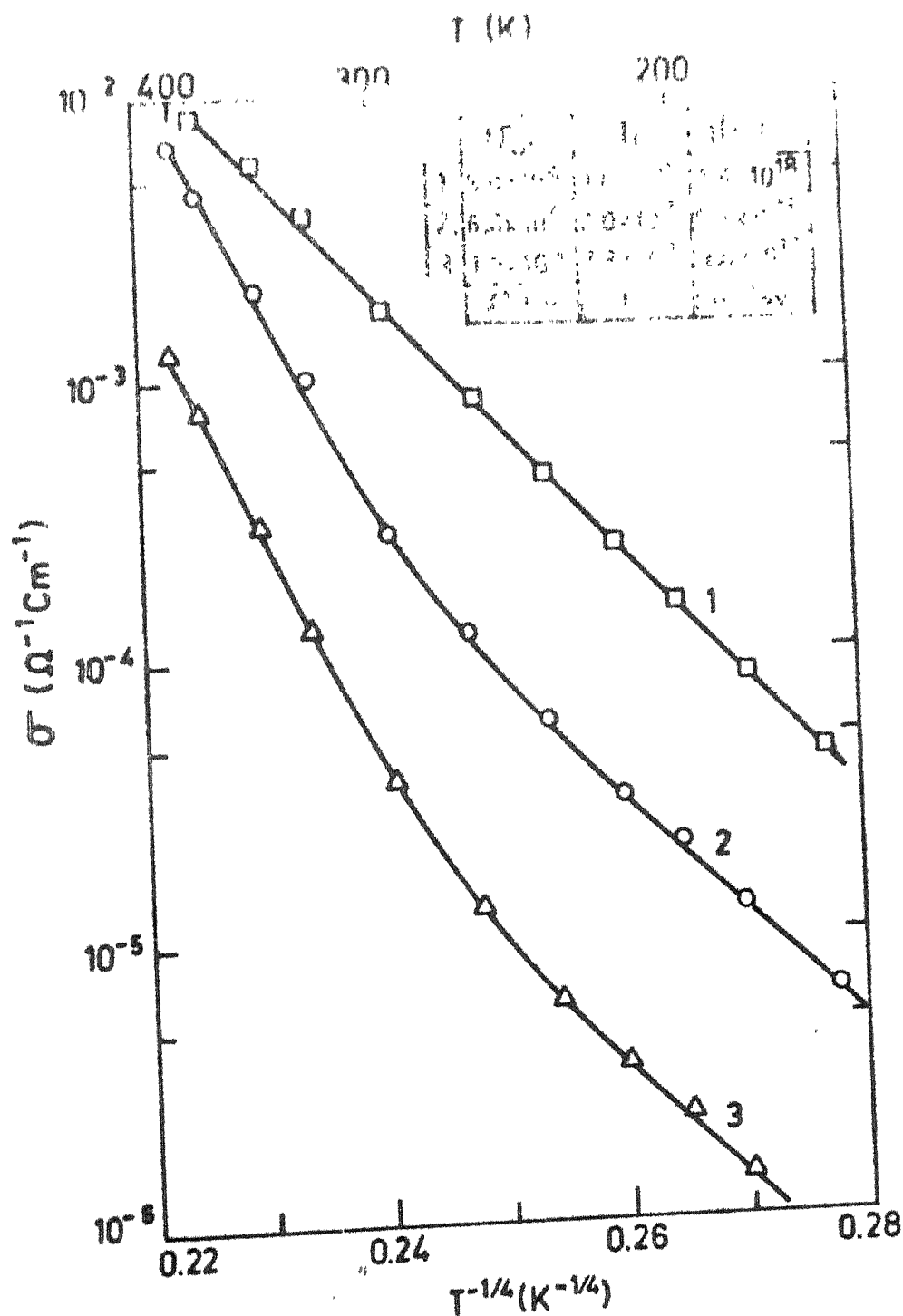


Fig. 2.4 : Conductivity (σ) versus $T^{-1/4}$, Curve 1 (evaporated a-Ge), Curve 2 (evaporated a-Ge:Li) and Curve 3 (evaporated, a-Ge:H).

$1/T^{1/4}$ for a-Ge, a-Ge:Li and a-Ge:H (curves 1,2 and 3 respectively). Curve 1 is a straight line in the range of the temperature of study. Curves 2 and 3 show $T^{-1/4}$ behaviour below $T = 250\text{K}$. Values of the prefactor σ_{OH} , constant T_0 , and $g(E_f)$ calculated using the measured slope T_0 (Eq.14) are listed in a Table given in Fig.(2.4). The slope T_0 upon hydrogenation and lithium diffusion remains almost constant (within a factor of 5), but the intercept at $T = \infty$ (σ_{OH}) decreases by about four orders of magnitude. Looking at the dependence of σ_{OH} and T_0 on $g(E_f)$, (Eqs. 13 and 14), this combination is not expected.

Similar results were observed by Lewis¹⁵ on sputtered hydrogenated samples having different concentration of hydrogen. In addition the value of $g(E_f)$ can also be calculated using Eq.(13) from the measured σ_{OH} . However, the calculated values are too large to be acceptable, as has been reported by others as well³¹. The difficulty with σ_{OH} may be related to one or more of the following points.

- (i) Whereas the slope T_0 can be determined fairly accurately, the value of σ_{OH} may have large errors because it is the value of the intercept at $T = \infty$.
- (ii) The expression of σ_{OH} is different as obtained from percolation and Mott's theory whereas T_0 expression is almost the same³.

(iii) The fit to the $T^{1/4}$ law is merely an accident and a different explanation is necessary.

Lewis¹⁵ explained the constant value of S for a-Ge considering NNH in a narrow thermally isolated band near the Fermi level rather than VRH. The expressions for σ and S are given by¹⁵

$$\sigma(T) = \nu R^2 \rho(1-\rho) e^{-2\alpha R} e^2 f(T)/6 kT \quad (A)$$

and

$$S(T) = -(k/e) \ln[(1-\rho)/\rho\rho] \quad (B)$$

where R is the average hopping distance, ρ is the temperature independent fractional occupancy of the band, ρ is the electron degeneracy factor and $f(T)$ depends on the dynamics of the electron-phonon interaction. The exact form of $f(T)$ is a complicated expression resulting from a collection of hopping rates³². Since the temperature dependence of $f(T)$ is not known with any certainty, from the theory, the observed T dependence of $f(T)$ is used by Lewis to infer that $\ln(f/T) \propto T^{-3/8}$. Further, since ρ is independent in this case, Eq.(B) implies that S should be independent of temperature, as observed.

In above discussion, it has been assumed that the amorphous films are homogeneous. But there are many experimental evidences, which show that these films are heterogeneous⁷. These films have a microscopic closed

network of voids⁷. It is likely that at the surfaces of these voids some band bending occurs and this will lead to potential fluctuations⁷. Even without microscopic voids, charge and potential fluctuations are expected to result from variations in density and composition. A quantitative analysis of experimental results is not yet possible using heterogeneous model.

In conclusion, lithium diffused and hydrogenated ^{to} a-Ge appear/have a large density of localized states and are not photoconducting, in contrast with the hydrogenated a-Si:H. The knowledge of the distribution of density of states and the position of the Fermi-level in the mobility gap, along with the mode of conduction as a function of temperature, suffices one to predict $S(T)$ and $\sigma(T)$ for a homogeneous a-semiconductor. However, since none of these are known in a-Ge (pure, hydrogenated or lithium diffused) with any confidence. The number of parameters become too large to make any quantitative predictions. Further, in reality these films are heterogeneous and a quantitative analysis for a heterogeneous system does not exist.

REFERENCES

1. A.J.Lewis, G.A.N.Connell, W. Paul, J.R.Pawlik and R.J.Temkin, in Tetrahedrally Bonded Amorphous Semiconductors, edited by M.H.Brodsky and W.Brenig (Taylor and Francis, London, 1974), p. 335.
2. S.Kumar and S.C.Agarwal, in Proc. of Symposium on Non-cryst. Solids, edited by S.C.Agarwal, I.I.T. Kanpur (1980).
3. N.F.Mott and E.A.Davis, Electronic Processes in Non-crystalline Materials, (Clarendon Press, Oxford, 1979).
4. N.F.Mott, Adv. Phys. 16, 49 (1967).
5. H.Fritzsche, Solid State Commun. 2, 1813 (1971).
6. D.K.C.MacDonald, Thermoelectricity (John Wiley & Sons, New York, 1962).
7. H.Fritzsche in Amorphous and Liquid Semiconductors, ed. J.Tauc (Plenum Press, New York, 1974).
8. A.Miller and E.Abrahams, Phys. Rev. 120, 745 (1960).
9. N.F.Mott, Philos. Mag. 19, 835 (1969).
10. P.Nagels, in Amorphous Semiconductors, edited by M.H.Brodsky (Springer Verlag, New York, 1979).
11. V.Ambegoakar, B.I.Halperin and J.S.Langer, Phys. Rev. B4, 2612 (1971).
12. M.Cutler and N.F.Mott, Phys. Rev. 181, 1336 (1969).
13. P.Nagels, M.Rotti and R.Gevers J. Non Cryst. Solids, 59 & 60, 65 (1983).
14. D.Emin in Electronic and Structural Properties of Amorphous Semiconductors: edited by P.G.LeComber and J.Mort (Academic Press, London 1973).
15. A.J.Lewis, Phys. Rev. B14, 658 (1976).
16. D.I.Jones, P.G.LeComber and W.E.Spear, Phil. Mag. B41, 439 (1980).

17. W.Beyer, A.Medeisis and H.Mell, Commun. Phys. 2, 121 (1977).
18. P.G.LeComber and W.E.Spear, Phys. Rev. Lett. 25, 509 (1970); D.I.Jones, P.G.LeComber and W.E.Spear; Phil. Mag. 36, 541 (1977).
19. H.Fritzsche, Solar Energy Materials, 3, 447 (1980).
20. W.Beyer and H.Overhof, Solid State Commun. 31, 1 (1979).
21. W.Beyer and H.Overhof in 'Hydrogenated Amorphous Silicon; edited by R.K.Willardson and A.G.Beer (Academic Press, New York, 1984), Vol. 21C.
22. Vijay Kumar, M.Tech. Thesis, I.I.T. Kanpur (1980).
23. Aruna Rajvanshi, M.Phil. Thesis, I.I.T. Kanpur (1980).
24. L.Maissel and P.Glang; Handbook of Thin Film Technology (McGraw Hill, New York, 1970).
25. D.White, K.S.Seshadry, D.F.Dever, D.E. Mann and M.J.Linevsky, J. Chem. Phys. 39, 2463 (1963).
26. D.I.Jones, W.E.Spear and P.G.LeComber, J. Non. Cryst. Solids, 20, 259 (1976).
27. W.Beyer and J.Stuke in: Proc. 5th International Conference on Amorphous and Liquid Semiconductors, Garmisch-Partenkirchen, edited by J.Stuke and W.Brenig (Taylor and Francis, London, 1974), p.251.
28. S.M.Sze, Physics of Semiconductor Devices, (Wiley Eastern Limited, New Delhi, 1981).
29. K.Shahi, Phys. Stat. Sol. (a) 41, 11 (1977).
30. H.Mell, (in Proc. of Conference given in Ref.27), p.203.
31. S.C.Agarwal, S.Guha and K.L.Narsimhan, J. Non. Cryst. Solids, 18, 429 (1975).
32. A.J.Lewis, Phys. Rev. B13, 2565 (1976).

CHAPTER 3

UNDOPED AND LITHIUM DOPED a-Si:H

This chapter is divided into two parts. In part A, conductivity and thermopower study of undoped and lithium doped a-Si:H is given and in part B gradient doping of lithium is studied.

3A: Conductivity and Thermopower

3A.1 Introduction

The density of localized states at the Fermi level in hydrogenated amorphous silicon (a-Si:H, $g(E_f) \sim 10^{17} \text{ cm}^{-3} \text{ eV}^{-1}$) is much less in comparison with hydrogenated a-Ge ($g(E_f) \sim 10^{18} \text{ cm}^{-3} \text{ eV}^{-1}$)¹. This difference is probably because Ge-H bond is less strong with respect to its competitors (Ge-Ge bonds) in a growing film, than is the Si-H bond with respect to its competitors². Because of the low density of states, a-Si:H films can be doped n-type or p-type³.

In this chapter, we present our measurements of conductivity (σ) and thermopower (S) in undoped and Li doped a-Si:H and compare them with those available in the literature, on evaporated a-Si as well as a-Si:H.

In the next section, the d.c. glow discharge system used to prepare a-Si:H films is described.

Interstitial doping of lithium is achieved by thermal diffusion. In section 3A.3, transport properties of a-Si:H and unhydrogenated a-Si⁴ are compared. In the same section, the effect of light soaking on the transport properties of undoped and lithium doped a-Si:H is described. In section 3.4, results are discussed with the available theoretical models and it is shown that these models are not adequate to explain completely the transport properties of samples in the light soaked and heat-dried states. It seems that the potential fluctuations caused by heterogeneities and charged defect centers modify the conduction processes.

3A.2 Preparation and Characterization

a-Si:H films are prepared by d.c. glow discharge of a mixture of 3% SiH₄+ 97% argon⁵. The design of the discharge chamber is shown in Fig.3.1. An aluminium plate of 10 cm. diameter is used as the anode and an aluminium grid as the cathode. The substrates (usually 7059 glass, having predeposited nichrome contacts) are kept about 1 cm away from the grid on a stainless steel plate, which can be heated with the help of an internal heater.

The typical deposition parameters are

Substrate temperature	= 580K
Pressure	= 1 Torr

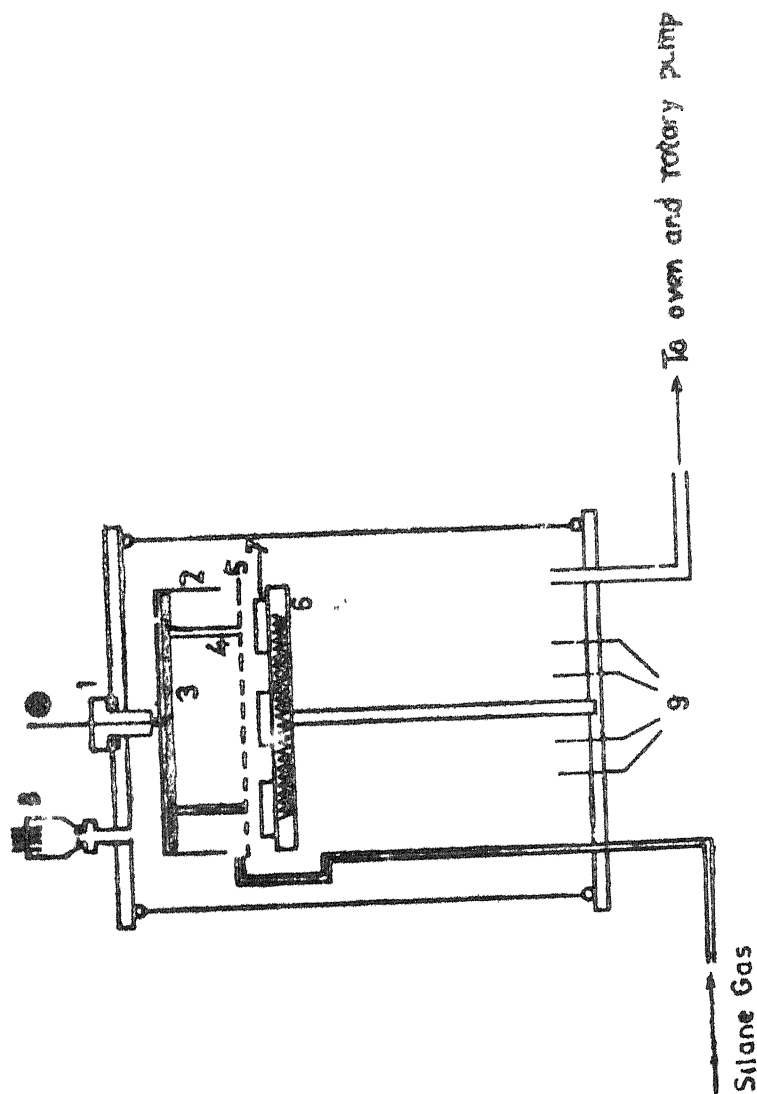


Fig. 3.1 : d.c. glow-discharge system, 1. High tension feed, 2. Cathode, 3. Anode, 4. Ceramic post, 5. Electrical feed through, 6. Steel plate containing heater, 7. Substrates, 8. Electrode plate jaws, 9. Electrical feed through

Distance between anode and the screen	= 2.5 cm
Power density	= 40 m W/cm ²
Deposition rate	= 1 Å/sec.

The films are characterised⁶ by electron microscopy and IR spectroscopy by using carbon coated copper grids and c-Si wafers respectively as the substrates. They are amorphous (Fig.3.2) and contain hydrogen (Fig.3.3). The identification of the various modes of vibration is also shown in Fig.3.3 and is in agreement with the literature⁷.

For doping with lithium, undoped a-Si:H films are kept in a vacuum coating unit and a layer of 100-200 Å thick Li is deposited as described in Chapter 2. The substrate temperature is ~200°C at the time of evaporation, and the films are allowed to anneal at this temperature for 8 hrs after evaporation of Li. Samples are etched by 10% HF to remove excess Li at the surface and finally cleaned with deionized water and vapours of isopropyl alcohol. Roughly estimating from the thickness of Li layer, we get about 4 at% of Li in a-Si:H films of 1 μm thickness. These films are heavily doped and give an increase in conductivity by a factor of 10^5 at room temperature. To get a less amount of Li in a-Si:H, Li is deposited on substrates kept at $T_s = 100^\circ\text{C}$ for one hour. Samples after etching with HF and cleaning with deionized water and vapors of isopropyl alcohol are again annealed at 200°C for two hours. In these lightly doped samples, conductivity increases by a

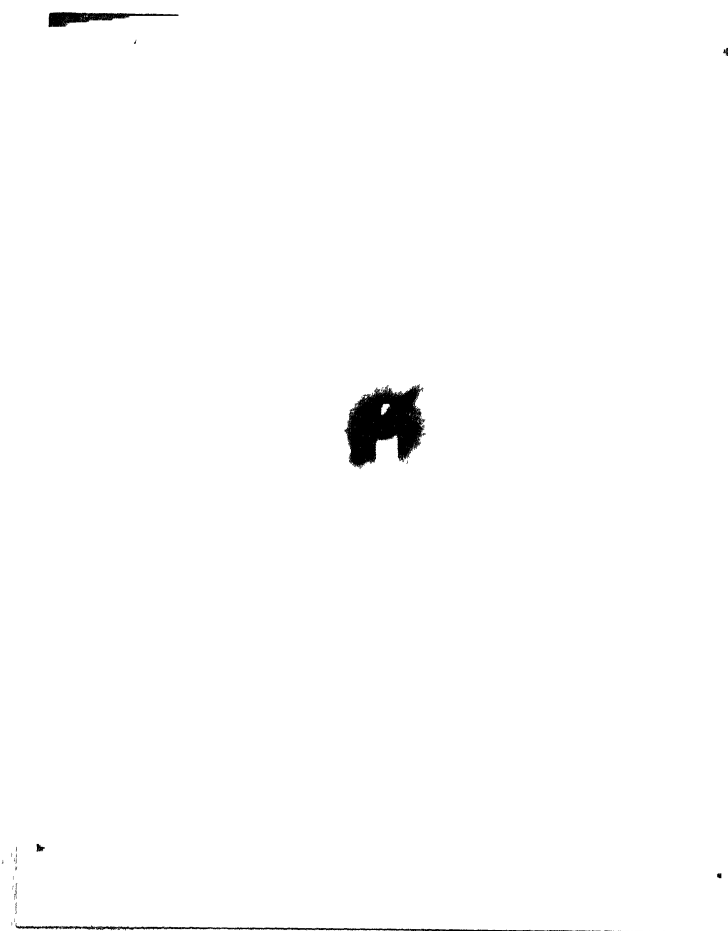


Fig. 3.2 : Electron diffraction micrograph of
a-Si:H deposited at $T_s = 580\text{K}$

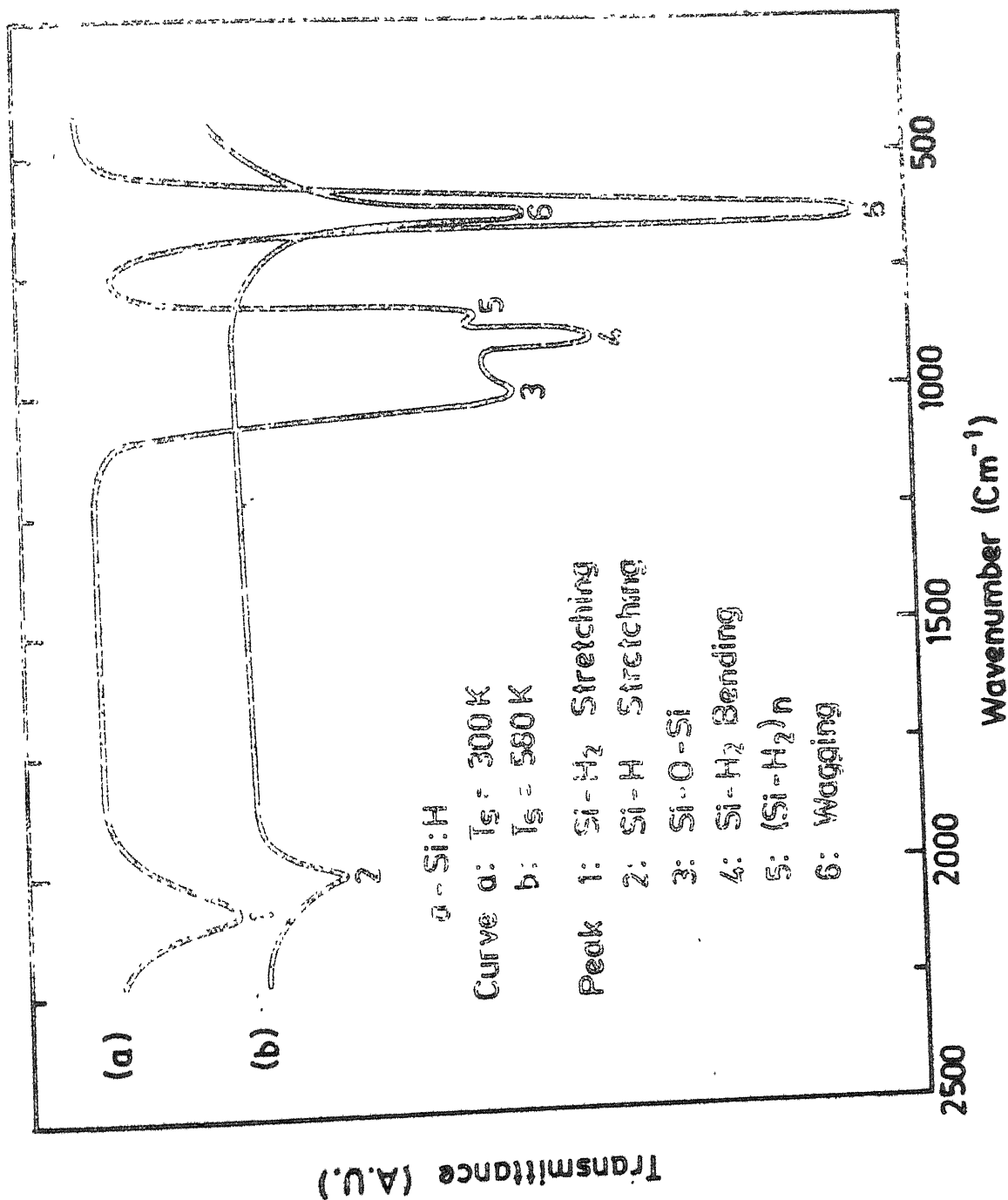


Fig. 3.3 : I-R spectra of a-Si:H, a : sample deposited at $T_s = 300\text{K}$
 b : sample deposited at $T_s = 580\text{K}$

factor 10^2 at room temperature. On comparing with Beyer and Fischer results⁸, rough estimation of Li concentration in these (lightly doped) films is about 100 ppm. Possibility of thermal diffusion of Li at low temperatures shows that it goes as interstitial impurity in a-Si:H lattice⁸.

3A.3 Experimental Results

Conductivity (σ) and thermopower (S) measurements are done on Li doped as well as undoped a-Si:H films using the cryostat described earlier (see section 2.2b). It is difficult to measure S for samples having resistance more than 10^{10} Ω . Therefore, S measurements on undoped samples are possible only at high temperatures ($T > 380K$). However, on highly doped samples, it is possible to measure ' S ' in the full temperature range of study ($450K > T > 200K$).

a) Effect of Hydrogenation:

Study of σ and S for evaporated unhydrogenated a-Si⁴ and hydrogenated a-Si:H have been done by many workers^{8,9,10}. It has been shown that the properties of a-Si:H prepared by glow-discharge are very similar to those prepared by sputtering in hydrogen atmosphere¹⁰.

To compare σ and S for hydrogenated a-Si:H with evaporated a-Si, results published on a-Si by Beyer and Stuke⁴ are used. Fig.(3.4a) and (3.4b) show σ and S versus $1/T$ respectively. In Fig.(3.4a), curve 1 is for a-Si:H

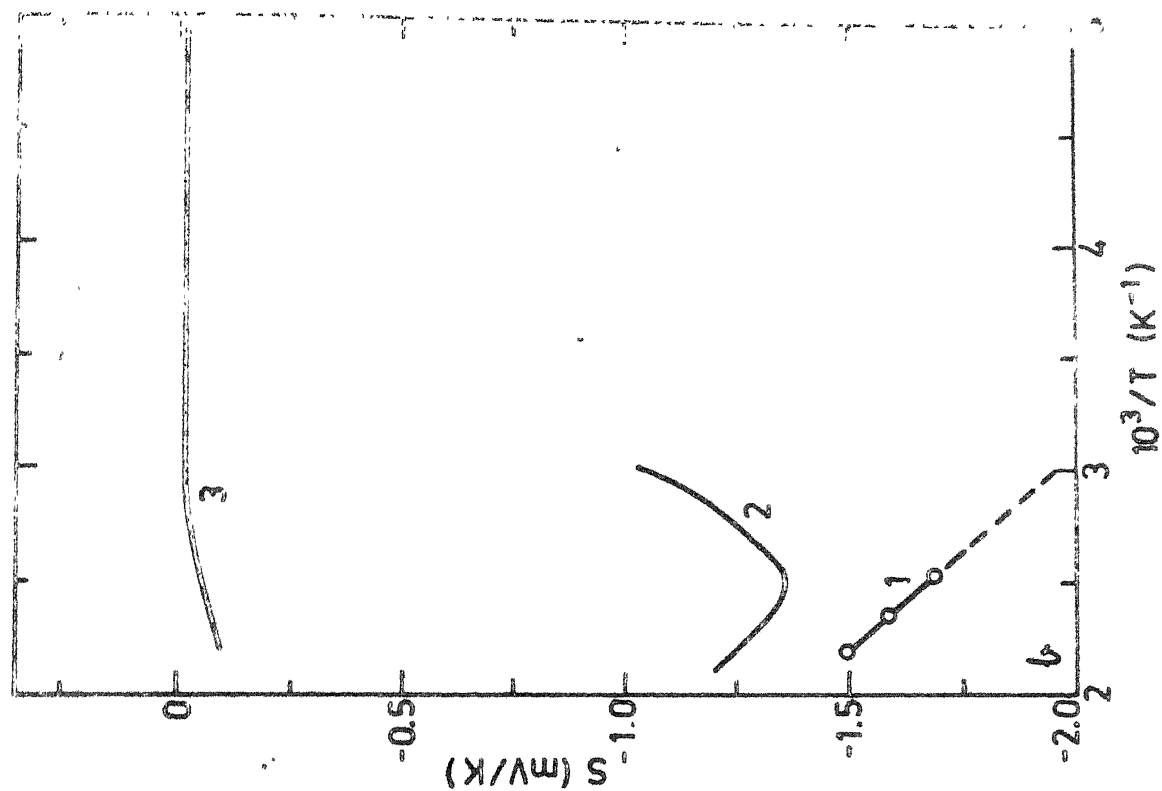
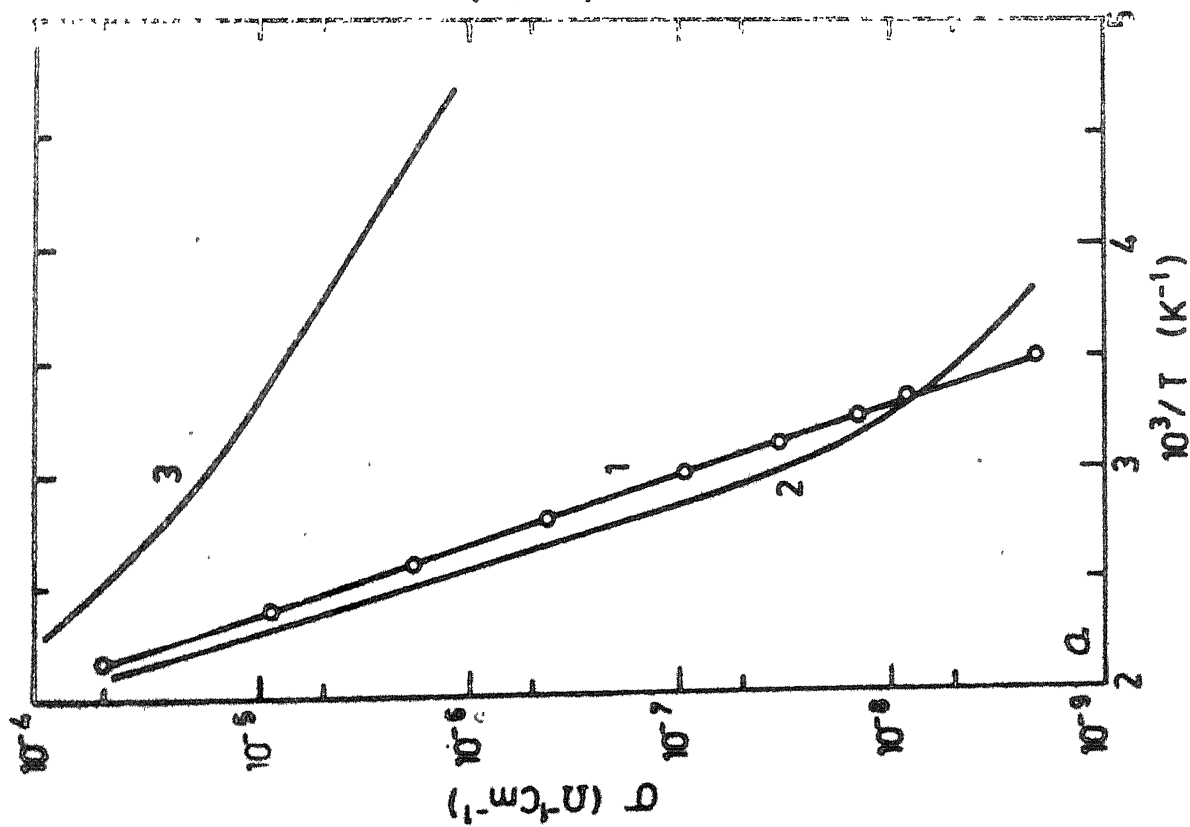


Fig. 3.4a : Conductivity (σ) versus $1/T$; (3.4b) Thermopower (S) versus $1/T$, Curve 1. Undoped a-Si:H ($T_g = 300^\circ\text{C}$), Curve 2. Evaporated a-Si ($T_A = 290^\circ\text{C}$), Curve 3. Evaporated a-Si ($T_A = 310^\circ\text{C}$). Curves 2 and 3 are from ref.4.

deposited at $T_s = 300^\circ\text{C}$ and with deposition rate $r = 1\text{\AA}/\text{S}$. Curve 2 is for evaporated a-Si deposited with $r = 2\text{\AA}/\text{S}$ at $T_s = 230^\circ\text{C}$ and annealed at $T_A = 290^\circ\text{C}$. Curve 3 is evaporated a-Si with $r = 16\text{\AA}/\text{S}$, $T_s = 230^\circ\text{C}$ and annealed at $T_A = 310^\circ\text{C}$. Among the reported results of many samples⁴, these two samples are chosen for comparison because their annealing temperatures are close to the deposition temperature of a-Si:H.

σ versus $1/T$ curves (1) and (2) are linear and quite close to each other above $T = 300\text{K}$. Activation energy E_σ for curve 1 is 0.65 eV and for curve 2 it is 0.75 eV. Curve 2 deviates from linearity below $T = 300\text{K}$, while curve 1 remains linear. σ for a-Si, evaporated at higher rate, (curve 3) is completely different in comparison with a-Si:H (curve 1) and slow deposited a-Si (curve 2). Curve 3 for σ does not show a single activation energy for conductivity.

Behaviour of S is completely different in all three samples. S for all samples is negative in the range of temperature of measurements. In Fig.(3.4b), curve 1, for a-Si:H, is linear with a slope $E_s = 0.62\text{ eV}$. This is in agreement with the reported behaviour^{8,9,10}. The magnitude of S for a-Si(2) is maximum at $T = 400\text{K}$. For higher temperatures $T > 400\text{K}$, it shows single slope $E_s = 0.60\text{ eV}$. For $T < 400\text{K}$, its magnitude decreases with

continuously varying slope. At very low temperatures, measurements of S are not possible⁴. Behaviour of S for evaporated a-Si(3) is similar to that of a-Ge. It has a small negative constant value for $T > 360K$ and its magnitude increases at higher temperatures.

The negative S and almost the same values of E_C (0.65 eV) and E_S (0.62 eV) for a-Si:H show that the conduction is due to electrons in the extended states⁹. Results of σ and S for evaporated a-Si are explained by Beyer and Stuke⁴ in a fashion similar to the explanation given for evaporated a-Ge. It involves assuming a bipolar conduction in the extended states at high temperatures and hopping conduction in the localized states at low temperatures, (Eqs.(17) and (18) in sec.(2.2)).

The difference between the results of evaporated Si and glow discharge deposited a-Si:H can be interpreted in terms of the presence of hydrogen in the latter. Hydrogen is known to saturate dangling bonds³.

The difference in evaporated a-Si(2) and (3) was attributed to differences in deposition parameters. The main difference between deposition parameters for these two samples is the rate of deposition. It is reported that a-Si films have a strong affinity to oxygen¹¹ and the amount of oxygen incorporated depends upon the rate of deposition¹¹. Films prepared with $r = 2A^\circ/S$ contain about

10% oxygen. Oxygen may also saturate dangling bonds¹¹.

However the differences between the a-Si:H and evaporated a-Si containing oxygen, show that the role played by hydrogen and oxygen must be quite different. The density of states in the best evaporated a-Si (annealed, oxygen incorporated, but not hydrogenated) is much larger than a-Si:H. Therefore it appears that hydrogen reduces the density of states not only by saturating the dangling bonds, but also by reducing strains in a-Si:H lattice¹¹.

3A.3b. Effect of Light Soaking on σ and S in the Doped and Li doped a-Si:H

Light soaking (Staebler-Wronski effect)¹² changes the conductivity and thermopower of the undoped and doped a-Si:H samples. The conductivity may increase or decrease after S-W, and has been roughly correlated with the position of the Fermi level in the mobility gap¹³. Heat-drying (annealing at 150°C for two hours) brings back the original values of conductivity and thermopower. Annealing below 120°C for 2 hrs does not change the light soaked state. Annealing at temperatures between 120°C to 150°C is slow and it takes about 2 hours at 150°C to bring a light soaked sample back to its original state. This is in agreement with Jang et.al.¹⁴. They reported annealing temperatures above 130°C for lightly phosphorus doped and undoped a-Si:H samples.

In this section, conductivity and thermopower results for undoped and doped samples in heat dried as well as light soaked states are given in Fig.(3.5) giving σ vs. $1/T$ for an undoped a-Si-H sample in annealed and light soaked states. Heat-dried samples are represented by the state A and light soaked samples by the state B. White light (60 mW/cm^2 from tungsten lamp) for 10 hours is used for light soaking. At $T = 295\text{K}$, in state A, $\sigma(A) = 8.5 \times 10^{-9} \text{ } \Omega^{-1} \text{ cm}^{-1}$ and reduces to $\sigma(B) = 2 \times 10^{-9} \text{ } \Omega^{-1} \text{ cm}^{-1}$ in state B. Sample in state B is heated and σ is measured at different temperatures. At 150°C , initially $\sigma(B) = 10^{-5} \text{ } \Omega^{-1} \text{ cm}^{-1}$, and increases to $\sigma(A) = 1.7 \times 10^{-5} \text{ } \Omega^{-1} \text{ cm}^{-1}$ after annealing for 2 hours at this temperature (heat drying). In heat-dried state, the sample follows the curve A while heating and cooling. In state A, $E_g = 0.65 \text{ eV}$ and $\sigma_0 = 8 \times 10^2 \text{ } \Omega^{-1} \text{ cm}^{-1}$ and in state B, $E_g = 0.78 \text{ eV}$ and $\sigma_0 = 1.4 \times 10^4 \text{ } \Omega^{-1} \text{ cm}^{-1}$. These results are in qualitative agreement with the literature. Although the magnitude of the change in σ and E_g from state A to state B is smaller than reported by Stasblier and Wronski¹², it is about the same as reported by other workers¹⁵. Figs.(3.6a) and (3.6b) show $\sigma(T)$ and $S(T)$ respectively, for lithium doped samples in the heat-dried state (A) and in the light soaked state (B). Results for the undoped sample, in state A, are shown by curves U(A) in Fig.3.6, for comparison. No measurements of S in state B for this sample are shown, since its resistance is too high to make these measurements for $T > 390\text{K}$, and since

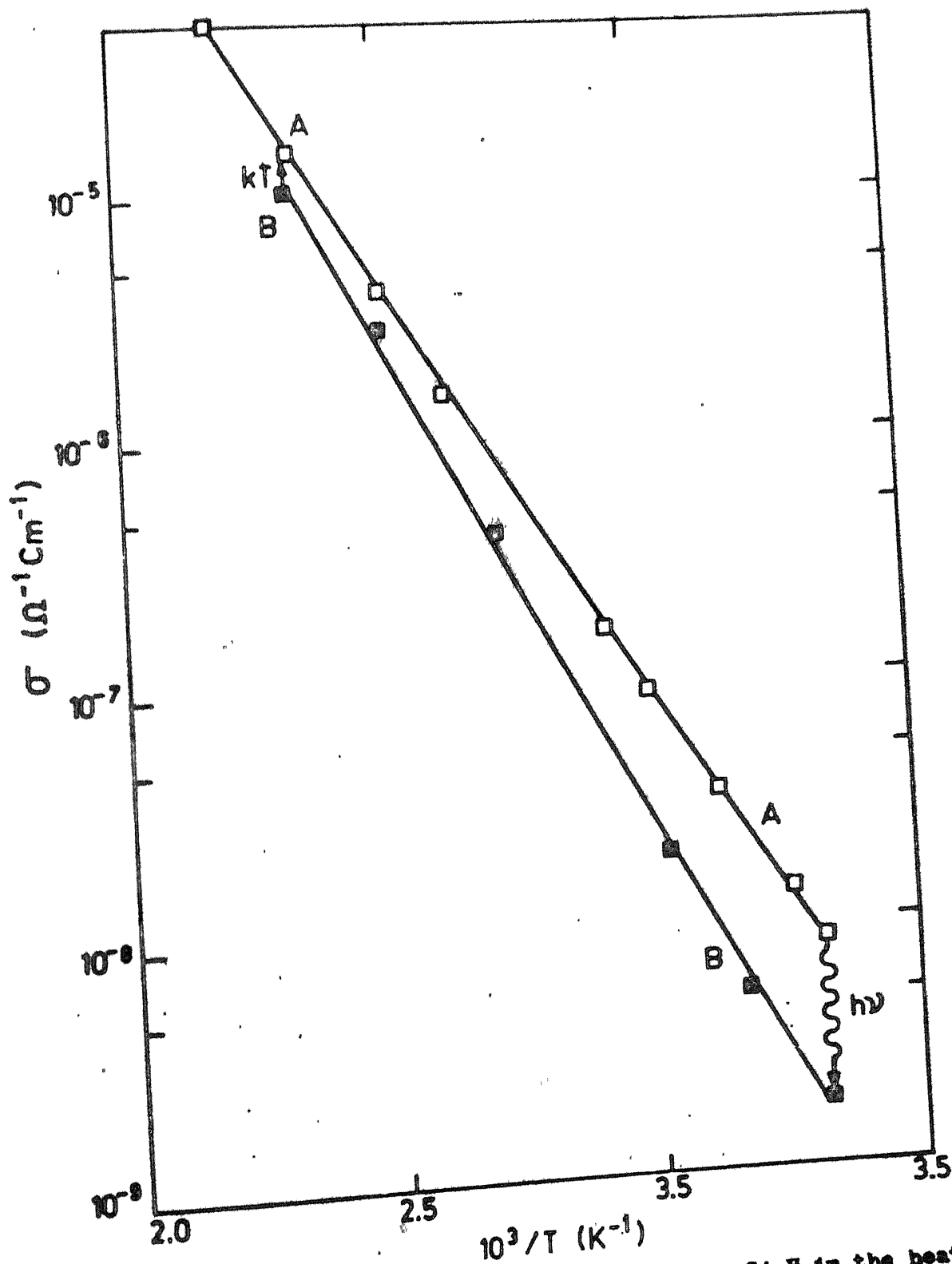


Fig.3.5 : Conductivity (σ) versus $1/T$ for undoped a-Si:H in the heat-dried state (A) and in light soaked state (B).

state B starts getting annealed at T higher than 390K. Curves 1(A) and 1(B) are for a lightly doped sample in states A and B respectively. At $T = 295\text{K}$, in state A, $\sigma(A) = 3 \times 10^{-6} \text{ cm}^{-1}$ reduces to $2 \times 10^{-6} \text{ cm}^{-1}$ after light soaking for ten hours. As the sample in state B starts getting annealed at about 390K, the sample is heated to 370K and then cooled down to room temperature σ and S are measured while cooling and are reported by the closed triangles (curve 1(B)) in Fig.3.6. σ and S measured after heat-drying the sample are given by open triangles (curve 1(A) in Fig.3.6). σ versus $1/T$ curves are straight lines in both states A and B. In state A, $E_{\sigma} = 0.48 \text{ eV}$, and $\sigma_0 = 4.8 \times 10^{21} \text{ cm}^{-1}$. These change to $E_{\sigma} = 0.51 \text{ eV}$ and $\sigma_0 = 1.3 \times 10^{23} \text{ cm}^{-1}$ in state B. Magnitude of S (curve 1(B), Fig.3.6b) reduces after light soaking. In state A, slope of S versus $1/T$ curve changes continuously in the temperature range of measurements. Near $T=340\text{K}$, the slope E_s is about 0.30 eV and increases to $E_s = 0.55 \text{ eV}$ at $T = 400\text{K}$, while (activation energy of conductivity) $E_{\sigma} = 0.48 \text{ eV}$ remains constant in this temperature range.

No change in conductivity of highly doped samples is observed after light soaking. Curve 2 (A,B) in Fig.(3.6a) shows σ for a sample highly doped with Li in states A and B. It shows a kink at $T = 380\text{K}$ for $T < 380\text{K}$, $E_{\sigma} = 0.14 \text{ eV}$ and $\sigma_0 = 1.0 \times 10^{21} \text{ cm}^{-1}$ and for $T > 380\text{K}$, $E_{\sigma} = 0.22 \text{ eV}$ and $\sigma_0 = 6.0 \times 10^{21} \text{ cm}^{-1}$. A kink in σ for heavily doped samples

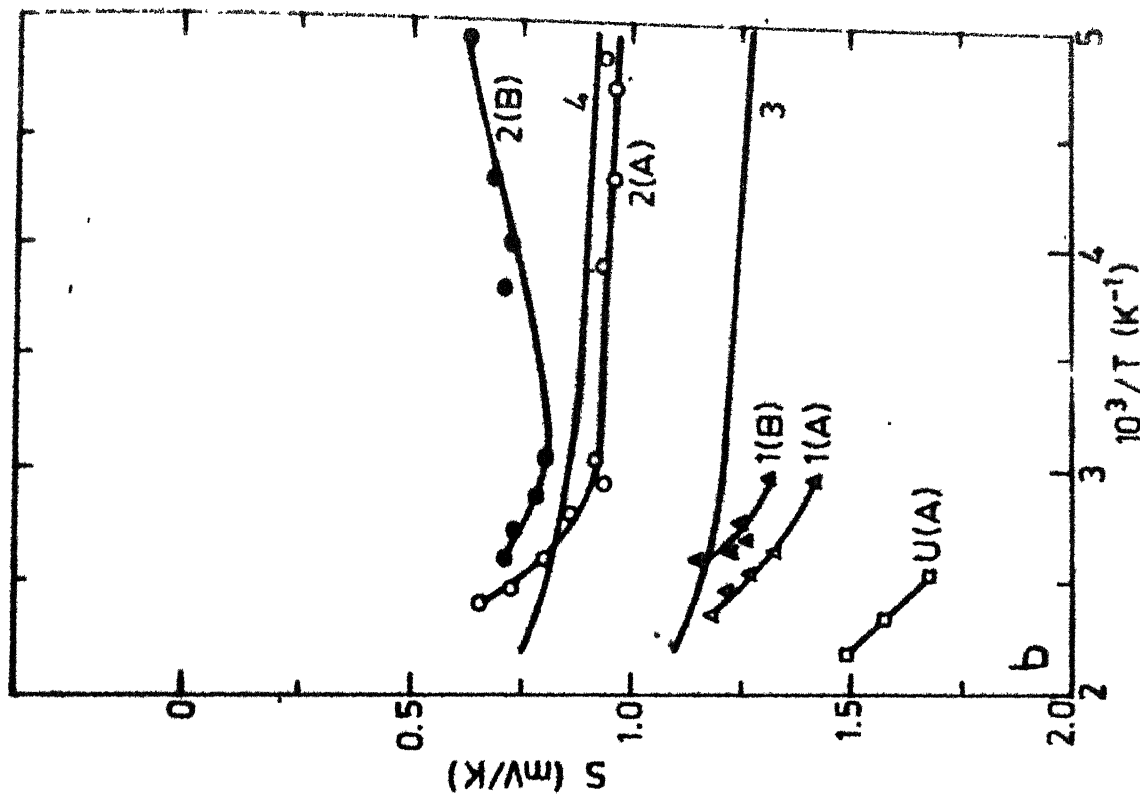
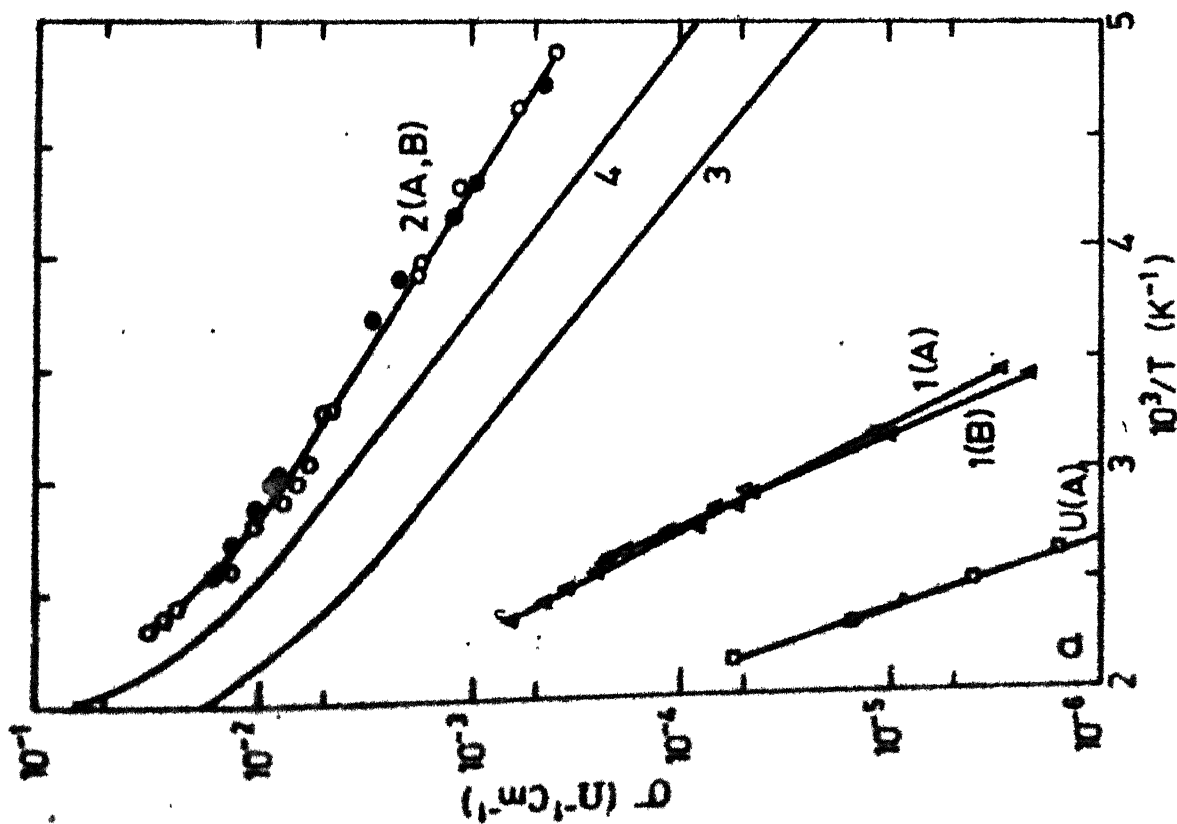


Fig. 3.6a : Conductivity (σ) versus $1/T$ and (3.6b) Thermopower (S) versus $1/T$ in the heat-dried state (A) and light soaked state (B). Curve U, Undoped a-Si:H, Curve 1, Lightly Li doped a-Si:H, Curve 2, Heavily Li doped a-Si:H, Curves 3 and 4 are for Li annealed a-Si:H respectively (ref.8).

(interstitially and substitutionally both) are also observed by other workers^{9,10,16}.

In contrast, however S changes significantly upon light soaking in this sample (curves 2A, 2B in Fig.3.6b). In state A, (curves 2A, in Fig.3.6B), S varies very slowly at low temperatures with $E_s = 0.03$ eV and $E_s = E_\sigma$ by 0.11 eV. Its magnitude decreases with continuously varying slope above room temperature, and $E_s = E_\sigma$ at high temperatures. Magnitude of S decreases upon light-soaking. In state B (curve 2B in Fig.3.6b), $S = -0.81$ mV/K is maximum at $T = 320$ K. It decreases slowly at low temperatures. This behaviour of S in state B (curve 2B) is similar to that of a slowly evaporated and annealed unhydrogenated a-Si (cf. Fig.3.4b). This shows that light soaking in a-Si:H (Li) is creating some defects which are similar to those in unhydrogenated samples.

Bayor and Fischer⁸ have measured σ and S on lithium doped samples. However, no results are available on the effect of light soaking in their samples. For comparison, σ and S for a lithium diffused sample⁸ (annealed at 400°C) are given by curve 3 in Fig.(3.6a) and Fig.(3.6b) respectively. Results for a lithium implanted sample³ (annealed at 300°C) are given by curve 4 in Figs.(3.6a) and (3.6b). T dependence of σ is similar for curves 2(A,B), 3 and 4 in Fig.(3.6a). T dependence of S

for these curves (2A, 3 and 4 in Fig.3.6b) is similar at low temperatures ($T < 300\text{K}$) but is different at high temperatures ($T > 300\text{K}$). In our samples (curve 2A) slope E_S of S versus $1/T$ is negative and increases continuously at high temperatures, and becomes more than E_σ . For curves 3 and 4, $E_S \approx E_\sigma$. The difference in the magnitude of σ and S in heavily lithium doped samples of our lab. and that of Beyer et.al.⁸ may be due to the different substrate temperature T_S and the annealing temperature T_A . T dependence of conductivity of heavily phosphorus doped a-Si:H (not shown here) is the same as that of lithium doped samples^{9,10,16}. The behaviour of S for P doped a-Si:H is similar to Li doped samples at low temperatures but the results obtained at high temperatures differ in different groups^{9,10,16}.

We summarize below the important features of transport in undoped and lithium doped a-Si:H.

1. Thermopower results show that the undoped and doped samples are n-type and lithium acts as an interstitial donor in a-Si:H.
2. With interstitial doping of lithium in a-Si:H, conductivity of a-Si:H can be increased by a factor of 10^5 to 10^6 and E_σ can be varied from 0.65 eV to 0.15 eV. The prefactor σ_0 reduces from about $10^3 \text{ A}^{-1} \text{ cm}^{-1}$ to less than 10^{-1} cm^{-1} upon doping.

3. E_{σ} and E_s are almost same in undoped samples at high temperatures.
4. For lithium doped samples, $E_s \sim E_{\sigma}$ at low temperatures and $E_s \sim E_{\sigma}$ at high temperatures.
5. Light soaking increases E_{σ} and σ_0 for undoped and lightly doped samples. It does not have any effect on conductivity of highly lithium doped a-Si:H samples. However, it reduces the magnitude of thermopower. The behaviour of S for light-soaked, heavily doped samples is similar to that of the unhydrogenated annealed evaporated sample.

3A.4 Discussion

A detailed interpretation of transport properties of a-Si:H presents major fundamental problems with the available information about the localized states in the mobility gap. It is therefore difficult to arrive at definite quantitative conclusions. Among the general aspects which appear to lead invariably to difficulties in interpretation are the following: (i) The temperature dependence of the reference energy levels such as the Fermi level and mobility edges¹³. (ii) Changes in the distribution of density of states by doping and role of added donor or acceptor levels in the hopping transport¹⁶. (iii) The presence of the space-charge regions at the front

surface and at the film-substrate interface and variation of space-charge region with temperature¹³. (iv) Role of the potential fluctuations caused by heterogeneities²³.

(i) Variation of σ_0 with E_σ :

The most important feature of the conductivity data of a-Si:H films is the variation of the conductivity prefactor σ_0 with doping and preparation conditions¹³. This is observed by all workers in glow-discharge a-Si:H¹³ as well as in sputtered a-Si:H¹⁰. From the Kubo-Greenwood formulae for σ_0 , one expects σ_0 to be independent of E_σ ¹¹. Experimentally it is observed that σ_0 is a function of the activation energy E_σ and follows the relation¹⁶

$$\sigma_0 = \sigma_{00} \exp (A E_\sigma) \quad (1)$$

with $\sigma_{00} = 1 \text{ cm}^{-1}$ and $A = 10 \text{ eV}^{-1}$.

This behaviour of σ_0 with E_σ is known as the Meyer Neldel Rule (MNR)¹⁷. This empirical rule is observed in different types of heterogeneous materials¹⁶, but it is not yet fully understood.

Fig.(3.7) shows the variation of σ_0 as a function of E_σ for a-Si:H samples containing different amount of lithium in heat-dried and light soaked states. Triangles in Fig.(3.7) represent σ_0 and E_σ reported by Beyer and Overhof

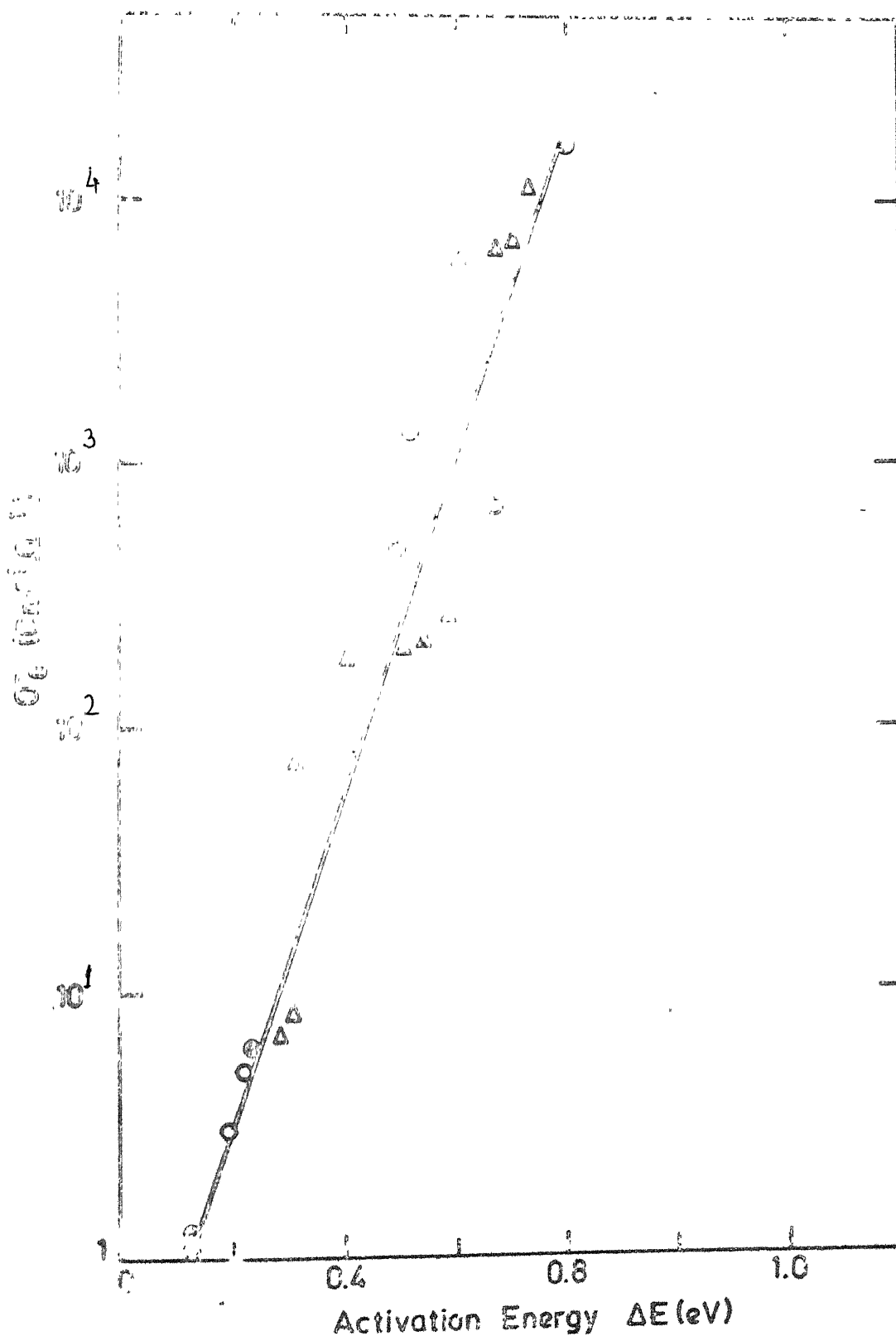


Fig. 3.7 : Conductivity prefactor (σ_0) versus conductivity activation energy (E), open circles are for heat-dried state and closed circles for light soaked state. Triangles are for a-Si:H (L1) samples from ref.16. Open, low temperature range and closed, high temperature range.

for a-Si:H (Li) samples¹⁶. Open triangles are for low temperature region and closed triangles for high temperature region.¹⁶ σ_0 versus E_σ curve follows Eq.(1) with $A = 15 \text{ eV}^{-1}$. This value of A compares well with the published value for n-type and p-type doped samples¹³. In literature, value of A between 10 to 35 cm^{-1} is reported^{13,16}.

Beyer and Overhof¹⁶ have shown that, if we consider the function $Q(T) = \ln \sigma + \frac{es}{kT}$ (see section 2.2), then the films are found to be rather insensitive to doping and to the preparation conditions. According to this, the wide variation of σ_0 must be ascribed to effects that do not alter the transport path.

Jones et.al.¹⁹ calculated the effect of statistical shift of the Fermi level with temperature on σ_0 . They calculated the temperature coefficient, δ , (Eq.21) section 2.2) using the density of states curve²⁰ obtained by field effect experiment on undoped a-Si:H and found that δ is negligible for $E_\sigma < 0.4 \text{ eV}$. But the experimentally observed decrease¹⁹ in σ_0 by about four orders of magnitude in this range of E_σ is difficult to explain. For doped samples, basic problem in this analysis is that the distribution of density of states may change with doping¹⁶.

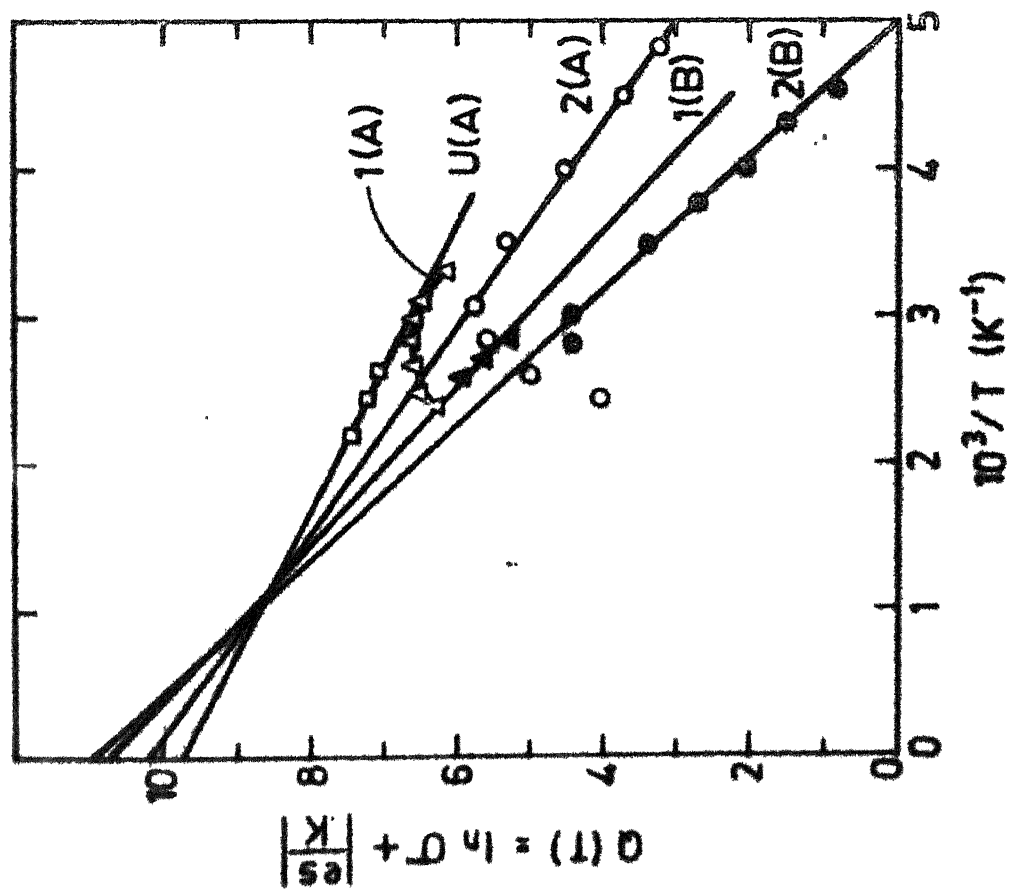
Beyer et.al.¹⁸ have observed for a variety of doped and undoped a-Si:H samples that $Q(T)$ versus $1/T$ curves (Eq.2.3, section 2.1) are straight lines in $150 < T < 550 \text{ K}$

temperature range with $0.05 \text{ eV} < E_{\mu} < 0.25 \text{ eV}$ and $Q_0 \approx 10$. The difference in E_{σ} and E_s is attributed to the activation energy of the mobility.

The function $Q(T)$ is calculated for lithium doped and undoped samples. $Q(T)$ versus $1/T$ curves are shown in Fig.(3.8). Curves U(A), 1(A) and 2(A) are for undoped lightly doped and heavily doped samples respectively in the heat dried state. Curves 1(B) and 2(B) are for lightly and heavily doped samples respectively in the light soaked state. Curves U(A) and 1(B) are linear within the small temperature range of measurements. Curves 1(A), 2(A) and 2(B) are not linear for $T > 330\text{K}$. Below $T = 330\text{K}$, all of them are linear, although because of limited data it can not be said so for curve 1(A) with certainty.

From the linear region of these curves, slopes (E_{μ}) and intercept with $1/T = 0$ axis (Q_0) are calculated and are listed in a Table given in Fig.(3.8). We see that the value of Q_0 is same (about 10) for these samples as expected. However, there is a variation in E_{μ} between 0.035 to 0.25 eV. These observations are in agreement with Beyer and Overhof results¹⁶.

The deviations from linearity, of curves 1(A), 2(A) and 2(B), at high temperatures are indicative of the presence of more than one transport mechanism¹⁶. Change in the sign of $Q(T)$ versus $1/T$ slope may be due to bipolar



Sample	$E_{\mu}(\text{eV})$	Q_0
U (A)	0.03	9.8
1 (B)	0.25	11.0
2 (A)	0.15	10.2
2 (B)	0.24	10.7

Fig. 3.8: $Q(T)$ versus $1/T$, $E_{\mu} = E_g - E_{\mu}$, Q_0 is the intercept of $Q(T)$ versus $1/T$ curve $1/T = 0$.

conduction¹⁶. Paul and Anderson¹⁰ have also observed deviations from linearity in $Q(T)$ versus $1/T$ curves for phosphorus doped sputtered samples.

(ii) Variation of E_μ by Doping:

The difference in E_σ and E_s ($E_\mu = E_\sigma - E_s$) is explained by various transport processes in the literature. Spear et.al.¹⁹ explained this difference by assuming NNH in band tails, thermally activated by about 0.1 eV. However, Beyer and Overhof¹⁶ pointed out that at low T , VRH near E_f may be more important, as the nearest neighbours can not be defined in a tail with a rapidly rising density of states function. Grunewald and Thomas²¹ considered VRH near Fermi level in doped films and for a density of states distribution rising exponentially as

$$g(E) = g_0 \exp(E/kT_0) \quad (2)$$

with kT_0 as the characteristic energy of tail states, that

$$E_\mu = 3.5 kT_0$$

The observed increase in E_μ , upon doping may thus imply that T_0 increases, i.e. sharpness of band tails decreases with doping.

Dohler²² suggested that the large value of E_μ may be due to a strong temperature shift of the energy of maximum conduction²². He separated the temperature dependent and independent parts of $\sigma(T)$ and $S(T)$ starting from the Kubo-Greenwood formulae (Eqs.1 and 2 in Section 2.2). He calculates the contribution to the transport at any energy E ($\sigma(E)$), from a Laplace transformation of the temperature-dependent prefactor $\sigma_0(T)$. Overhof and Beyer¹⁶ have discussed that, by a Laplace back transform $\sigma(E)$ can be computed directly from $Q(T)$. As a result $\sigma(E)$ rises over many orders of magnitude in a range of a few tenths of an electron-volt. Upon doping, the shape of $\sigma(E)$ is altered significantly. $Q(T)$ depends very sensitively on the actual shape of $\sigma(E)$ over a broad range of energies. The observed linear behaviour of $Q(T)$ appears to be accidental. It is then hard to explain why $\sigma(E)$ changes upon doping in a way that does not destroy the linear $Q(T)$ relation. Further, they pointed out, that the Fermi level position derived directly from the model leads to a Fermi level shift that can not be accounted for by any density of states model¹⁶.

Another explanation has also been proposed, by Overhof and Beyer²³. They assume that the conduction takes place in the extended states above the mobility edge E_c , and $E_\mu - kT$ is due to spatial fluctuations of E_c . The origin of these fluctuations might be density fluctuations

(in homogeneities), strain fields, and potential fluctuations caused by charged centers. Assuming a random distribution of charged centers, and neglecting the other effects, the numerical calculations yield

$$E_{\mu} = 0.83 \text{ eV} \left[(L/A^0)n_c \right]^{1/2} \quad (3)$$

where n_c is the concentration of charged centers and

$$L = (g(E_F)E_{\mu})^{-1/3}$$

is the screening length determined by the density of states at the Fermi level $g(E_F)$. A typical value of $E_{\mu} = 0.1 \text{ eV}$, can be explained by, $n_c = 10^{18} \text{ cm}^{-3}$ and $g(E_F) = 10^{16} \text{ cm}^{-3} \text{ eV}^{-1}$. It is thus a characteristic feature of this model that the concentration of charged centers (n_c) is appreciably larger than the concentration of deep gap states $g(E_F)^{23}$. This is too large²³. So it appears that other two possibilities related with the inhomogeneity and strain fields may have to be considered to explain the behaviour fully.

(iii) Variation in E_{μ} by Light Soaking:

The difference in E_{μ} for curves 2(A) and 2(B) in Fig.(3.5) is about 0.1eV. Hauschildt et.al.²⁴ calculated $Q(T)$ for a phosphorus doped sample in the heat-dried and light soaked states. $Q(T)$ versus $1/T$ curves are straight lines in both states, in the temperature range 200K to 500K. The slope, E_{μ} changes from 0.09 eV in the

heat-dried state to 0.21 eV upon light soaking. This increase in E_{μ} (by about 0.1 eV) upon light soaking is the same as in our lithium doped sample.

Hauschildt et.al.²⁴ compared the shift in E_{μ} caused by phosphorus doping and by light soaking. They have shown that the changes in E_{μ} and E_{σ} for doping are different than the changes in E_{μ} and E_{σ} by light soaking. Our data, on Li doped samples in the heat-dried state and light-soaked state, support observations of Hauschildt et.al.²⁴.

Hauschildt et.al.²⁴ have shown that the increase in E_{μ} by light soaking is difficult to understand in terms of the transport models used to explain the variation of E_{μ} by doping. They suggested the increase in E_{μ} is caused by an increase in the potential fluctuations upon light soaking. Main difficulty in quantitative analysis results from the assumption that the charged defect centers are randomly distributed, because it requires a large concentration of these defects. If the charged centres are generated inhomogeneously during the exposure, they may give rise to much stronger fluctuations and thus might explain the observed increase in E_{μ} upon light soaking.

(iv) Deviation of $Q(T)$ versus $1/T$ Curves from Linearity:

The change in sign of the slope of Q versus $1/T$ curves in high temperature region indicates bipolar conduction¹⁶.

Negative S and small E_G show that the Fermi level lies close to the conduction band mobility edge in Li-doped samples. Probability of hole transport is negligible. In a-Si:H (Li) samples, the possibility of Li^+ ions contributing to conduction process can be checked by estimating the magnitude of ionic conductivity in a-Si lattice. Diffusion mobility of Li^+ ions in a-Si lattice is expected to be smaller than in c-Si. It may be more on the surface of a void within the sample, but it is highly improbable to have a continuous interconnected voids across the length of the sample. Diffusion mobility of Li^+ ions in c-Si lattice at $T = 400\text{K}$ is about $\mu(\text{Li}^+) \approx 4 \times 10^{-10} \text{ cm}^2/\text{Vs}$ ²⁵. Taking this value of mobility for a-Si:H, and density of Li^+ ions of the order of 10^{20} cm^{-3} , the conductivity due to Li^+ ions will be of the order of $2.5 \times 10^{-8} \text{ cm}^{-1}$ at $T = 400\text{K}$. Experimentally observed conductivity is of the order of 10^{-2} cm^{-1} , which is much larger than the ionic conductivity. Hence, the contribution of Li^+ ions to conductivity and thermopower in a-Si:H (Li) samples will be negligible (also section 2.5).

The unusual behaviour at high temperatures may be due to a change in the doping efficiency¹⁶ as the temperature increases. It is known that the majority of the impurities are built in as neutral atoms and only a small fraction (about 3% in case of Li)²⁶ act as dopant. At high temperatures, ionization of impurities may increase.

An increase in charged donor levels may modify the distribution of localized states and hence the conduction processes.

Another difficulty, in the interpretation of the transport properties of a-Si:H is due to the nonavailability of information about the role of space-charge layers present at the front surface and the film substrate interface²⁷.

The presence of these space-charge layers have been detected by various experiments, for example, surface photovoltage (SPV)^{28,29} and adsorbate induced conductance measurements³⁰. The unusual behaviour of S at high temperatures may be caused by the conduction of charge of opposite polarity in the surface layers.

Although, SPV shows the presence of a space-charge layer, it does not give the magnitude and the direction of band-bending at the surface²⁹. Since no information about the band-bending and its variation with temperature is available at present, it is difficult to estimate the effect of space-charge layers on the transport.

In conclusion, a-Si:H films can be doped with lithium by thermal diffusion at temperatures about 200°C. The variation of σ_0 with E_g upon doping and light soaking follows the empirical Meyer Neldel rule for heterogeneous semiconductors. A statistical shift of the Fermi level and the mobility edges with temperature, which depend upon the distribution of localized states and the position of the

Fermi level, may be responsible for this.

Understanding of transport mechanisms in undoped and doped a-Si:H with the help of theoretical models based on a homogeneous material is not complete. Doping as well as light soaking increase heterogeneities and charged defect centers. The types of defect centers created by doping and light-soaking are different. Without considering the potential fluctuations caused by heterogeneities and charged defect centers, it is difficult to predict the transport mechanism.

3B. Gradient Doping

3B.1 Introduction:

Lithium acts as an interstitial donor in crystalline³¹ as well as in hydrogenated a-Si:H³². In crystalline semiconductors a concentration gradient of impurities has been found to give rise to a photovoltage^{33,34}. Gradient doping can be used to increase the efficiency of solar cells³⁵. Here, we present similar effects in a-Si:H, by doping it with a gradient of Li^+ ions. When a lithium doped sample is subjected to an electric field at high temperatures and cooled down in presence of the electric field, a gradient of concentration of Li^+ ions gets frozen along the length of the sample. A photovoltage (V_{oc}) of the order of 100 mV and a short circuit current density (J_{sc}) of about 10^{-3} A/cm^2 for a white light flux 100 mW/cm^2 are observed in a gradient doped sample. This behaviour of gradient doped a-Si:H is similar to the phenomenon observed in crystals.

Section 2 describes the experimental techniques. I-V characteristics are studied in dark and light. The gradient profile is measured by probing the sample along the length, it is found that the potential gradient is almost linear. To increase the solar energy conversion efficiency of a Schottky barrier samples with a series

combination of a Schottky barrier at the surface and a linear voltage barrier in the bulk are fabricated. But this did not give encouraging results. The probable reasons for this and conclusions are discussed in section 3.

3B.2 Experiment:

Highly photoconducting a-Si:H films deposited on 7059 corning glass substrates, having predeposited coplanar NiCr electrodes, are loaded in a standard coating unit. Lithium is deposited on top of the films kept at $T_s = 470K$. To obtain a gradient of Li^+ ions along the length of the sample, an electric field of about $E = 10^3 V/cm$. is applied between electrodes 1 and 2, as shown in Fig.(3.9) of an a-Si:H sample immediately after lithium evaporation. This field is kept on for two hours at 470K and during the cool down of the sample to room temperature ($T=300K$).

To prepare samples having a series combination of a voltage gradient in the bulk and a Schottky barrier at the surface, the sandwich geometry is used. Initially, a layer of a-Si:H of thickness about 2000\AA is deposited on a substrate having a predeposited NiCr electrode for the back contact. This layer of a-Si:H is heavily doped with lithium by depositing $\sim 100\text{\AA}$ thick film of lithium and thermally diffusing it as before. The doped film is

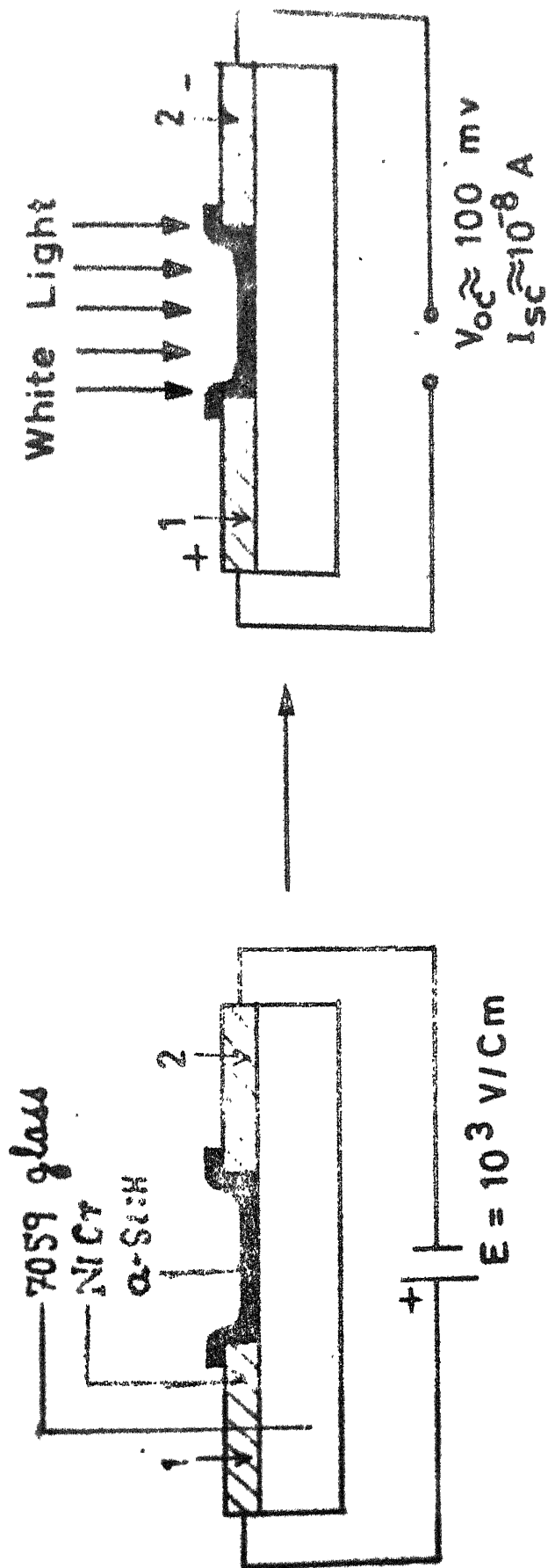


Fig.3.9 : Lithium diffusion in presence of the electric field.

etched with 10% HF to remove excess Li from the surface and cleaned with deionized water and in vapors of isopropyl alcohol. After this, the sample is reloaded in the glow-discharge system and a second layer of undoped a-Si:H of thickness about 10^{-4} cm is deposited. Finally a layer of 200Å thick Pd is deposited on top of the etched surface of undoped a-Si:H to fabricate the Schottky barrier.

3B.3 Results and Discussion

Figure (3.10) shows the I-V characteristics for a gradient doped sample having a planar geometry of electrodes in dark and in presence of light. I-V curve is symmetric in dark but has the form shown in Fig.(3.10) in presence of light. Electrode of the sample to which positive field had been applied becomes positive upon shining light. The applied voltage V (for I-V characteristic) is considered to be positive, when the electrode which becomes positive upon shining light is positively biased. The intercept of I-V curve in light to the voltage axis, is the open circuit voltage (V_{oc}) .95 mV and the intercept on the current axis is the short-circuit current (I_{sc}) 10^{-8} A. For $V > V_{oc}$, the current through the sample under light is positive and for $V < V_{oc}$, it is negative. The I-V characteristic for an a-Si:H (Li) sample without gradient is shown in Fig.(3.11), it is symmetric in dark as well as

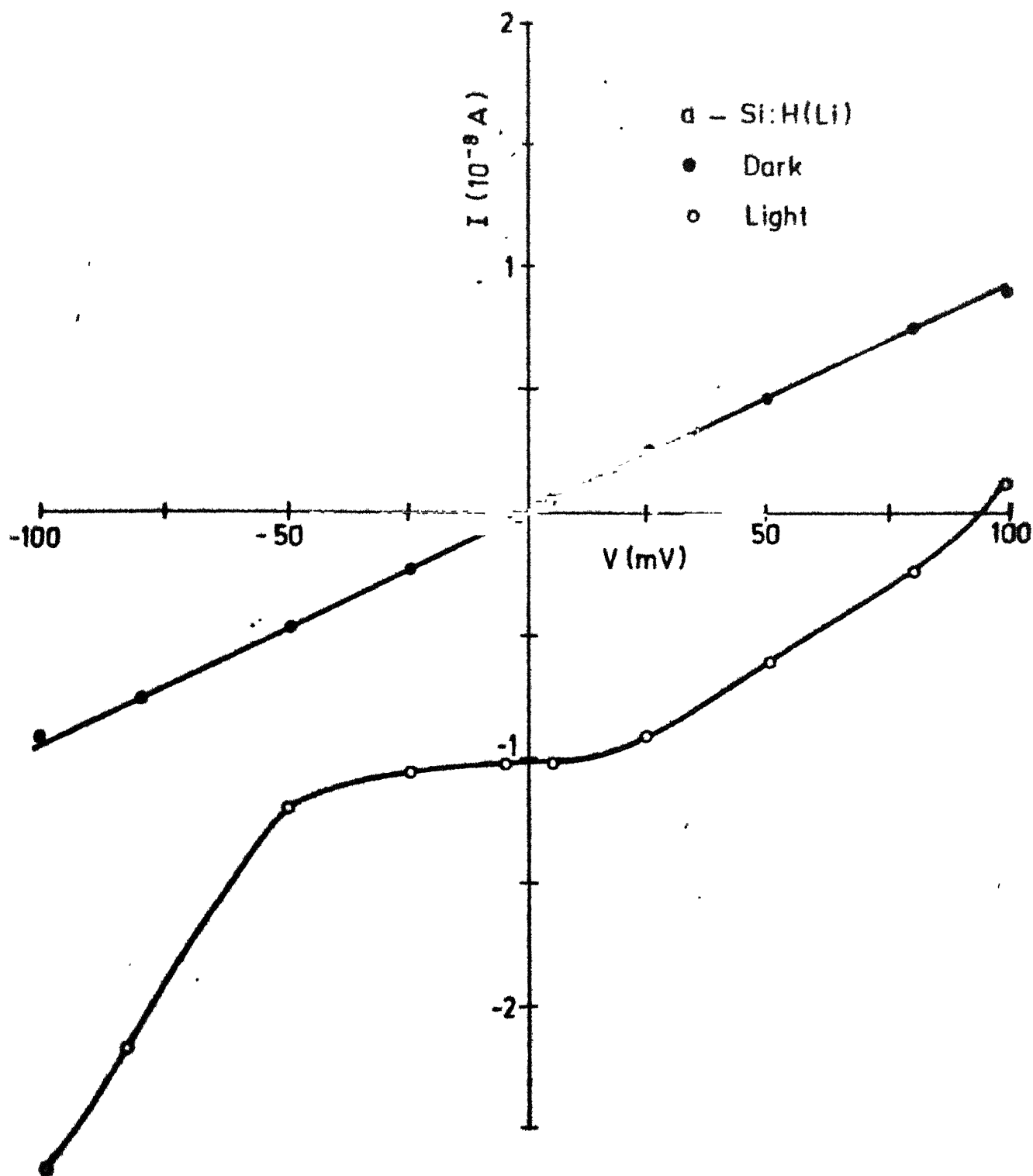


Fig.3.10 : Current (I) versus voltage (V) for a gradient doped a-Si:H (Li) in dark and light (flux = 100 mW/cm²).

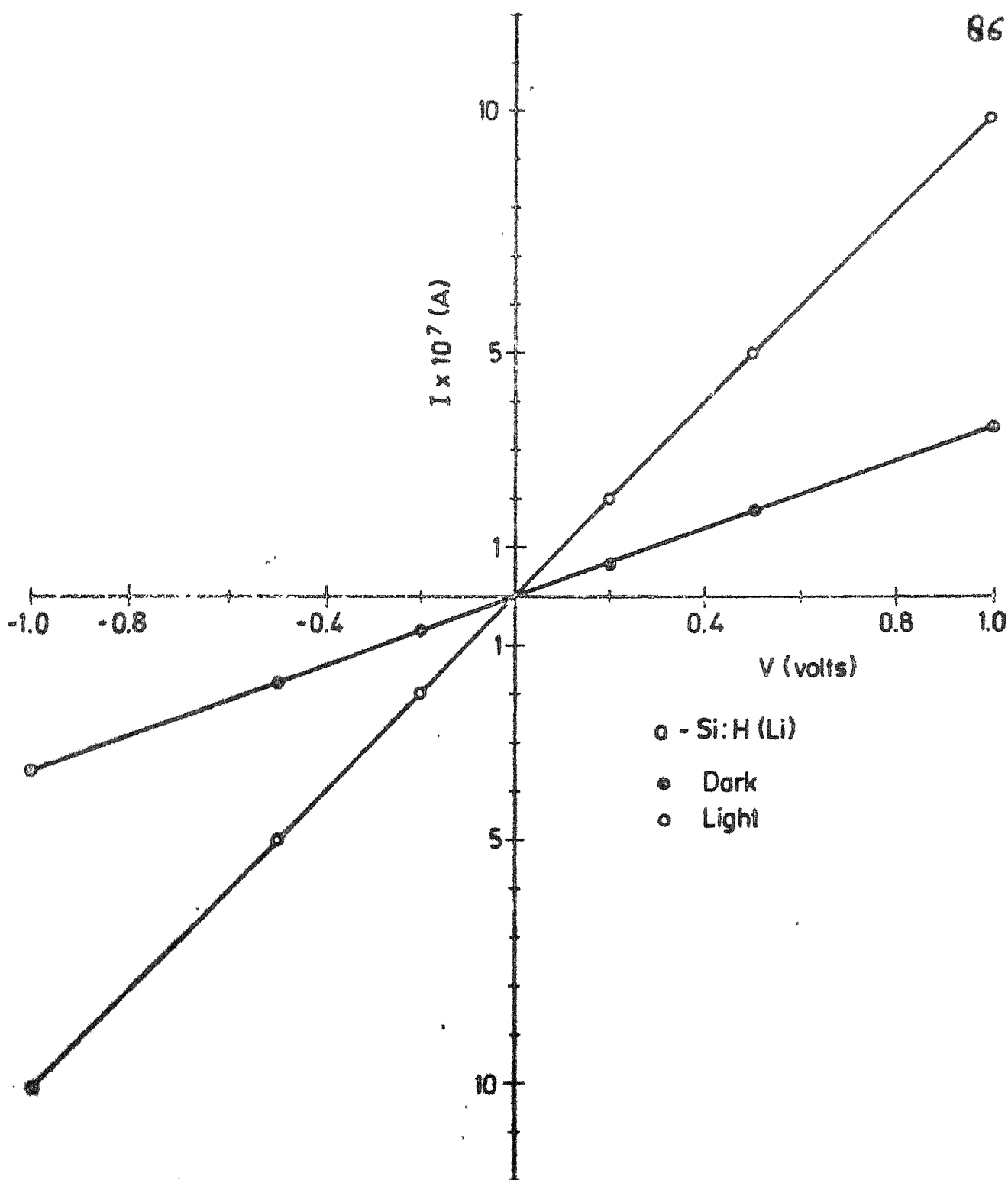


Fig.3.11 : Current (I) versus voltage (V) for an a-Si:H (Li) samples without gradient in dark and light (flux = 100 mW/cm^2).

in light.

V_{oc} remains unchanged upon storing the samples in a dissicator for a period of several months at room temperature $T = 300K$, and upon annealing at $450K$ for two hours. However, annealing at $450K$ for four hours in presence of an electric field ($E = 10^3$ V/cm) with reversed polarity, reverses the sign of V_{oc} as shown in Fig.(3.12). This shows that even at the high temperature

$T = 450K$ the directional movement of Li^+ ions is possible only in the presence of an electric field.

To measure the voltage gradient along the length of the sample, a-Si:H films are deposited on 7059 glass-substrates, having predeposited four NiCr electrodes 0.5 cm apart as shown in Fig.(3.13a). The width of the NiCr strip is 0.5 mm. For creating Li gradient an electric field at high T is applied between the two outer most electrodes. The photovoltage (V_{oc}) in the gradient doped sample is measured between different electrodes. Fig.(3.13b) shows V_{oc} as a function of distance (x) measured from one of the extreme electrodes. We see that the distribution of photovoltage is almost linear along the length of the sample.

The observation of a photovoltage in ^{the} samples subjected to an electric field during Li diffusion, can be understood qualitatively in terms of a gradient

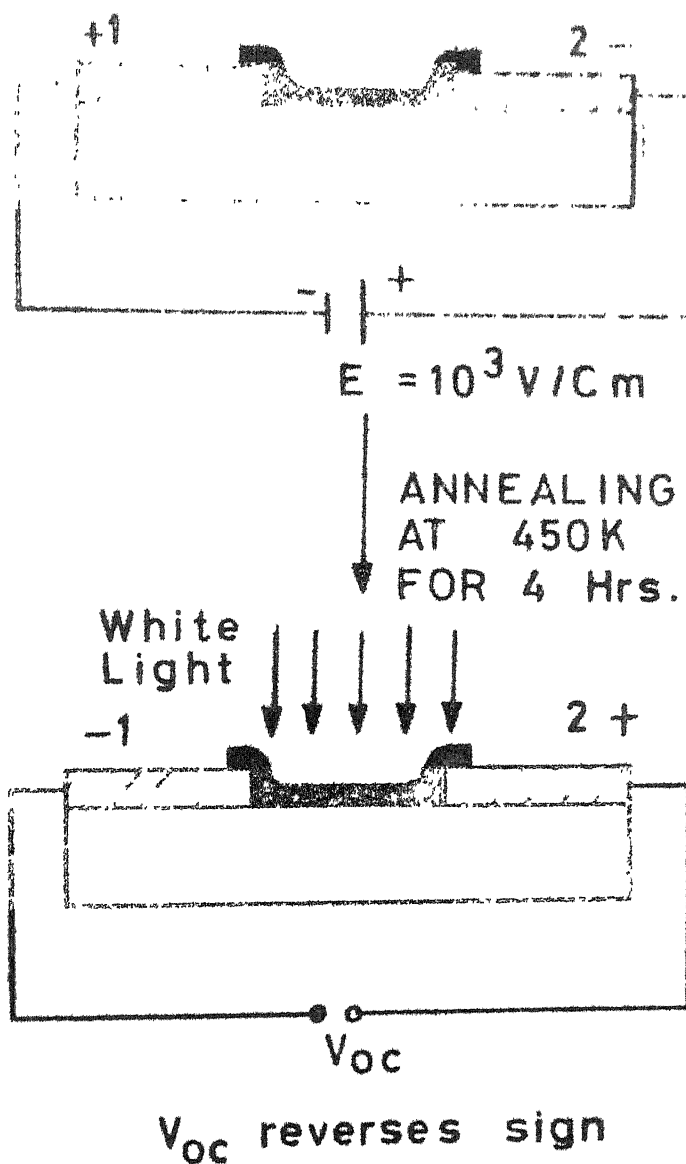


Fig.3.12 : Annealing in presence of an electric field reverse polarity of the photovoltage.

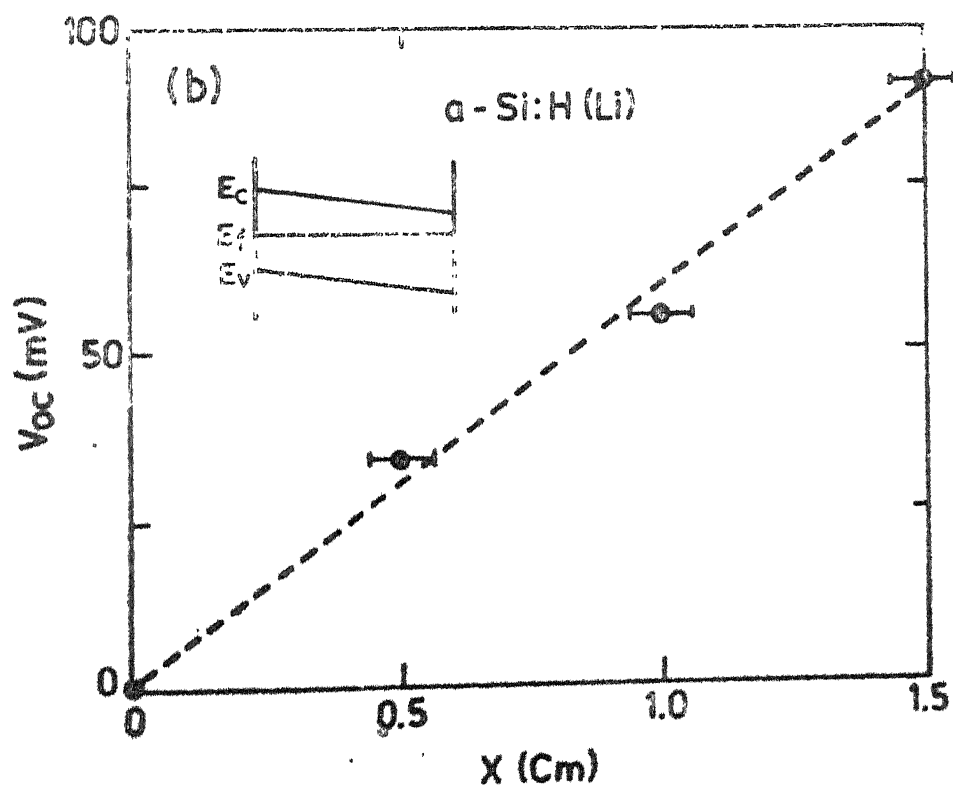
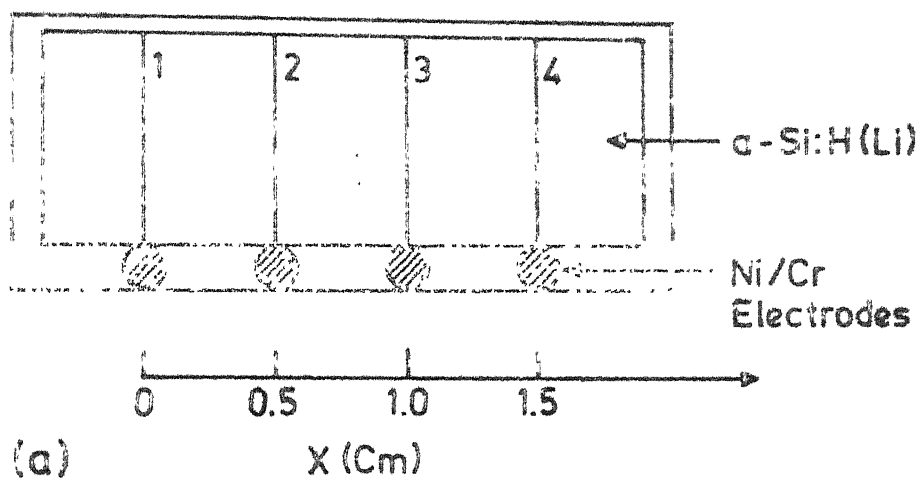


Fig. 3.13a : Geometry of the sample to measure potential profile,
(3.13b) Photovoltage (V_{oc}) versus distance (x).

of Li^+ ions along the length of the sample. Since identical electrodes are used, the contact effect^{35,36} is expected to be small. In addition, the use of coplanar geometry of electrodes rules out the Dember effect as the cause of the observed photovoltage, since it (Dember) is expected to be observed in a direction parallel to the incident light^{35,36} (for a further discussion, see section 4.4). Since the mobility of Li in c-Si is high, ($\mu(\text{Li}) 10^{-8} \text{ cm}^2/\text{V-s}$ at $T = 470$), we can expect a gradient of Li^+ ions upon application of an electric field at high T . This might give rise to a built-in potential, which although helps in separating the charged photocarriers, is expected to be quite small, since the I-V characteristic in dark is symmetric and linear. Further, it appears that the potential gradient is almost linear throughout the sample as evidenced by the linearity of the photovoltage along the length of the sample. A possible linear potential gradient in the sample is shown in Fig.(3.13a). The sign of the observed photovoltage is consistent with the above hypothesis.

Fig.3.14a shows the Schottky barrier geometry. A potential barrier at the surface is formed by making a contact with a metal of high work function (in this case Pd). The back of the sample has an ohmic contact (with NiCr) and the bulk remains neutral. This configuration is denoted by NiCr/a-Si:H/Pd. The electron-hole

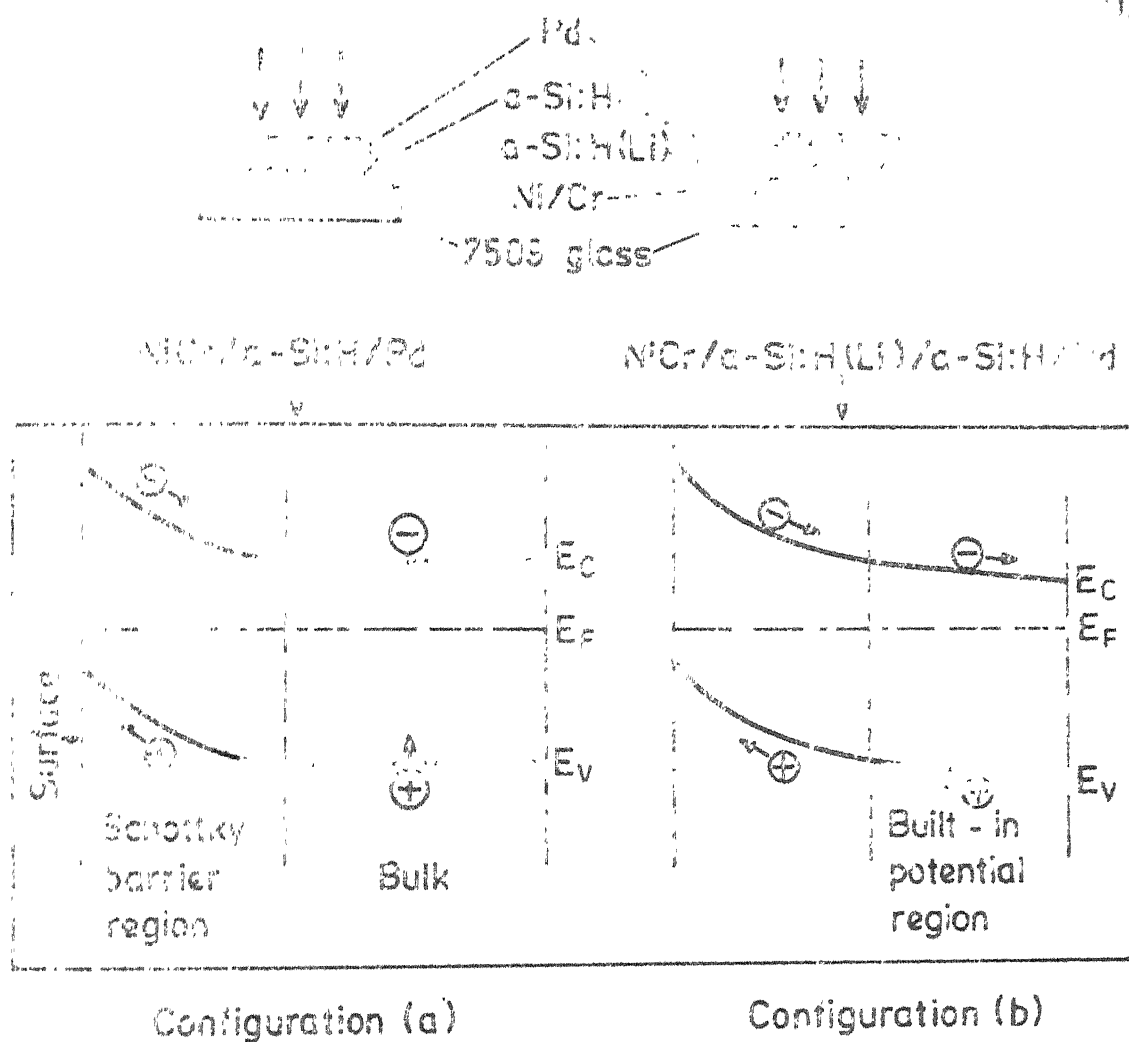


Fig. 2.14 : Schottky barrier with the neutral bulk (configuration a) and with a built in potential in the bulk (configuration b).

pairs generated near the barrier get separated by the built-in field, before they recombine. However, a large number of free carriers generated by light in the bulk get lost by recombination, since there is no field in this region to separate them. Also, we can have a bulk with a linear potential gradient as shown in Fig.(3.14b). We can expect an increase in the charge collection efficiency. To check this idea, samples are fabricated in a configuration NiCr/a-Si:H(Li)/a-Si:H/Pd as shown in Fig.(3.14b). After annealing the sample in this configuration we expect diffusion of Li^+ ions from first a-Si:H layer to second a-Si:H layer, thus giving rise to a potential gradient in the bulk.

Surprisingly, the current density reduced drastically by a factor of $\sim 10^3$, although V_{oc} increased by a factor of 2. V_{oc} and J_{sc} of a few Schottky barriers in configurations (a) and (b) are given in Table No.(3.1). One would expect less series resistance, because the sample resistance in configuration (b) than in (a), because Li acts as a donor and increases the conductivity of a-Si:H by several orders of magnitude. The increase in resistance may be due to the presence of an oxide layer at the interface of a-Si:H(Li) and a-Si:H layers. In the fabrication process, sample was exposed to air while taking out from the glow-discharge system for Li doping and also at the time of reloading. This exposure to air for a few minutes after etching may be

TABLE 3.1V_{oc} and J_{sc} in Configurations 'a' and 'b'

S.No.	Configuration	Flux 100 mW/cm ²	
		V _{oc} mV	J _{sc} A/cm ²
1.	Pd/a-Si:H/NiCr	300	7x10 ⁻³
2.	Pd/a-Si:H/NiCr	280	5x10 ⁻³
3.	Pd/a-Si:H/a-Si:H(Li)/NiCr	630	1.5x10 ⁻⁶
4.	Pd/a-Si:H/a-Si:H(Li)/NiCr	520	1.5x10 ⁻⁶
5.	Pd/a-Si:H/a-Si:H(Li)/NiCr	680	2.5x10 ⁻⁶
6.	Pd/a-Si:H/a-Si:H(Li)/NiCr	610	2.7x10 ⁻⁸
7.	Pd/a-Si:H/a-Si:H(Li)/NiCr	510	1.3x10 ⁻⁸

enough for the formation of an oxide layer at the surface. Although, we were unable to increase the conversion efficiency of Pd/a-Si:H/a-Si:H(Li)/NiCr Schottky barriers, by gradient doping, an increase in the efficiency of p-i-n solar cells is reported by Konagai et.al.³⁷. These authors investigated the effect of graded boron-doping during the i-layer deposition. The fabrication of the p-i-n layers is done in a single system without exposing the sample to air. It is found that the characteristics of the cells strongly depend on the graded doping profile of boron and the high efficiency of 9.45% is obtained with the linear, graded doping profile. It therefore appears possible, to see an increase in the efficiency in the case of Schottky barrier solar cells also, if we improve the fabrication procedure (e.g. avoiding exposure to air).

In conclusion, a gradient of Li^+ ions in a-Si:H can be obtained by thermal diffusion of Li in presence of an electric field.

REFERENCES

1. A.Madan, P.G.LeComber, W.E.Spear, J. Non. Cryst. Solids., 20, 239 (1976).
A.J.Lewis, G.A.N.Connell, W.Paul, J.R.Pawlik and R.J.Tempkin, in Tetrahedrally Bonded Amorphous Semiconductors, edited by M.H. Brodsky, S.Kirkpatrick and D.Weaire, A.I.P. Conf. Proc. No.20, 1974; p.27.
2. W.Paul in Fundamental Physics of Amorphous Semiconductors; edited by F.Yonezawa (Springer-Verlag, New York, 1981), p.72.
3. W.E.Spear and P.G.LeComber, Solid State Commn. 17, 1193 (1975).
4. W.Beyer and J.Stuke, in Proc. 5th Int. Conf. on Amorphous and Liquid Semiconductors, edited by J.Stuke and W.Brenig (Taylor and Francis, 1974), p.251.
5. D.S.Misra, P.N.Dixit and S.C.Agarwal, Bull. Mater. Science, 3, 347 (1981).
6. D.S.Misra, Ph.D.Thesis, I.I.T. Kanpur (1984).
7. G.Lucovsky, in Fundamental Phys. of Amorphous Semiconductors, edited by F.Yonezawa (Springer-Verlag, New York, 1981), p.87.
8. W.Beyer and R.Fischer; Appl.Phys.Lett., 31, 850 (1977).
9. D.I.Jones, P.G.LeComber and W.E.Spear, Phil. Mag. B36, 541 (1977).
10. D.A.Anderson and W.Paul, Phil. Mag., 45, 1 (1982).
11. N.F.Mott and E.A.Davis, Electronic Properties of Non-Crystalline Materials (Clarendon Press, Oxford, 1979).
12. D.L.Staebler and C.R.Wronski, Appl.Phys.Lett., 31, 292 (1977).
13. H.Fritzsche, Solar Energy Mat., 3, 447 (1980).

14. J.Jang, T.M.Kim, J.K.Hyun, J.H.Yoon and C.Lee,
J.Non. Cryst. Solids, 59&60, 429 (1983).
15. S.Guha, Bull. Mater. Science, 2, 317 (1980).
16. W.Beyer and H.Overhof in Hydrogenated Amorphous
Silicon, edited by R.K.Willardson and
A.G.Beer, Vol. 21C, (Academic Press, New York,
1984).
17. W.Meyer and H.Neldel, Z.Tech. Phys. 18, 588 (1937).
18. W.Beyer and H.Overhof, Solid State Commun. 31, 1
(1979).
19. W.E.Spear, D.Allan, P.G.LeComber and A.Gaith,
Phil. Mag. B41, 419 (1980).
20. A.Madan, P.G.LeComber and W.E.Spear, J.Non. Cryst.
Solids, 20, 239 (1976).
21. M.Grunewald and P.Thomas, Phys. Stat. Solidi
(b) 94, 125 (1979).
22. G.Döhler, Phys. Rev. B19, 2083 (1979).
23. H.Overhof and W.Beyer, Phil. Mag. B43, 433 (1981).
24. D.Hauschildt, W.Fuhs and H.Mell, Phys. Stat. Solidi,
(b) 111, 171 (1982).
25. E.M.Pell, Phys. Rev. 119, 1014 (1960).
26. H.Overhof and W.Beyer, J.Non. Cryst. Solids,
35&36, 375 (1980).
27. H.Fritzsche, in Electronic and Transport Properties
of Hydrogenated Amorphous Silicon, edited by
J.I.Pankove (Academic Press, 1984).
28. B.Goldstein and D.J.Szostak, Surface Sci., 99,
235 (1980).
29. S.Kumar and S.C.Agarwal, to be published.
30. M.Tanilian, Phil. Mag. B45, 435 (1982).

31. R.L.Aggarwal, P.Fisher, V.Mourzine and A.K.Ramdas, Phys. Rev. 138A, 882 (1965).
32. W.Beyer and R.Fischer, Appl.Phys. Lett., 31, 850 (1977).
33. Z.Trousil, Czech. J. Phys., 6, 96 (1956).
34. J.Tauc, Rev. Mod. Phys., 29, 308 (1957).
35. R.H.Buke, Photoconductivity of Solids (John Wiley & Sons, N.Y. 1960).
36. A.Many, Y.Goldstein and N.B.Grover, Semiconductor Surfaces (North-Holland, Amsterdam, 1965).
37. M.Konagai, K.S.Lim, P.Sichanugrist, K.Komori and K.Takahashi in Proc. of the 16th IEEE Photovoltaic Specialists Conference, Florida, p.1321.

CHAPTER 4

SURFACE PHOTOVOLTAGE IN a-Si:H

4.1 Introduction

The presence of a charged layer at the surface of a semiconductor can be detected from the measurement of surface photovoltage (SPV)¹. The change in the surface potential upon illumination is the measured SPV¹. If the contribution of the surface states is small it can be shown that the effect of light is to flatten the bands and thus to reduce the potential at the surface². Thus in this case the sign of SPV gives the direction of band bending at the surface. If however, surface states contribute, Garrett and Brattain³ have shown that the SPV for low intensity of light can differ from the expected value by a small amount. It has been observed that, in c-Si⁴, Cd-S⁵ and In-Sb⁶, the low intensity SPV may not give band bending depending upon surface conditions. However, Many et.al.⁷ have argued that at high intensities, the surface potential tends to zero, even if surface states participate, unless some "special surface-state parameters" are involved. Although this statement has been shown to be untrue by Frankl and Ulmer⁸, the impression given by Many et.al.⁷ seems to persist, and many SPV measurements at high intensities are done in the hope of finding the surface potential.

Upon shining light the change in surface potential may be caused by either (i) a redistribution of charge between surface states and the space charge region, or (ii) a redistribution of charge within the space charge region without involving surface states. Since charge neutrality requires that the charge in surface states (Q_{ss}) should be equal and opposite to space charge (Q_{sc})

$$Q_{ss} + Q_{sc} = 0$$

For processes described in (i) the change in Q_{sc} , $\Delta Q_{sc} = - \Delta Q_{ss}$ and in (ii) $\Delta Q_{sc} = 0$.

Johnson² gave a theory of SPV at high injection levels and developed a method of graphical analysis to show how the surface potential changes under illumination. His analysis shows that light injection tends to flatten the bands for procedure (ii), but may and may not do so for process (i) where the space charge changes. In the case of crystalline Ge and Si the analysis implies that at high intensities SPV will directly give the band bending within one kT/e , of process (ii) dominates.

Clearly, if it can be ensured that $Q_{sc} = 0$ in light (i.e. $\Delta Q_{sc} = - Q_{sc}$), the observed SPV will be equal to the surface potential even in case (i). However, this can not always be guaranteed and the observed SPV can be either positive or negative depending on the ratio of the capture cross-sections for electrons and holes of

surface states^{6,8}. In the case of a-Si:H, Fritzsche⁹ has argued that Q_{sc} most probably is not zero in presence of light because the charges may be separated too far spatially and energetically to equilibrate.

In the present work, Johnson's graphical analysis² is applied for a-Si:H, considering a continuous distribution of localized states in the mobility gap. In section 4.2, a relation between the space charge density (Q_{sc}) and the surface potential (V_s) is derived in dark and in presence of light, by solving Poisson's equation for V_s . It is shown that in a-Si:H, process (ii) gives negligible SPV and a change in Q_{sc} is necessary (i.e. process (i)) to observe a finite SPV. In section 4.3, the method of measurement of SPV using pulsed light (chopped light) is described. In the next section, the effects of repetition frequency (f), intensity (I) and energy ($h\nu$) of the pulsed light are discussed. Effects of etching, aging and ambient air on SPV have also been studied. In addition SPV at the free surface and the film substrate interface has also been measured as a function of temperature. These measurements show that the SPV does not give band bending. This supports the theoretical results of the section 4.2, since finite SPV means a change in Q_{sc} for a-Si:H and therefore surface state parameters are expected to govern the SPV. In the last section (4.5), effect of light soaking (Staebler-Wronski effect)¹⁰ on SPV is

described. In this experiment, samples are exposed to a sequence of light soaking and moisture similar to Tanilian¹¹. However, in addition to the dark conductance (G), the SPV is also measured. It is observed that the SPV is sensitive to the sequence of illumination and moisture. From these measurements, it is concluded that the light soaking changes the surface as well as the bulk states in a-Si:H.

4.2 Theory of Surface Photovoltage

In this section we shall give a graphical method similar to that of Johnson² to obtain SPV in a-Si:H.

1) Solution of Poisson's Equation in Dark and Light

The energy band diagram, in presence of light, as a function of thickness (x) for an undoped sample with an accumulation layer is shown in Fig.4.1. In bulk, E_c and E_v are the conduction band and valence band mobility edges, E_f is the Fermi energy level in dark, E_{fn}^t and E_{fp}^t are the quasi Fermi energy levels for trapped electrons and holes respectively in light. In the space-charge region, the electrostatic potential $V(x)$ at the point x is positive for downward band bending and energy level (E) is shifted by an energy (-eV), e being the magnitude of the electronic charge. It is well known that there is a continuous distribution of localized states in the

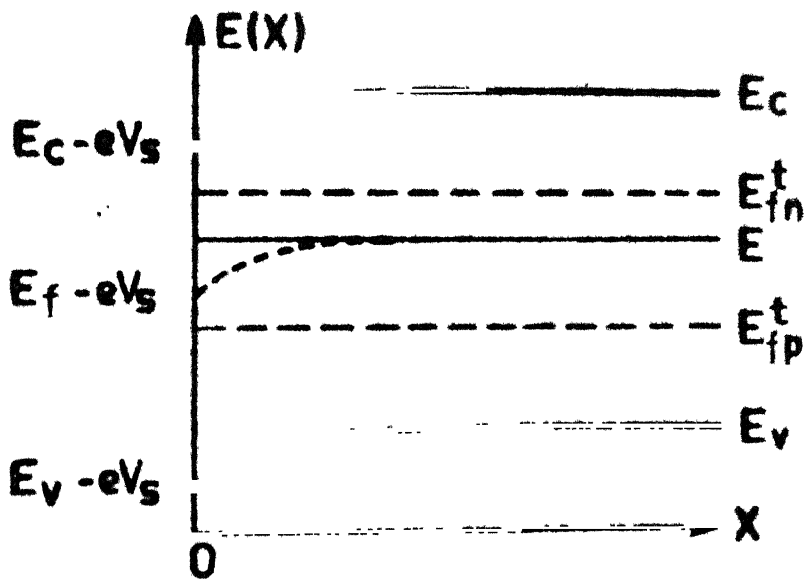


Fig.4.1 : Energy band-diagram for a-Si:H with an accumulated surface in light. E_c and E_v are mobility edges, E_f is the Fermi level in dark, E_{fn}^t and E_{fp}^t are quasi Fermi levels for trapped carriers. Potential V is positive and energy level E in bulk is shifted to $E - eV_s$ at the surface.

mobility gap of a-Si:H¹². We estimate the density of states between 10^{16} to 10^{17} cm⁻³ eV⁻¹ at the Fermi level in our undoped samples¹³. Using Shockley Read Statistics¹⁴, Simmons and Taylor¹⁵ have derived the occupation probability of an energy level lying in the mobility gap in non-equilibrium conditions. For convenience, it is assumed that the quasi Fermi levels are flat upto the surface. The traps are monovalent, and those existing below E_f are neutral when filled with an electron and that the traps positioned above E_f are neutral when empty. Further assuming that the ratio R of the cross-sections for electrons and holes is constant for all energy levels, the probability of occupation $f(E, E_{fn}^t)$, of an energy level E above E_f by an electron is¹⁵

$$f(E, E_{fn}^t) = \frac{Rn_b}{Rn_b + p_b} \frac{1}{1 + \exp(E - E_{fn}^t)/kT} \quad (1)$$

where n_b and p_b are the free electron and hole densities in the bulk and the probability of occupation of an energy level below E_f by a hole is

$$1 - f(E, E_{fp}^t) = \frac{p_b}{Rn_b + p_b} \frac{1}{1 + \exp(E - E_{fp}^t)/kT} \quad (2)$$

The potential $V(x)$ at a distance x from the surface satisfies the Poission's equation

$$\nabla^2 V(x) = - \rho(x)/\epsilon \quad (3)$$

where $\rho(x)$ is the effective charge density and ϵ is the permittivity of the medium.

Charge density $\rho(x)$ in non-equilibrium condition is given by

$$\begin{aligned} \rho(x) = e \left[\int_{-\infty}^{E_V} g(E) \left\{ f(E, E_{fp}) - f(E, E_{fp} + eV) \right\} dE \right. \\ + \int_{E_V}^{E_f} g(E) \left\{ f(E, E_{fp}^t) - f(E, E_{fp}^t + eV) \right\} dE \\ + \int_{E_f}^{E_c} g(E) \left\{ f(E, E_{fn}^t) - f(E, E_{fn}^t + eV) \right\} dE \\ \left. + \int_{E_c}^{\infty} g(E) \left\{ f(E, E_{fn}) - f(E, E_{fn} + eV) \right\} dE \right] \quad (4) \end{aligned}$$

where E_{fn} and E_{fp} are the quasi Fermi levels for free electrons and holes respectively and $g(E)$ is the distribution of density of states. In Eq.(4), first and forth integrals give contribution to the density of free carriers (ρ_0) due to holes and electrons respectively and second and third integrals give density (ρ_t) of trapped holes and electrons respectively. For convenience these integrals are represented by I_1 , I_2 , I_3 and I_4 respectively. These integrals can be evaluated using Eqs.(1) and (2) and the standard Fermi distributions $f(E, E_{fp})$ and $f(E, E_{fn})$ for free carriers. Average values of $g(E)$ at the valence and

conduction band mobility edges $g(E_v)$ and $g(E_c)$ are taken for I_1 and I_4 respectively; and constant density of states $g(E) = g_0$ is taken for I_2 and I_3 . With these assumptions, integrals are carried out and are given by

$$I_1 = p_b(\exp(-v)-1) \quad (5)$$

$$I_4 = n_b (1 - \exp(v)) \quad (6)$$

$$I_2 = \frac{kTg_0p_b}{Rn_b+p_b} \ln \frac{1+\exp(-\beta(E_v - E_{fp}^t))}{1+\exp(-\beta(E_v - E_{fp}^t)+v)} \cdot \frac{1+\exp(\beta(E_{fp}^t - E_f)+v)}{1+\exp(\beta(E_{fp}^t - E_f))} \quad (7)$$

and

$$I_3 = \frac{kTg_0Rn_b}{Rn_b+p_b} \ln \frac{1+\exp(-\beta(E_c - E_{fn}^t)-v)}{1+\exp(\beta(E_c - E_{fn}^t))} \cdot \frac{1+\exp(\beta(E_f - E_{fn}^t))}{1+\exp(\beta(E_f - E_{fn}^t)-v)} \quad (8)$$

where $\beta \equiv 1/kT$ and $v \equiv eV/kT$.

These integrals hold good both in light and in dark.

In dark, these integrals can be obtained by putting

$E_f = E_{fn}^t = E_{fp}^t$ and using dark values of n_b and p_b . To evaluate I_3 and I_4 , in light, information about the quasi Fermi levels for the trapped charges is necessary. Assuming that the quasi Fermi levels for free carriers are the same as for the trapped carriers, ($E_{fn}^t = E_{fn}$, $E_{fp}^t = E_{fp}$), one can estimate the positions of the quasi Fermi levels from photoconductivity data. Let us estimate them for a high

intensity which gives saturated value of SPV and about four orders of photoconductivity. For an undoped sample, with activation energy (E_G) = 0.65 eV and band gap $E_G = 1.6\text{eV}$, various differences in energy levels in I_2 and I_3 are

$$E_c - E_{fn}^t = 0.4\text{eV}; E_{fn}^t - E_f = 0.25\text{eV}$$

$$E_f - E_{fp}^t = 0.55\text{eV} \text{ and } E_{fp}^t - E_v = 0.4\text{eV}$$

These energy differences are calculated assuming

$E_c - E_{fn} = E_{fp} - E_v$. This will be true if light creates an equal number of free electrons and holes. Although, this is not likely to hold since the free hole concentration is probably smaller because of larger capture of holes¹⁶. This assumption is not likely to change the conclusions in a qualitative manner.

Using these energy differences and neglecting appropriate terms, the summation of I_2 and I_3 becomes

$$\begin{aligned} I_2 + I_3 &= -g_0 kT v \left(\frac{p_b + Rn_b}{Rn_b + p_b} \right) \\ &= -g_0 kT v \end{aligned}$$

Hence, the trapped charge density will be

$$\rho_t(x) = -e g_0 kT v(x) \quad (9)$$

Although, Eq.(9) is derived for high intensity of light, it

also holds good in dark, because it is independent of terms involving quasi Fermi levels. It may be interesting to note that the $\psi(x)$ given by Eq.(9) is the same when Fermi distributions are approximated by a step function using zero temperature statistics⁹.

$$\frac{e}{kT} \frac{d^2 \psi(x)}{dx^2} = - \frac{\rho(x)}{\epsilon} = \frac{e}{\epsilon} \left[n_b (e^{\psi} - 1) - p_b (-e^{-\psi} + 1) + g_o kT \psi(x) \right] \quad (10)$$

Equation (10) and

$$\frac{d\psi}{dx} \frac{d^2 \psi}{dx^2} dx = \frac{kT}{e\epsilon} \int \rho(x) \frac{d\psi}{dx} dx$$

will give

$$\left(\frac{d\psi}{dx} \right)^2 = \frac{2kT}{e\epsilon} \int \rho(x) d\psi \quad (11)$$

and the space-charge density (per unit area) Q_{sc} is given by Gauss's law

$$Q_{sc} = \pm \left| \frac{d\psi}{dx} \right| = \pm \sqrt{2\epsilon} \left| \int \rho(x) d\psi \right| \quad (12)$$

where positive sign is for negative ψ and vice versa.

Using Eqs.(11) and (12), the charge per unit area given by

$$Q_{sc} = \pm \sqrt{2q\epsilon} \left[n_b (e^{\psi_s - \psi_s} - 1) - p_b (e^{-\psi_s + \psi_s} - 1) + \frac{g_o kT \psi_s^2}{2} \right]^{1/2} \quad (13A)$$

Corresponding expression for the case of constant impurity concentration and complete ionization in a crystalline semiconductor⁷ is

$$Q_{sc} = \pm \sqrt{2q\epsilon} \left[n_b (e^{v_s} - v_s - 1) - p_b (e^{-v_s} + v_s - 1) \right]^{1/2} \quad (13B)$$

It may be noted that Eq.(13) gives the relationship between the surface potential and the space-charge density Q_{sc} , for all intensities of light including zero. One has only to put the correct free carrier densities n_b and p_b in the bulk for the intensity of illumination under consideration.

ii) Graphical Analysis of SPV

Figure 4.2A shows the graphical plot of Eq.(13A) in dark, curve (1), and (curve 2) and (curve 3) are for medium and high illuminations respectively, for an undoped a-Si:H sample, having depleted surface, with $g_0 = 10^{17} \text{ cm}^{-3} \text{ eV}^{-1}$ and activation energy $E_\sigma = 0.65 \text{ eV}$. In dark, $n_b = 5 \times 10^8 \text{ cm}^{-3}$ and $p_b = 5 \times 10^3 \text{ cm}^{-3}$. n_b and p_b increase to $n_b + \Delta n_b$ and $p_b + \Delta p_b$ in presence of light. For the high intensity curve 3 in Fig.4.2A, we have chosen $\Delta n_b = 5 \times 10^{12} \text{ cm}^{-3}$ which corresponds to a change by about 4 orders of magnitude in conductivity upon shining light. Curve 2 is for $\Delta n_b = 5 \times 10^{10} \text{ cm}^{-3}$. Further, for the sake of simplicity

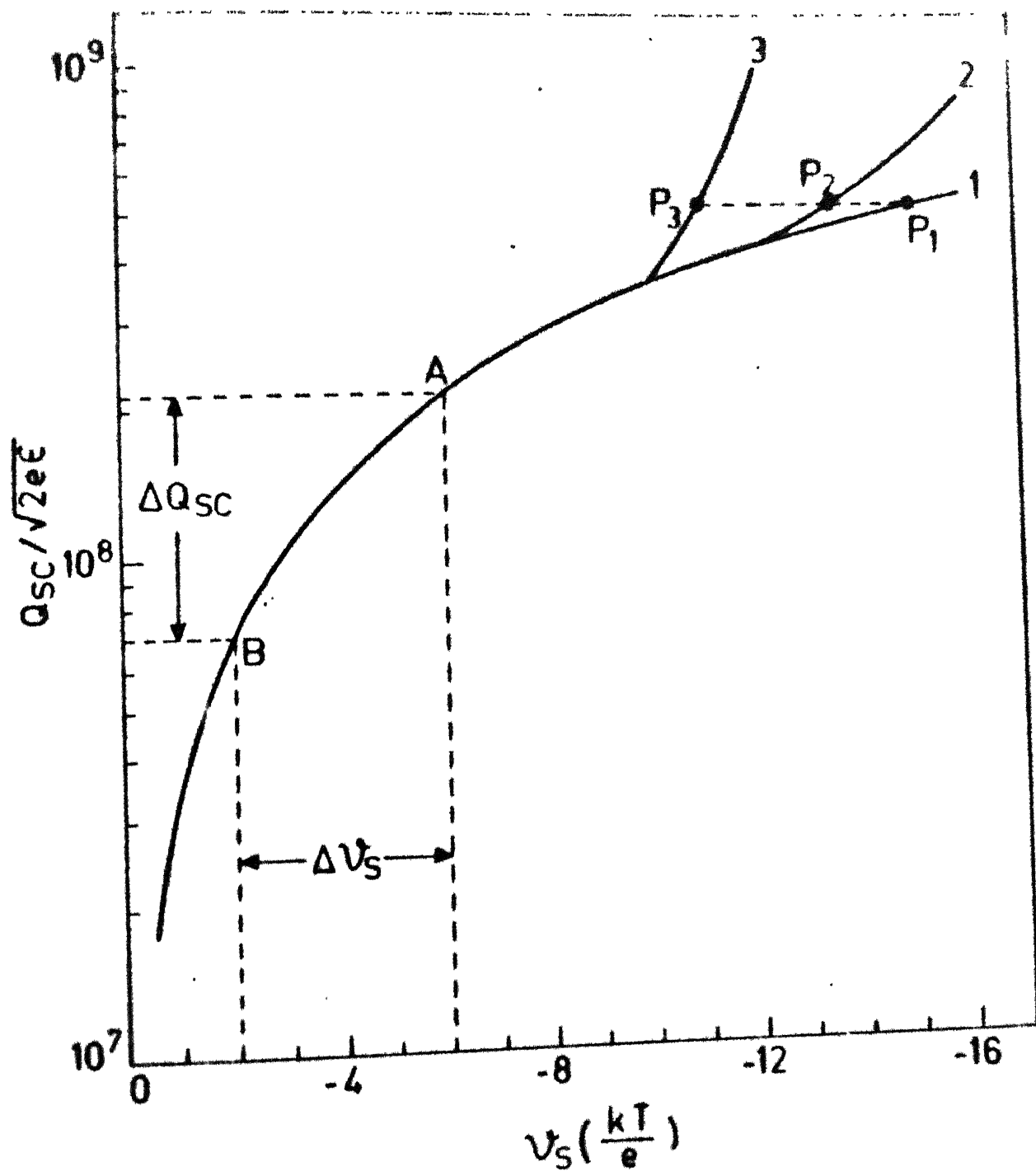


Fig.4.2A : Space-charge density Q_{sc} versus surface potential V_s for a p-n junction with negative space charge region in dark (1) and light (2 : $\Delta n_0 = 5 \times 10^{16} \text{ cm}^{-3}$ and 3 : $\Delta n_0 = 5 \times 10^{17} \text{ cm}^{-3}$).

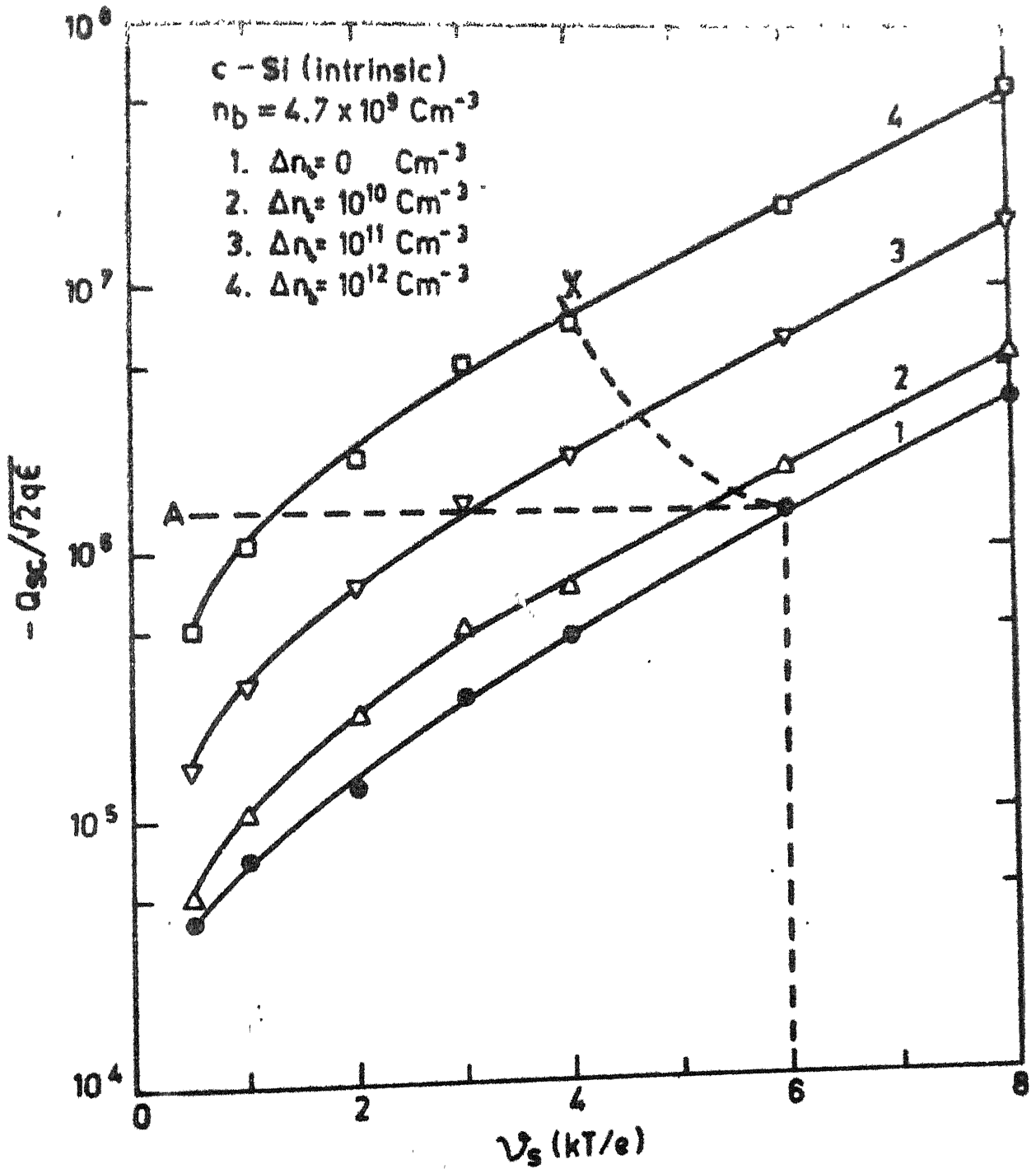


Fig.4.2B : Space-charge density Q_{sc} versus surface potential V_s for $c-Si$ (intrinsic) with negative space-charge region in dark (1) and light (2 : $\Delta n_0 = 10^{10} \text{ cm}^{-3}$, 3 : $\Delta n_0 = 10^{11} \text{ cm}^{-3}$, 4 : $\Delta n_0 = 10^{12} \text{ cm}^{-3}$)

Δp_b has been taken to be equal to Δn_b . As mentioned earlier, this need not be true, but will not affect the conclusions drawn here, corresponding curves for the depleted surface are obtained simply by changing the signs of Q_{sc} and v_s in Fig.4.2A. Q_{sc} vs. v_s curves calculated using Eq.(13b) for c-Si (intrinsic) with an electron accumulation layer are shown in Fig.4.2B. Curve 1 is for dark ($n_b = p_b = 4.7 \times 10^{-9} \text{ cm}^{-3}$). Curves (2,3 and 4) in light are shifted to the left of the curve 1 for all values of v_s , even for small intensities of light. In contrast, for a-Si:H, curves 2 and 3 in Fig.4.2A under illumination coincide with curve 1 in dark upto $v_s = 10$. This feature is quite different as compared to the similar curves for c-Si. This difference between c-Si and a-Si:H arises primarily because the latter has a continuous distribution of localized states and $\rho_0 \ll \rho_t$.

In the case of c-Si, using light pulses of appropriate frequency, it has been possible to keep the Q_{ss} and hence the Q_{sc} constant during the experiment¹⁸. In this case, the system in Fig.4.2B moves along a horizontal line. The line A applies to a particular case, where initial v_{si} in dark is 6. The values of the surface potential for different intensities of light are described by the intersections of line A with the Q_{sc} curves. The quantity $\Delta v = v_{sf} - v_{si}$ is the photovoltage. If Q_{ss} changes during the injection, the system will move along a path, other

than A; on the line X, for example. The path of the system will depend upon the properties of surface states. In fact, Δv could remain constant or even change sign depending upon the path followed by the system. Experimentally, in the case of c-Si¹⁸ and c-Ge², it has been observed that the large-signal surface photovoltage is not very sensitive to fast surface states. Therefore SPV measurement with high injection light to suppress the contribution from the slow states is a fairly reliable tool for determining surface potential. However, for small signal SPV, the contribution from surface states might not be negligible as compared to the contribution from the redistribution within the space-charge. It has been observed in the case of crystalline Si, that the SPV may not be zero even if $v_s = 0$ ^{4,8}.

Let us now consider SPV in a-Si:H. In Fig.4.2A, the curves 2 and 3 under illumination, coincide with curve 1 in dark upto $v_s = 10$. Now if the surface states do not participate, Q_{sc} remains constant upon shining light. Let the system be at P_1 on the curve 1 in dark. In light, the system moves along a horizontal line intersecting curves 2 and 3 at P_2 and P_3 respectively. The expected SPV is then surface potential difference between P_1 and P_2 for $\Delta n_b = 5 \times 10^{10} \text{ cm}^{-3}$ and between P_1 and P_3 for $\Delta n_b = 5 \times 10^{12} \text{ cm}^{-3}$.

Clearly, if v_s in dark is less than 10 (which is normally the case for a-Si:H)¹⁷, this procedure will predict a zero SPV, since curves 1, 2 and 3 overlap. Further, the observed SPV in a-Si:H is not zero (and is in fact more than 100 mV in some cases), we must question our assumption that Q_{sc} is unchanged and the system moves along a horizontal line. A significant change in Q_{sc} can be only by exchanging charges with the surface states, since the density of free carriers for $|v_s| < 10$ is too small. Therefore, for a change in Q_{sc} by an amount ΔQ_{sc} , the surface states charge Q_{ss} must change by $\Delta Q_{ss} = -\Delta Q_{sc}$. In that case, the system need not move in a horizontal line and the observation of a large SPV can be explained. For example, if in dark the system is at A, Fig. 4.2A, corresponding to $v_s = 6$, it can move to B, and give $SPV = 4kT/e$, if we allow for a change in Q_{sc} , $\Delta Q_{sc} \approx 1.5 \times 10^8 \sqrt{2e\epsilon}$ Coulomb upon shining light. Since the dark and illuminated curves coincide in this region, the path of the system from A to B must not deviate from this curve in this case. It is interesting to note that ΔQ_{sc} may be positive or negative depending on the nature of surface states, and so the observed photovoltage could even be of opposite sign for the same initial value of v_s . For the example cited above, $SPV = 4kT/e$ (≈ 100 mV at $T=300K$), $\Delta Q_{ss} = 10^{-8}$ Coulomb, and this gives surface states density participating in charge transfer of the order of $10^{11} \text{ cm}^{-2} \text{ eV}^{-1}$. This

number is quite reasonable and agrees with other measurements of surface states density^{11,17}.

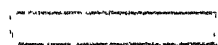
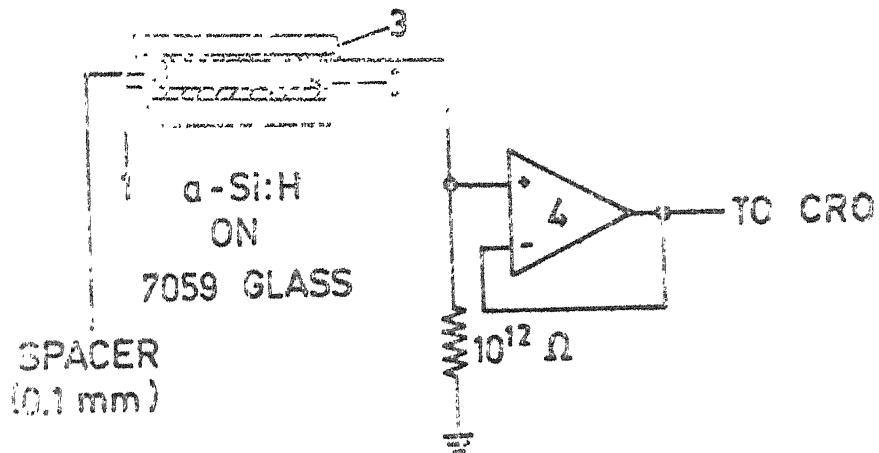
Thus we are led to the following conclusion, unless the band bending at the surface of a-Si:H is unreasonably large, the SPV in a-Si:H will be governed entirely by the change in the space charge Q_{sc} , which depends upon the properties of surface states. Although a constant density of states is assumed, a more realistic density of states will imply higher $g(E)$ near band edges and will strengthen this conclusion.

Thus we are led to the following conclusion, that if the surface potential is less than $10kT/e$ in a-Si:H, then one will observe a finite SPV for the process (i) (i.e. $\Delta Q_{sc} = -\Delta Q_{ss}$) and the SPV will be zero for the process (ii) (i.e. $\Delta Q_{sc} = 0$). One expects for higher chopping frequency, ΔQ_{ss} will be negligible and hence SPV will also be negligible.

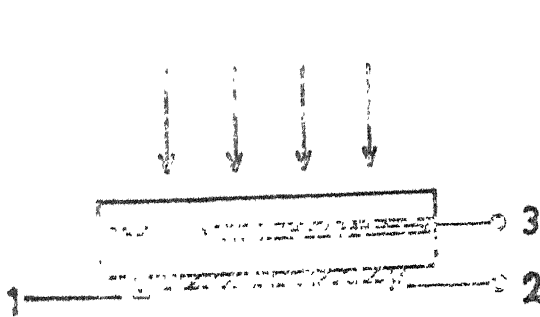
4.3 Experimental

The experimental system used for measuring SPV is shown in Fig.4.3A a-Si:H samples deposited on 7059 glass substrates, and of thickness $0.6 \mu m$ to $1.5 \mu m$, having two NiCr electrodes 1 and 2 with gap of 1 cm to 1.8 cm are used. Geometry of the sample is similar as used for thermopower measurements. To measure SPV at the front surface of the sample, a semitransparent electrode (3) is

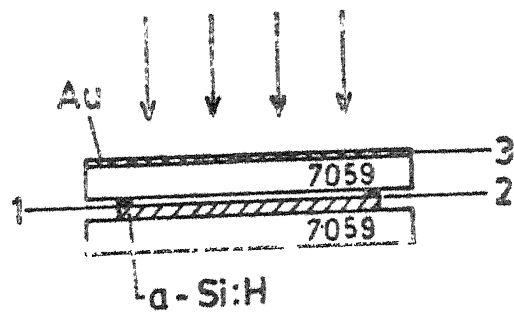
PULSED LIGHT


 FILTER


(A)



(B)



(C)

Fig.4.3A : Arrangement for the measurement of SPV. 3 is a semitransparent electrode. Electrodes 1 and 2 are for measurement of G and are grounded for SPV measurements. 4 is a FET input operational amplifier.

B : G and τ used to measure SPV at the back surface.

C : G and τ used to measure SPV at the front surface, keeping the same relation between electrode 3 and the sample same as in (B).

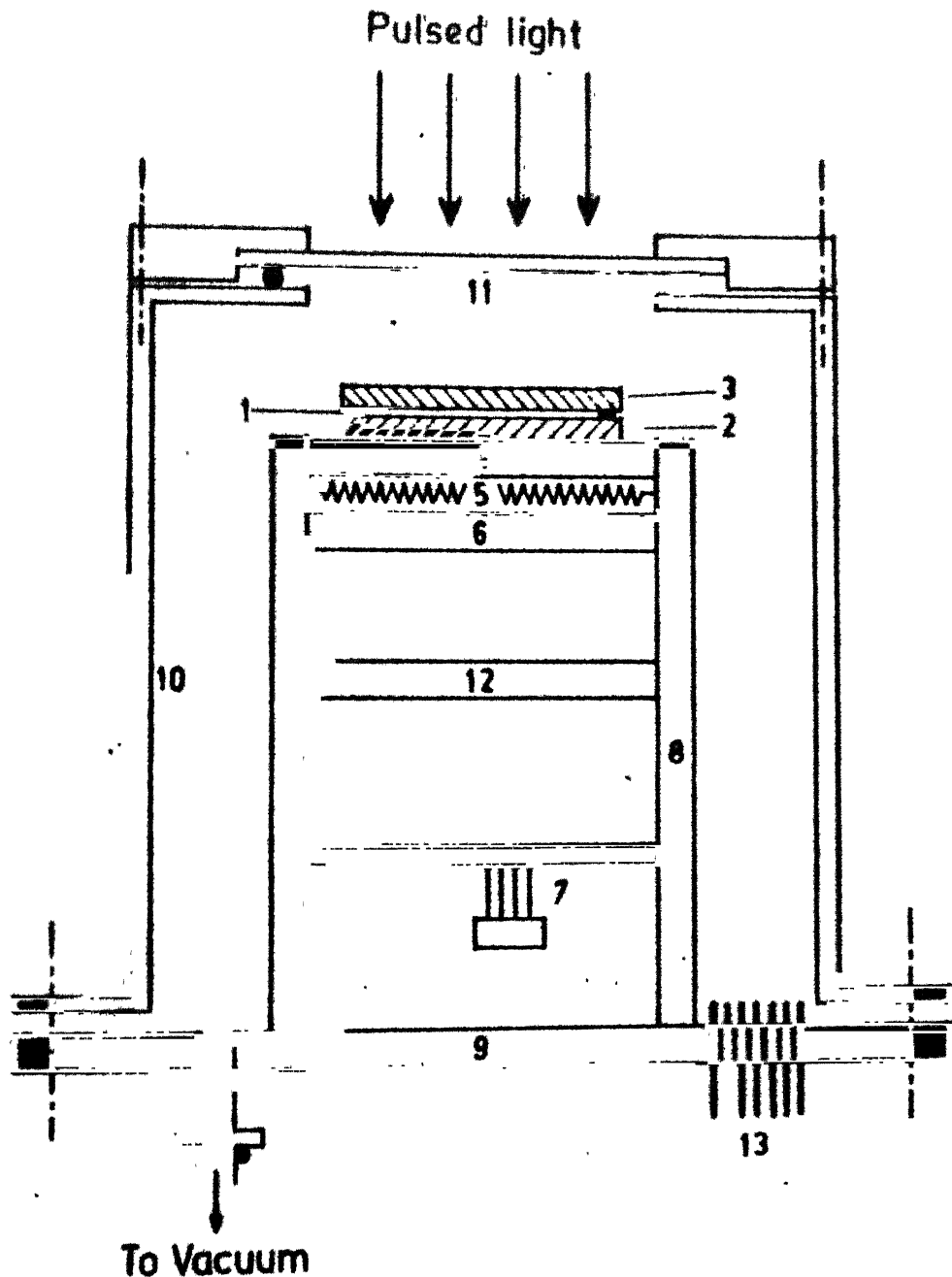


Fig.4.4 : System to measure SPV at different temperatures in vacuum.
 1 and 2.NiCr electrodes, 3.semitransport electrode,
 4.aluminium substrate holder, 5.heater, 6.another aluminium
 plate, 7.PNT input amplifier, 8.ceramic stand, 9.base plat
 having a vacuum line, 10.brass cylinder, 11.quartz window,
 12.heat shield, 13.feed throughs.

kept at a distance of 0.1 mm from the semiconductor surface. Semitransparent electrodes were made by depositing about 100 Å thick layer of gold on clean 7059 glass substrates. Electrode (3) is insulated from electrodes (1) and (2) by teflon tape. Pulses of light (f.w.h.m $\sim 3 \mu\text{s}$, repetition frequency $2.5 \text{ Hz} < f < 450 \text{ Hz}$) are allowed to fall on the sample through the semitransparent electrode. Illumination of the sample causes charge rearrangement, and the induced voltage is picked up by the semitransparent electrode. This signal is fed into a high input impedance buffer circuit before displaying on a CRO. Appropriate light filters are used to vary the energy of the pulsed light between 1.8 to 3 eV. Neutral density filters are used to vary the intensity.

The assembly of the sample, semitransparent electrode and buffer circuit is kept in a metallic system, Fig.4.4 . Sample with semitransparent electrode is kept on an aluminium base (4). Temperature can be varied by a heater (5) kept below the aluminium base. The heater is insulated by mica sheets and supported by another aluminium plate (6). A high input impedance operational amplifier (7), which acts as a buffer, is mounted inside the system to avoid any pickup. The specifications of the op.amp. are given in Table 4.1. It is kept at a distance of 10 cm from the heater assembly using a heat shield of stainless steel (12). All these parts are supported by four ceramic

Table 4.1SPECIFICATIONS OF 18007 AC FET INPUT
OPERATIONAL AMPLIFIER

Specifications	Typical	Maximum	Unit
Input Offset Voltage	15	30	mV
Input Offset Current	0.2		pA
Input Current (either input)	0.5	1	pA
Input Resistance	10^{12}		
Input Capacitance	2		pF
Large Signal Voltage Gain	20,000		
Output Resistance	75		
Output Short-circuit Current	25		mA
Supply Current	3.4	6.0	mA
Power Consumption	102	180	mW
Slow Rate	6.0		V/ S
Unity Gain Bandwidth	1.0		MHz
Transient Response (Unity gain)			
Risetime	300		nS
Operating Temperature Range	0°C to 70°C		

mounts (8) standing on a brass flange (9). The system is covered by a brass cylinder (10), having a quartz window (11) and the other end is supported on the flange with an 'O' ring between them. The flange (9) has feed throughs (13) for measuring SPV, conductance, and for heater and power supply to operational amplifier. The system can be evacuated to 10^{-5} Torr using a diffusion pump with liq. N_2 trap.

Most of the measurements on the free surface are done using the geometry shown in Fig.(4.3A). To compare SPV at the free surface and the film substrate interface in identical conditions, the geometry used is described in Fig.(4.3B,C). To measure SPV at the interface, the semitransparent electrode (3) is kept in such a way that the thin gold layer faces the substrate of the sample Fig.(4.3B). To avoid any damage to the gold layer, it is kept at a distance of 0.1 mm from the substrate. Total separation (d) between the interface and the gold layer is the sum of the thickness of the substrate (having sample) and 0.1 mm separation between the substrate and the gold layer. To measure SPV at the free surface, separation between the free surface and the semitransparent gold layer is kept equal to 'd'. This is achieved by keeping the semitransparent electrode such that the gold layer is not facing the free surface, so that the substrate (of the semitransparent electrode) is in between the gold layer and the

sample (Fig.4.3C). Using the teflon tape between the sample and the semitransparent electrode, the separation d becomes 1.1 mm.

Calibration of the System

To calibrate the system the technique used by others^{2,4} is used. The sample in Fig(4.3A) is replaced by a gold film. Square wave pulses of frequency between 2.5 Hz to 400 Hz are generated using a photodiode. These waves are fed to the gold film kept in place of the sample. Amplitudes of the direct signal from the photodiode and of the signal received through the circuit are compared. For geometry used in Fig(4.3A) the signal reduces by a factor of 2.9 and for geometries used in Fig.4.3B,C, it is reduced by a factor of 3.4 for all frequencies. SPV results measured in different geometries are corrected by appropriate calibration factors.

4.4 Experimental Results

SPV, on heat-dried samples, is measured with varying chopping frequency (f), intensity (I) and energy ($h\nu$) of the pulsed light. Although most of the time, SPV is measured by keeping the electrodes (1) and (2), Fig.(4.3), in dark, the results are unaffected if they are exposed to light. In the following the values of SPV quoted are the

peak heights (during light pulse) of SPV observed as time dependent signal on the CRO.

a. Frequency Dependence

Variation of SPV with repetition frequency (f) of the pulses is shown in Fig. (4.5A). For convenience, f is plotted on a logarithmic scale and SPV on a linear scale.

SPV is positive for all values of ' f ' between 2.5 Hz to 400 Hz. For $f < 4\text{Hz}$, SPV is almost constant and for higher frequencies, it decreases as $\text{SPV} \propto \ln(f)$. SPV due to one pulse takes typically about 250 ms to decay. At higher frequencies, SPV due to next pulse overlaps with the decaying SPV signal due to initial pulse. Also, at lower frequencies slower states can also contribute to SPV.

b. Dependence upon Intensity and Energy of Light

Fig. 4.5B shows variation of SPV as a function of the intensity of light, for two filters (allowing light of energy $1.6\text{ eV} < E_1 < 1.8\text{ eV}$ and $2\text{ eV} < E_2 < 2.8\text{ eV}$ respectively) measured on the free surface. Neutral density filters are used to ensure that the photocurrent from the light of energy E_1 is equal to that from E_2 at each intensity. For the band gap light (E_1) as well as the high energy light (E_2) SPV shows saturation at high intensities. One might try to explain this as being caused

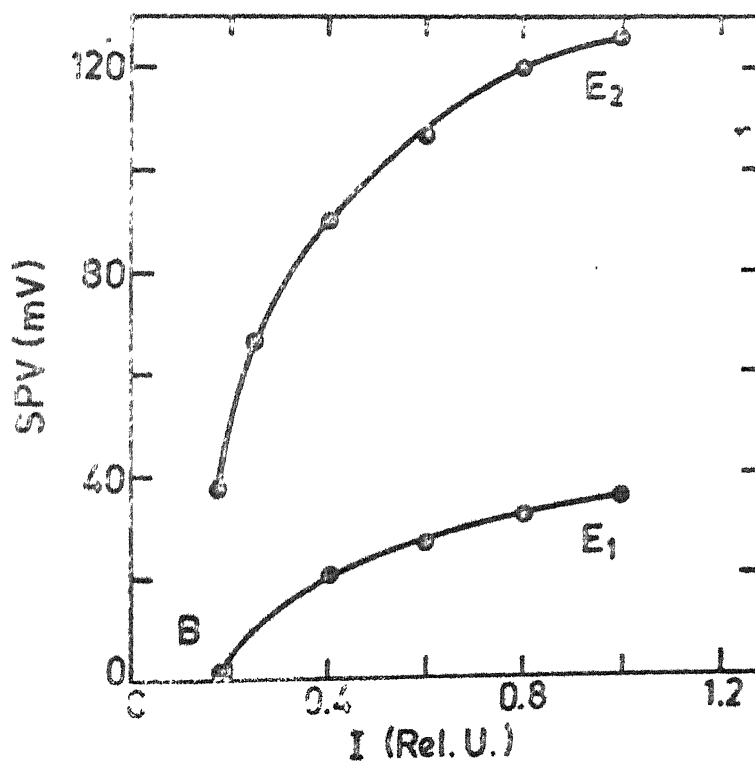
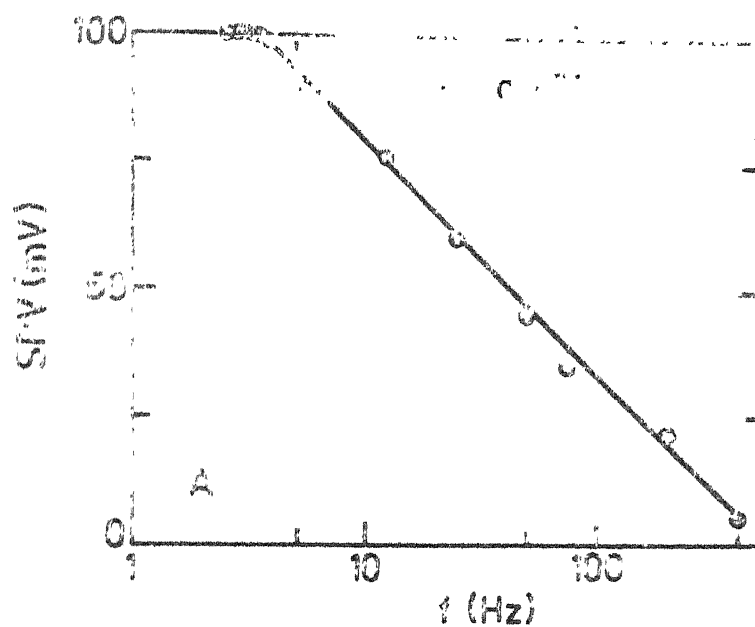


Fig.4.5A : SPV as a function of repetition frequency (f) of pulsed light on the front surface of a-Si:H sample.

Fig.4.5B : SPV as a function of intensity (I) of the pulsed light for optical gap light E_1 and high energy light E_2 .

by the Dember effect⁷. The Dember potential arises from the potential gradient set up internally to equalize the otherwise different electrons and holes diffusion currents in the direction of the incident light⁷. This takes place because of the difference in the mobilities of electrons and holes. This effect is negligible in an uniformly excited sample^{7,19}. Optical band gap light E_1 gives an uniform excitation of the sample, whereas E_2 gets absorbed near the front surface. Thus if Dember effect were large, it could explain the difference. However, this is not likely, since among other things the geometry of the electrodes used is not favourable for the Dember effect. We can however give a simpler explanation for this behaviour of SPV with E , which is given below. Since the band gap light (E_1) sees the front as well as the back surface, this difference may be because in this case the measured SPV will be the algebraic sum of the contributions from the front and the back. If we assume that the contribution to the SPV from the high energy light (E_2) comes only from the surface on which it is shown, this hypothesis can be checked. SPV is measured at the highest intensity by shining E_1 and E_2 at the back of the sample. It is found to be 70 mV for E_2 and -40 mV for E_1 . This shows that SPV at front is larger (125 mV) than at the back (70 mV). These are measured by using E_2 . For E_1 , we expect 55 mV

and -55 mV at the front and the back respectively. These are not very different from the measured values of 36 mV and -40 mV respectively, considering the qualitative nature of this simple explanation. This behaviour for low and high energies is observed for all samples. High energy light $E = 3$ eV is used for most of the measurements of SPV reported here, in order to avoid interference from the back surface.

c. Effect of Etching, Aging and Ambient

SPV and conductance have been measured to check the effect of etching, aging and ambient air on the free surface of a-Si:H samples. Light of energy $E = 3$ eV and pulsed frequency $f = 2.5$ Hz is used to measure SPV. Fig.4.6 shows the dark conductance (G) and SPV measured in different states of a sample, produced by etching heat-drying, aging and varying ambient. Heat dried sample (annealed in vacuum at 150°C , 2h) measured in vacuum is represented by the state A ($G = 1.45 \times 10^{-12} \Omega^{-1}$ and $\text{SPV} = 32$ mV). Etched sample (etched for 5 min in 10% HF and cleaned by deionized water and vapors of isopropyl alcohol) measured in air is given by the state B ($G = 1.1 \times 10^{-11} \Omega^{-1}$; $\text{SPV} = 7$ mV). After this the system is evacuated (state C) and G reduces to $8.5 \times 10^{-13} \Omega^{-1}$ and SPV increases to 17 mV. Now, the sample is heat-dried and the state D_1 ($G = 10^{-12} \Omega^{-1}$ and $\text{SPV} = 17$ mV) is reached. Sample is kept in a dessicator

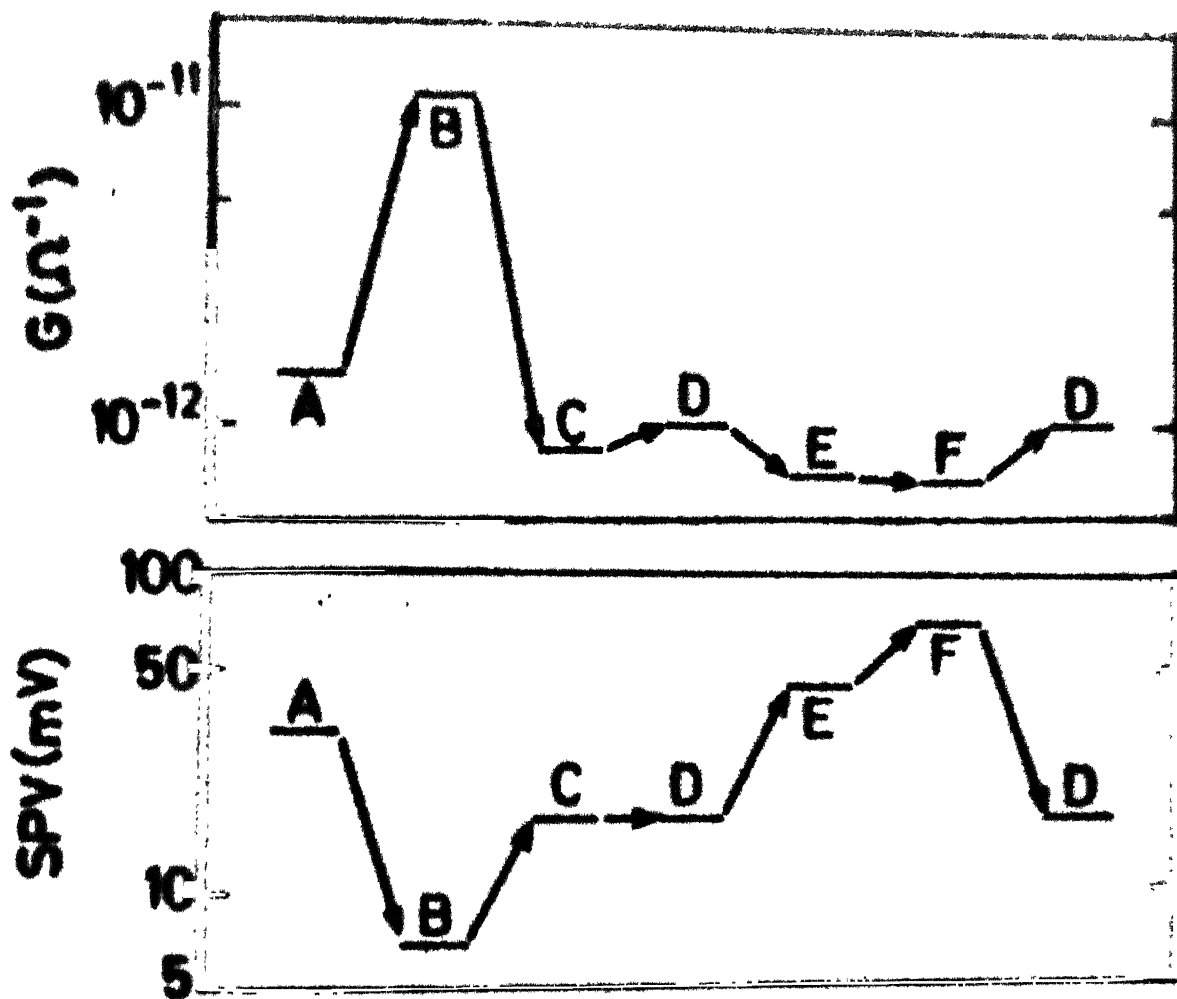


Fig.4.6 : Conductance (G) and SPV after different surface treatments of an a-Si:H sample. A (non-etched, heat-dried measured in vacuum), B (etched, measured in air), C (state B measured in vacuum, 10^{-5} Torr), D_1 (after heat-drying C, measured in vacuum), E (heat-dried after 15 days of D_1 , measured in vacuum), F (heat dried E after 30 days of D_1 , measured in vacuum), D_2 (after etching and heat drying F, measured in vacuum).

for 15 days. It is heat-dried and measured, state E ($G = 7 \times 10^{-13} \Omega^{-1}$, SPV = 45 mV). The process is repeated after 30 days and we obtain the state F ($G = 6.8 \times 10^{-13} \Omega^{-1}$, SPV = 70 mV). Etching and heat drying the sample in state F brings it to the state D_2 which is the same as the state D_1 .

d. Temperature Dependence

Fig.4.7 shows the SPV at the free surface and at the film substrate interface as a function of temperature (T) between 300 to 450K. Curves (1) and (2) are for a free surface obtained before and after etching. Curve (3) is the SPV for the back surface. All measurements are done on the heat-dried state. For non-etched front surface, (Curve 1) SPV is positive at room temperature, decreases linearly at higher temperatures and finally becomes negative at $T = 460K$. After etching and heat-drying, it reduces at room temperature (300K), but remains positive. It changes sign at $T = 380K$ and then it becomes more negative at higher temperatures (Curve 2). The temperature dependence of SPV at the back surface is quite different than at the free surface. It remains positive in the whole temperature range and shows a maxima at about 350K (Curve 3). It increases between $T = 300$ to 350K and then decreases linearly at higher temperatures.

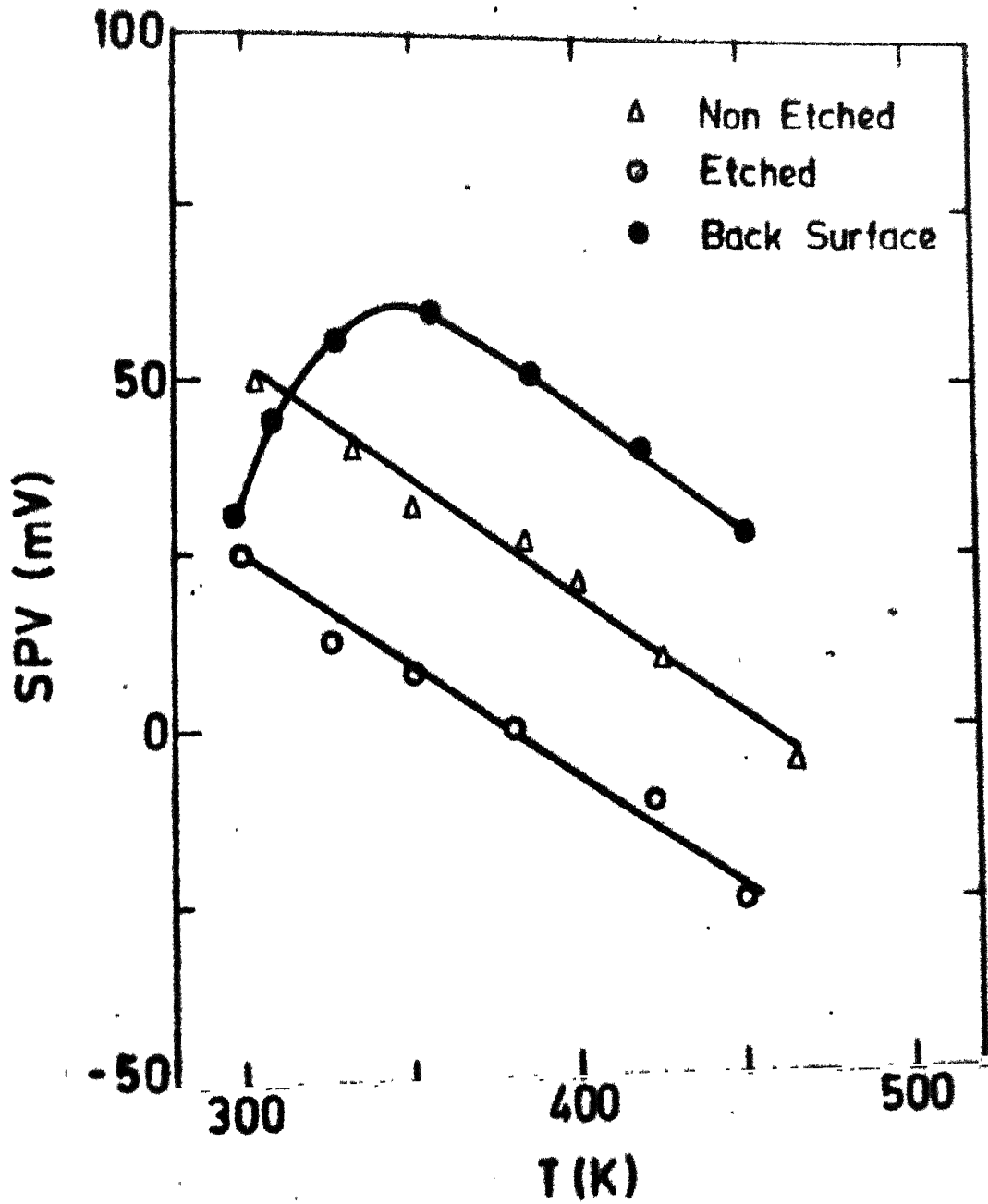


Fig.4.7 : SPV as a function of T for an a-Si:H sample. Curve 1 (non etched and heat-dried front surface), Curve 2 (etched and heat-dried front surface), and Curve 3 (heat-dried back surface).

The magnitude and the behaviour with T of SPV at the back surface is almost the same for all samples. However, although the T dependence of SPV at the front surface does not change from sample to sample, its magnitude shows a variation. It seems to depend on the sample history.

4.5 Interpretation

In the case of crystalline semiconductors, repetition frequency of pulsed light is usually chosen such that the charge in the surface states does not have time to change during illumination^{2,14}. Since overall neutrality must be preserved, injected carriers can not produce a net change in the space charge, but instead will cause a charge redistribution. In this situation, as discussed in section 4.2, the light injection reduces surface potential, i.e. the light tends to flatten the bands.

So in principle, it is possible to determine the direction as well as magnitude within a kT/q from the saturated value of SPV using high intensity excitations⁷. However as discussed in section 4.2 the situation becomes complex if charge exchange takes place between surface states and the space charge region. In this case, the SPV may not be relied upon to give direction and the magnitude of surface potential. Other contributions to the measured SPV may originate from a photovoltage generated at the

metal semiconductor contact (contact photovoltage) and from the Dember effect⁷. The contact photovoltage has been suppressed by keeping the contact in dark as suggested in the literature⁷. However, in the present case, the contact photovoltage turns out to be small since the measured SPV does not show any detectable difference, whether we expose the contacts to light or not. Further as discussed in section 4.4b, Dember effect is also negligible in our case.

a) Frequency Dependence

In Fig.4.5A, SPV is larger for lower frequencies. This can be explained by the fact that at lower frequencies more surface states (i.e. slow) can contribute to the charge transfer. At higher frequencies, the contribution from the surface states reduces, and one gets a situation of almost constant Q_{sc} near 1 KHz. The observation that the SPV tends to zero as f is increasing, supports the theoretical results (Section 4.2). This shows that there are very few surface states with time constant $< 1\text{ms}$, which contribute to SPV. SPV at low frequencies necessarily involves a transfer of charge between surface states and the space charge region (i.e. process (i) in section 4.1).

b) Intensity Dependence

If one assumes a reasonable band bending in dark ($v_s = 6 \text{ kT/e}$), it is possible to find out the charge transfer upon shining light. Using the Q_{sc} vs. v_s curve Fig.2.2, the saturated value of SPV at high intensity corresponds to a possible charge transfer $\approx 10^8 \sqrt{2e\epsilon}$ Coulombs from the surface states. This corresponds to a density of about $10^{11} \text{ cm}^{-2} \text{ eV}^{-1}$ surface states. These many surface states participating in charge transfer is also reported by others^{11,17}.

c) Change in Surface Conditions

Different surface treatments as described in section 4.4c are likely to change the surface potential v_s resulting in a change in G and SPV. The conductance (G) measured in a coplanar geometry is a function of the surface potential v_s and is given by⁹

$$G = \frac{w}{l} \sigma_o \int_0^t \exp \left[\frac{-(E_c - E_f)}{kT} + \frac{eV(x)}{kT} \right] dx \quad (14)$$

where w is the length of the electrodes and l is the separation between them, t is the thickness of the sample and $V(x)$ is the potential in the space-charge region. As an example we can find out the maximum possible change in G , if V_s changes from -0.1 eV to $+0.1 \text{ eV}$, for a sample of thickness $t=1.0 \mu\text{m}$ and taking the width of the

space-charge region $\approx 0.2\mu\text{m}$, in both accumulated and depleted surface conditions. Exact information about the potential distribution and its variation with surface potential is required to find out the dependence of G on surface potential (V_s). In the absence of any information about the potential distribution in the space-charge region, we use the following approximate method for our

calculation. Let us divide the space-charge region in 4 strips, each of thickness $0.05\mu\text{m}$ as shown in Fig.4.8. Potential drop from one strip to another is 0.025V . Using Eq.(14) for G , one gets $G(V_s = +0.1\text{V})/G(V_s = -0.1\text{V}) \approx 5$. Therefore, for a change in V_s from -0.1V to $+0.1\text{V}$, an increase in G by about a factor of 5 is expected.

Let us try to understand the results of Fig.4.6 giving G and SPV after different surface treatments in terms of the change in V_s . Since high intensity SPV in some cases gives surface potential⁷, let us assume for the sake of argument that it does so for a-Si:H also. We shall show that the results can not be explained in this manner.

Since the SPV is positive in all states (Fig.4.6) the bands must bend upwards as per our assumption. G increases by a factor of 7 in going from the state A to the state B. Starting from any reasonable value of v_s in state A. This increase in G would imply a downward band

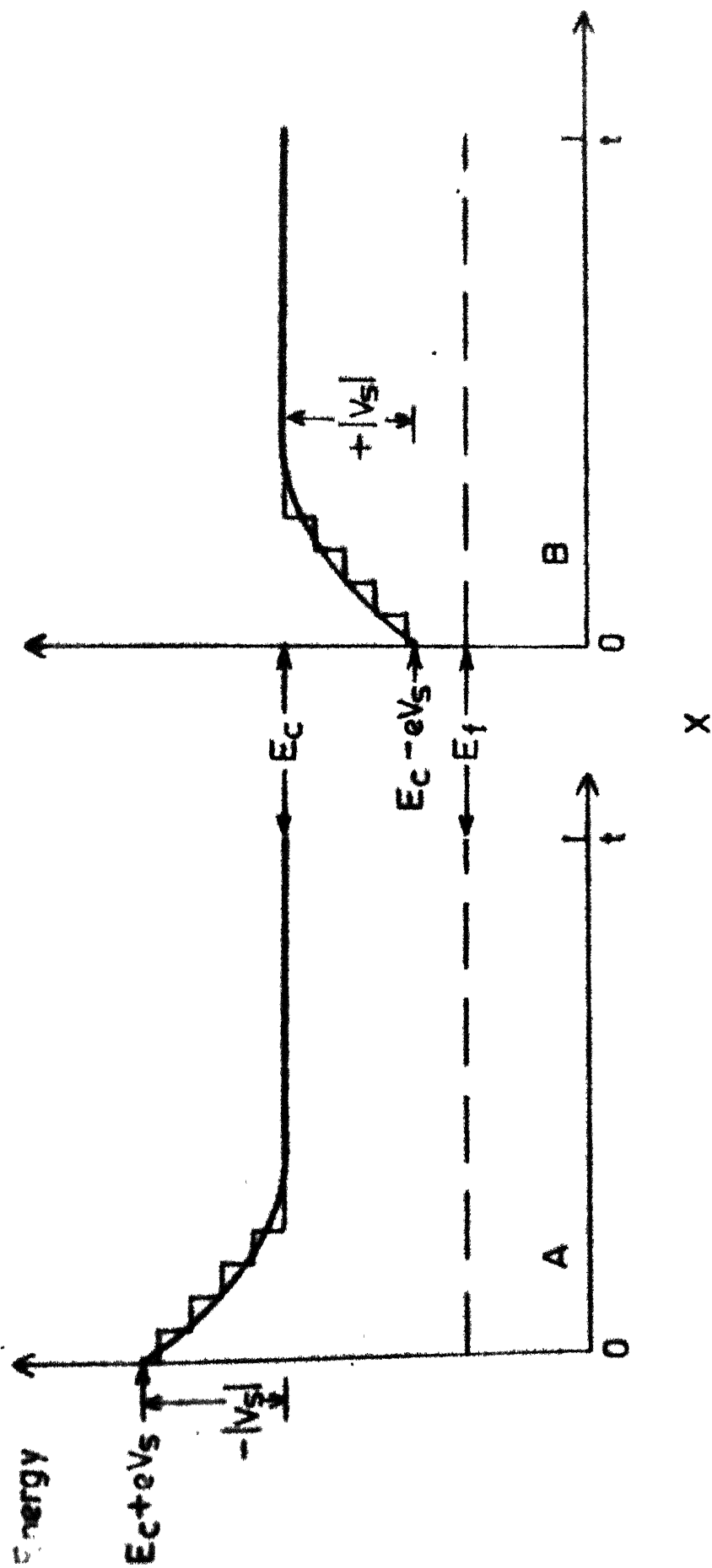


Fig.4.8 : Energy band diagram with upward band bending (A) at the surface ($V_s = -0.1V$) and with downward band bending (B) at the surface ($V_s = 0.1V$).

bending in the state B, as estimated using procedure outlined above. Therefore, one expects a negative SPV, in state B. But the observed SPV in this state is positive (+7 mV). Further, the increase in SPV by 10 mV from the state B to the state C is too small to explain the large decrease in G by a factor more than 10. The discrepancy is even more striking if we compare the state A with the state C. Whereas G in state A is larger than the state C, the SPV is smaller in the state C. Since SPV is positive and assumed to give upward band bending, this implies that the state A has more upward bending of bands than the state C. But then G for the state A should have been more than that of the state C. Thus, the results can not be understood, if SPV were to give the band bending at the surface.

d) Temperature Dependence

Yamagishi¹⁸ has measured the temperature dependence of SPV in c-Si(111) surfaces having a silicon-dioxide or a silicon-nitride layer. In both cases, SPV decreases linearly with temperature and becomes zero at higher temperatures. By assuming that the high intensity SPV measures the surface potential, the results could be explained in terms of the shift of the Fermi level in the bulk as a function of temperature¹⁸.

The measured SPV and G in states D, E and F (Fig.4.6) are also inconsistent with the hypothesis that SPV gives band bending. In this case, since heat-drying and aging are involved, one could argue that these may change the bulk states as well. But upon etching and heat-drying the sample in state F, state D is reproduced. Since the sample was heat-dried to start with and was heat-dried at several other stages, namely, D, E and F, it is improbable that this changes the bulk states. Further, since ingoing from state A to B to C, only the surface was affected, and the results could not be explained if the SPV were to give the band bending, it would be very surprising, if a different explanation were to hold in this case.

In the case of a-Si:H the observed variation of SPV with temperature is quite different than that of c-Si. SPV at the front surface decreases linearly but it changes sign as the temperature is raised instead of approaching zero as in c-Si with an oxide layer¹⁸. The temperature dependence of SPV at the back surface is even more puzzling. It increases initially, shows maximum at about $T=350\text{K}$ and then decreases linearly at high temperatures. It has been shown in section 4.4 that the SPV in a-Si:H does not give surface potential and is determined mainly by the extent of participation of surface states by changing Q_{sc} ($\Delta Q_{sc} = - \Delta Q_{ss}$). Hence the analysis of Yamagishi¹⁸ can not be applied which starts with the assumption that no surface

states participate in SPV.

In the present case the behaviour of SPV with temperature will depend upon the parameters of surface states, such as, capture cross-sections for electrons and holes, and their separation from the Fermi level and the mobility edges^{6,8}. In the absence of such information in a-Si:H, it is difficult to give a definite interpretation of the behaviour of SPV with temperature. Some general statement can however be made. The temperature dependence of SPV measured at the front and the back surface are different. In order to check, if this difference is because of an oxide layer which may be present at the front but not at the back surface, the sample was **etched** in an attempt to reduce the oxide at the front. Upon etching, the SPV at room temperature is about the same for the front and the back surface. However the T dependence is quite different.

This difference in T dependence can not be explained by a slowly growing oxide layer during the measurement of SPV at high T, since the value of SPV at room temperature is reproducible after the heat cycle. Although the presence of a thin oxide layer is expected to be present at the surface even after etching. The results seem to suggest that the difference between the front and the back surface states is not merely because of an oxide present at the front. This is not surprising, in any case, since the front surface is in vacuum and the back is in contact with the substrate

resulting in different surface state parameters at the front and the back. Also the plasma chemistry of silane in the beginning of the glow discharge may be different than at the end during the preparation, thus resulting in a different material and the back and the front⁹.

Other experiments^{20,21} have also indicated different behaviour of the front and the back surface space charge layers. Transient photoconductivity and charge collection experiments on Cr/a-Si:H/Cr sandwich geometry by Sreet et.al.² indicate a very different behaviour at the two surfaces. A possible explanation is that the initial deposition of a-Si:H yields material with a high defect density and the presence of an oxide layer and adsorbates affect the front surface. It indicates that the parameters related with the surface states are different for the front and the back surface.

Thus we conclude that the SPV in a-Si:H is mainly governed by the charge transfer between the surface states and the space charge region and it does not give the magnitude and the sign of the surface potential.

4.6 Light Soaking and SPV

4.6.a Experimental Results

Although it is difficult to infer the band bending in a-Si:H from SPV, we shall show that it is possible to find out, whether light soaking (Staebler Wronski effect) changes the surface or not by performing the following experiment. Conductance (G) and SPV are measured in different states of a-Si:H samples, obtained by exposing the heat dried sample to a sequence of light soaking and moisture and then in the reverse sequence (in a similar fashion to the experiment by Tanielian¹¹ in which he measured only (G). Procedure of this experiment will be clear from the Fig.4.9.

Fig.(4.9) shows the changes in G, observed for an undoped sample of a-Si:H (No.185), as a function of time, as the surface conditions are changed. A represents the heat dried state of the sample with $G=3.8 \times 10^{-13} \Omega^{-1}$. At time $t=0$, it is exposed to a white light (intensity 60 mW/cm^2). G increases to $1.2 \times 10^{-9} \Omega^{-1}$ in the presence of light, but then decreases slightly with time, reaching $7.5 \times 10^{-10} \Omega^{-1} \text{ cm}^{-1}$ in 6 hrs. (see Fig.4.9a). At $t = 6 \text{ hrs}$, the light is switched off and we obtain the light soaked state B, which has a smaller $G = 2.8 \times 10^{-13} \Omega^{-1}$. Now the sample is exposed to moist nitrogen (relative humidity $< 50\%$). In the presence of moisture, G first increases to $6 \times 10^{-13} \Omega^{-1}$ and then slowly decreases in about 3 hrs to $4.5 \times 10^{-13} \Omega^{-1}$ (state F). For the reverse sequence (Fig.4.9b) the sample

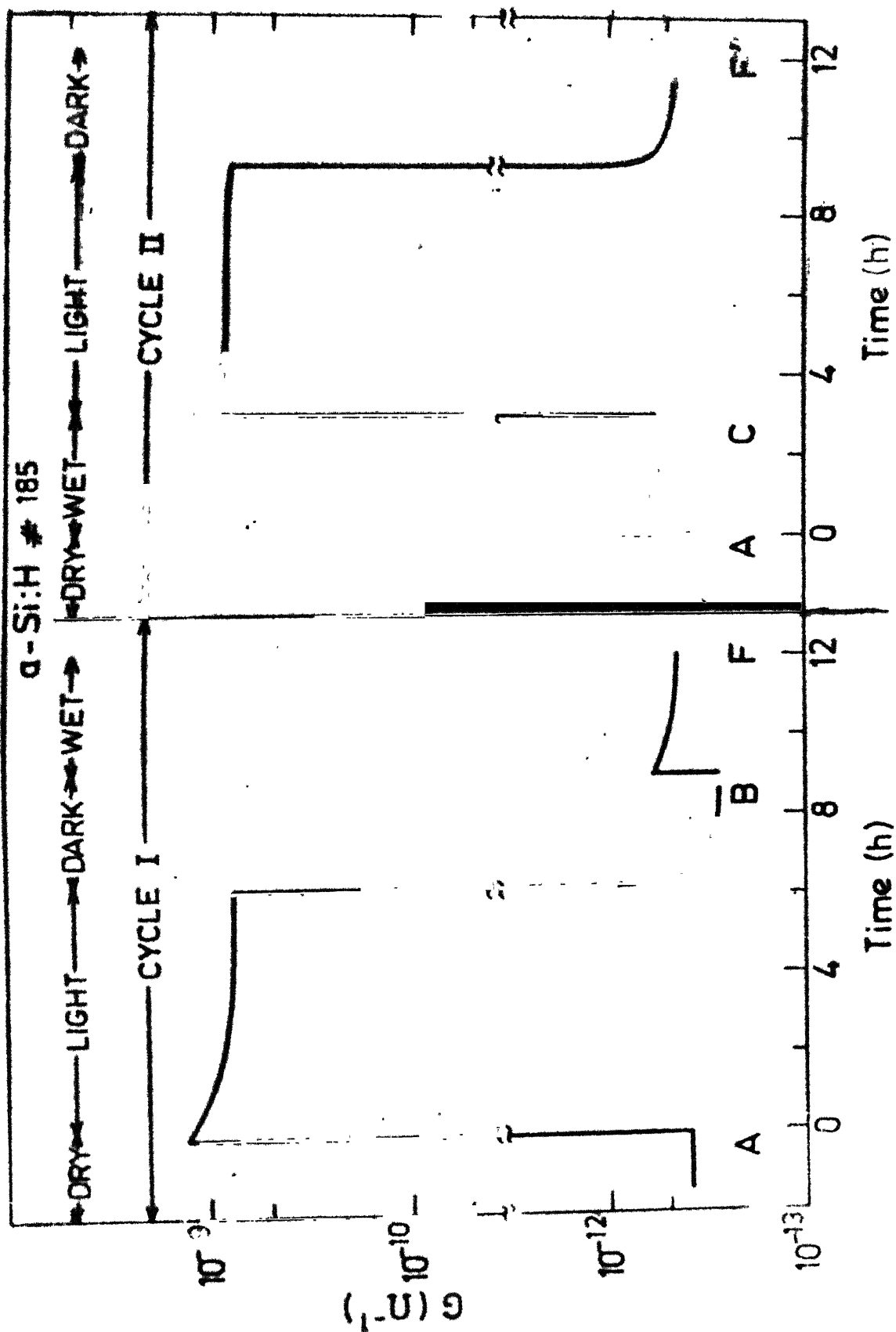


Fig.4.9 : Conductance (G) in different states of the cycle experiment for an α -Si:H sample. A (heat-dried state), B (light soaked state), F (state B in presence of moisture), C (state A in presence of moisture), F' (state C after light soaking).

is again heat dried. After heat-drying, the sample conductance comes back to state A. The heat-dried sample is exposed to moisture. G immediately increases to $8.5 \times 10^{-13} \Omega^{-1}$ and then decreases within time (≈ 3 hrs) to $5.6 \times 10^{-13} \Omega^{-1}$ in equilibrium (state C). Now, the sample is exposed to white light as before. The photoconductance reduces from $1.05 \times 10^{-9} \Omega^{-1}$ to $8 \times 10^{-10} \Omega^{-1}$ in six hours. The final conductance in dark (state F') is $4.7 \times 10^{-13} \Omega^{-1}$. These results agree qualitatively with those of Tanilian, and can be explained in a similar fashion¹¹ although the changes in G are much larger in his case.

The equilibrium values of G in each state are shown in the upper half of Fig.(4.10) for each of the cycles. The lower part of the figure shows SPV, measured with the high energy (3eV) and the band gap light (1.8eV), in different equilibrium states of the sample. In Fig.(4.11) results obtained on another undoped (sample No.184, solid lines) and after doping it lightly with lithium (broken lines) are given. The variation of G and SPV in different states shows a trend similar to that shown in Fig.4.10.

The first part of the Fig.(4.12) gives the effect of light soaking on SPV and G on a sample (No.186) before etching. States A' and B' represent the heat-dried and the light soaked states respectively and their G and SPV values show a trend similar to other non etched samples (Figs.4.10 and 4.11). The sample in state A' is etched and heat-dried

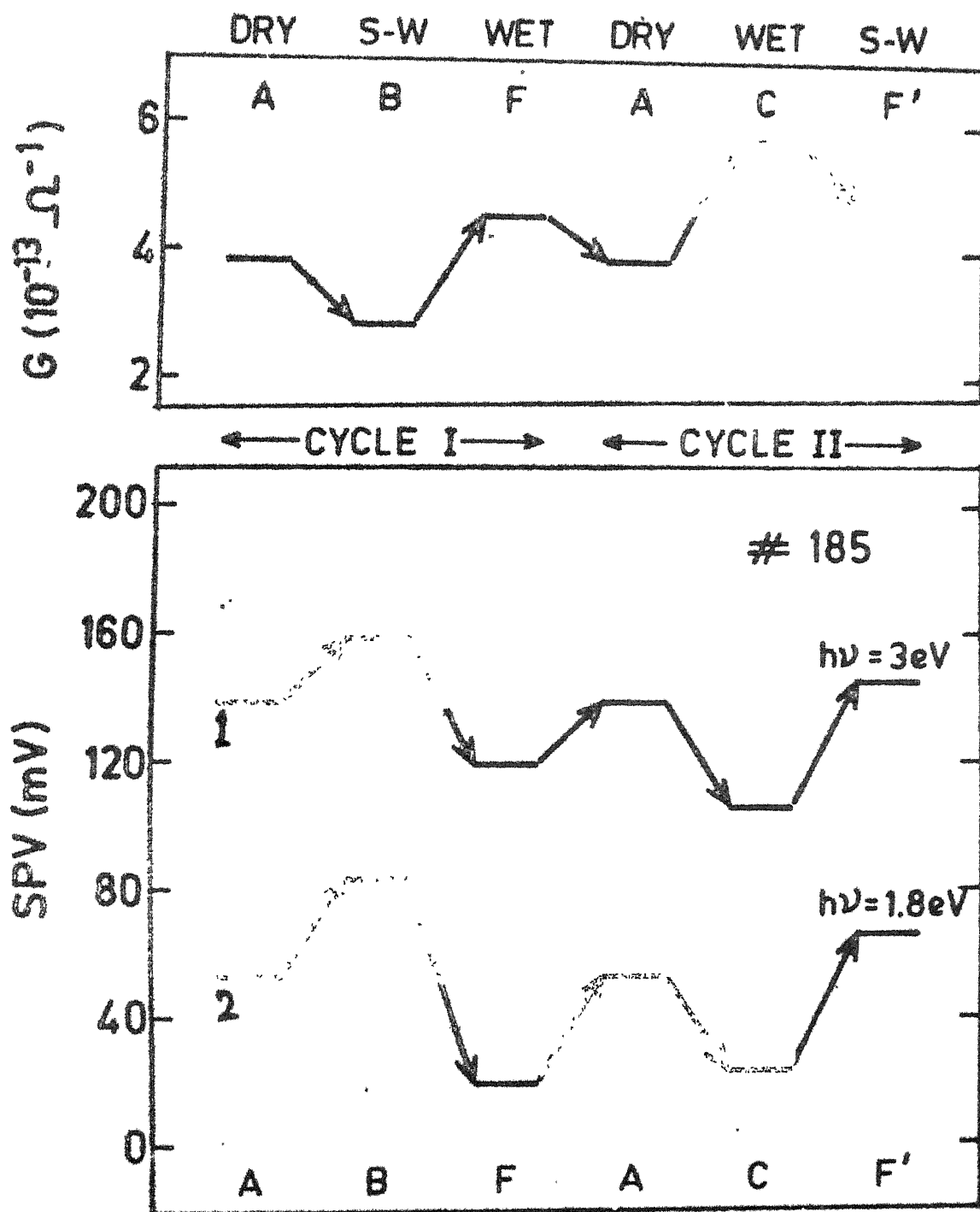


Fig. 4.10 : G and SPV in different states of the cycle experiment. G is in upper half of the figure and SPV in the lower half. SPV Curve 1 is for high energy light $E = 3\text{eV}$ and Curve 2 is for optical gap light $E = 1.8\text{eV}$.

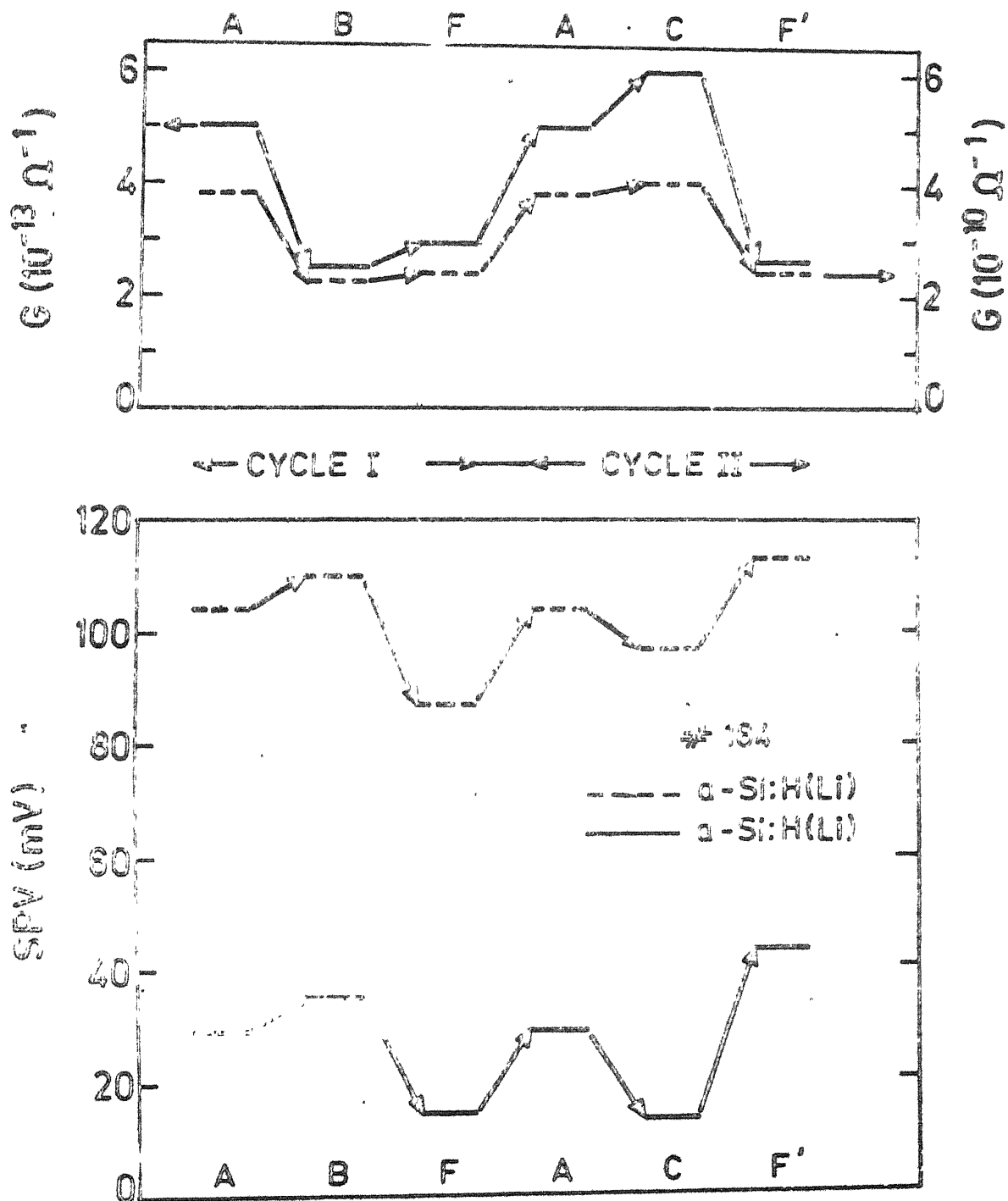


Fig.4.11 : G and SPV for an undoped α -Si:H sample and lightly Li doped α -Si:H (Li) sample in different states of the cycle experiment SPV is for optical gap light $E_1=1.8\text{eV}$.

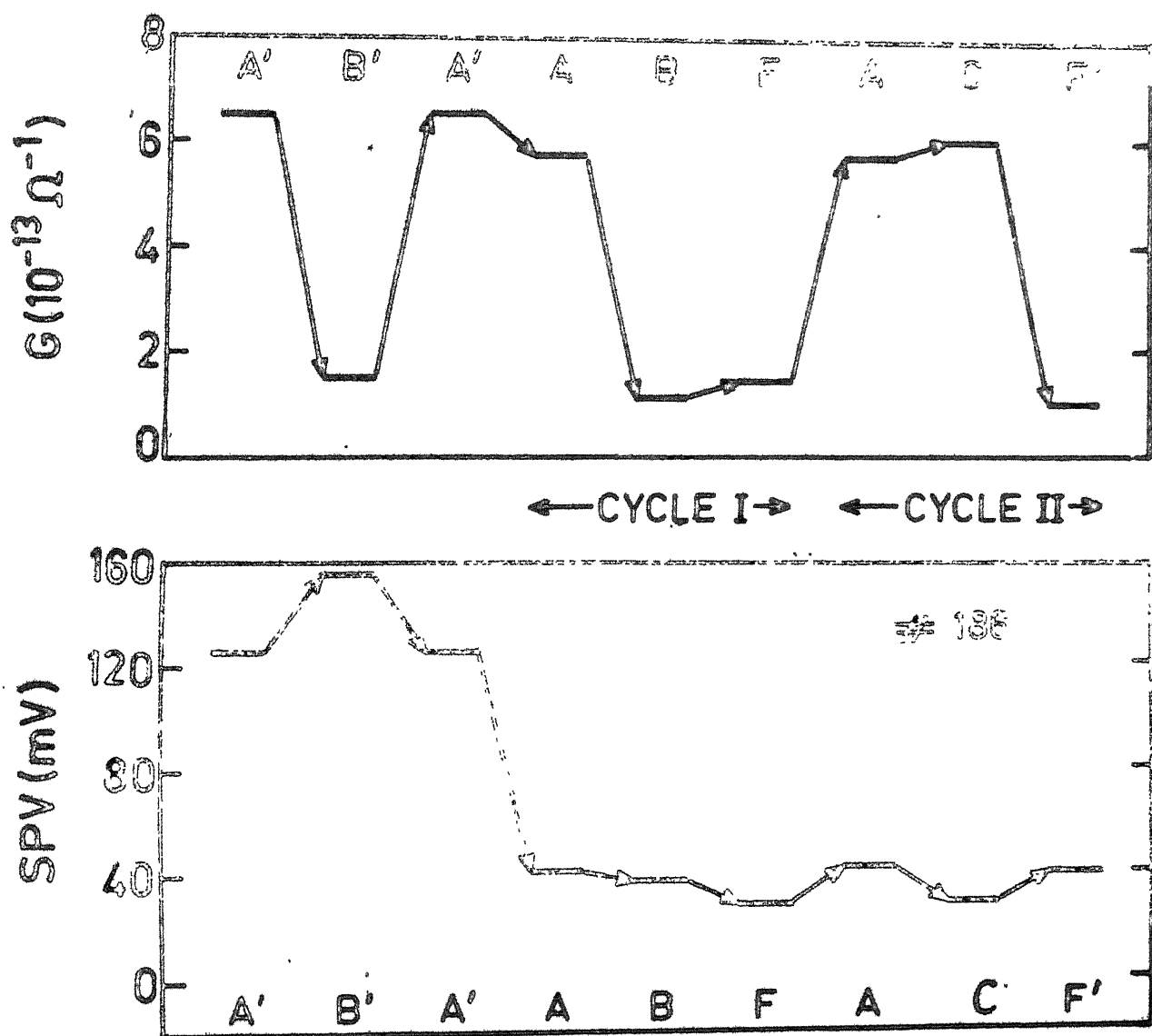


Fig.4.12 : G and SPV for an etched a-Si:H sample in different states of the cycle experiment. A' (non-etched, heat-dried state), B' (non-etched, light soaked state) A to F' states are same in the cycle experiment

to obtain the state A. The sample in state A is subjected to the light soaking, moisture cycles, as before (see Fig.4.12). On comparing the results on different samples in the cycle experiment, the following features are observed.

- 1) SPV is positive in all states of all the samples.

This positive sign is in agreement with the literature^{22,23}.

- 2) The change in G upon exposure to moisture is larger for the heat dried samples as compared to the light soaked ones, in agreement with Tonilian¹¹.

- 3) Moisture increases G and decreases SPV.

- 4) SPV is larger for the non-etched sample.

This is in agreement with Aker et.al.²²

- 5) Light soaking decreases G in all states of the samples, but its effect on SPV depends on whether the surface is etched or not. It (light soaking) increases SPV on the non-etched surface and decreases it (SPV) on the etched surface. Similar effect of etching on the change in SPV upon light soaking have also been observed by Aker et.al.²²

- 6) G in states F and F' is almost the same (in agreement with Tanilian¹¹). SPV in the state F' is always more than in state F.

- 7) There is no correlation between the change in conductance G and the change in SPV from one state to another, if we assume that the saturated value of SPV gives the magnitude and the direction of surface potential²². This is in agreement with the results already discussed in section 4.4.

4.6b Discussion

Water acts as a donor on the surface of many crystalline semiconductors and creates a band bending by causing a charge transfer between the adsorbed H_2O and the semiconductor⁷. This band bending creates an accumulation layer adjacent to the surface. Moisture (H_2O) increases the conductance upon adsorption in the case of the intrinsic and n-type samples¹. Increase of G upon exposure to moisture (states C and F) support this view.

The observation by Tanielian¹¹ that G decreases upon exposure to moisture for p-type a-Si:H, is a further indication and the observed changes in G are indeed caused by a change in the surface potential. Also, using adsorbates which are electron acceptors (e.g. O_2 and evaporated Se) it has been shown that G decreases in n-type a-Si:H, as expected¹¹. We also observed a decrease in G upon evaporation of a layer of Se onto undoped a-Si:H (which is slightly n-type) by a factor of about 10 for 1 μm thick sample.

If light soaking increases the density of states around the Fermi level in the undoped specimen, the magnitude of the change in G upon exposure to moisture is expected to reduce¹¹. This is indeed observed (see (2), in 4.5a) in all cases, in agreement with Tanielian¹¹. He points out that the observation that $G(F) \cdot G(F')$ (see (6), in 4.5a) is also consistent with the hypothesis that light-soaking affects the bulk states.

There is considerable debate in the literature about the origin of the change in G upon light soaking (sec.(5), sec.4.5a). Although we observed a decrease, an increase in G upon light soaking is also sometimes observed²⁵. The explanation is not quite clear. Whereas there is a lot of evidence to suggest that this is a bulk effect²⁶, as assumed by Tanielian, the experiments of Solomon¹⁷ and Hack and Madan²⁷ suggest that the light exposure affects the surface also. More recently, Hauschildt et.al.²⁸ measured conductivity and thermopower before and after light soaking and concluded that they can not be explained in terms of surface changes alone.

Let us now turn our attention to the SPV results. The magnitude of change in G implies that the surface potential in states C and F must be negative (see sec.4.4). If SPV were to give the surface potential, (as is usually in many crystals, but not in a-Si:H), one would expect a negative SPV in states C and F. But the observations are

opposite. Further, the decrease in G does not always mean an increase in SPV as observed after light soaking on the etched surfaces (A \rightarrow B, Fig.4.12).

Aker et.al.²² have explained changes in G in boron doped a-Si:H, after light soaking by assuming bulk changes and by an increase in metastable charged defects within the oxide layer at the surface. Difference in SPV in states A' \approx B' and A \rightarrow B (see 6 in sec.4.5a) may be due to increase in metastable charges within the oxide layer and this may be less on the etched surface having a thinner layer of oxide. These observations provide further support for the conclusion already reached in Sec.4.4, that SPV is not directly correlated with the surface potential in a-Si:H. However, even in this unfavourable situation, some conclusions about the origin of the effect of light soaking can be arrived as follows. The different values of SPV in the states F and F' show that the light soaking changes the surface as well as the bulk states. For the sake of argument, let us assume that light soaking changes the bulk states alone. Since the moisture affects only the surface, we should expect the same SPV in states F and F', which is contrary to the observations. This should specially hold for the sample No.184, whose activation energy does not change upon light soaking.

In conclusion, the light soaking changes the bulk as well as the surface of the sample. Surface changes depend upon the surface conditions, such as the presence of the oxide layer and adsorbates.

REFERENCES

1. W.H.Brattain and J.Bardeen, Bell. System Tech. J., 32, 1 (1953).
2. E.D.Johnson, Phys. Rev. 111, 153 (1958).
3. C.G.B.Garrett and W.H.Brattain, Phys. Rev., 99, 376 (1955).
4. V.M.Buimistrov, A.P.Garbon and V.G.Litovchenko, Surface Sci., 3, 445 (1965).
5. J.Lagowski, C.L.Balestra and H.C.Gatos, Surface Sci., 27, 547 (1971).
6. D.L.Lile, Surface Sci., 34, 337 (1973).
7. A.Many, Y.Goldstein and N.B.Grover, Semiconductor Surfaces (North-Holland, Amsterdam, 1965).
8. D.R.Frankl and E.A.Ulmer, Surface Sci., 6, 115 (1966).
9. H.Fritzsche, in Electronic and Transport Properties of Hydrogenated Amorphous Silicon; edited by J.I.Pankove (Academic Press, New York, 1984).
10. D.L.Staebler and C.R.Wronski, Appl. Phys. Lett., 31, 292 (1977); J.Appl. Physics, 51, 3262 (1980).
11. M.Tanielian, Phil. Mag., B45, 435 (1982).
12. A.Madan, P.G.LoComber and W.E.Spear, J. Non. Cryst. Solids, 20, 239 (1976).
13. D.S.Misra, Ph.D. Thesis (1984), I.I.T. Kanpur.
14. W.Shockley and W.T.Read, Phys. Rev., 87, 835 (1952).
15. J.G.Simmons and G.W.Taylor, Phys. Rev. B4, 502 (1977).
16. A.R.Moore, Appl. Phys. Lett., 37, 327 (1980).
17. I.Solomon, T.Ditl and D.Kaplan, J. Physics (Paris), 39, 1241 (1978).
18. H.Yamagishi, J. Phys. Soc. Japan., 25, 766 (1968).

19. C.E.Reed and C.G.Scott in Surface Physics of Phosphors and Semiconductors, edited by C.G.Scott and C.E.Reed (Academic Press, N.Y., 1975).
20. P.G.LeComber, W.E.Spear, R.A.Gibson, H.Mannspenger and F.Djamdji, J. Non.Cryst. Solids, 59&60, 505 (1983).
21. R.A.Street, Phys. Rev., B27, 4924 (1983).
22. B.Aker, Shao-Qi Peng, Song-yi Cai and H.Fritzsche, J.Non.Cryst. Solids, 59&60, 509 (1983).
23. B.Goldstein and D.J.Szostak, Surface Sci., 99, 235 (1980).
24. S.Kumar and S.C.Agarwal, Phil. Mag. (1984), to appear.
25. H.Mell and W.Beyer, J. Non.Cryst. Solids, 59&60, 405 (1983).
26. D.Adler, Solar Cells, 9, 133 (1983).
27. M.Hack and A.Madan, Appl. Phys. Lett., 41, 272 (1982).
28. D.Hauschildt, W.Fuhs and H.Mell, Phys. Stat. Solidi, b111, 171 (1982).

CHAPTER 5

SUMMARY AND CONCLUSIONS

The effect of lithium incorporation in a-Ge and on its transport properties is studied and compared with that of hydrogenation. Both reduce the number of dangling bonds and result in a smaller conductivity as compared to that of pure evaporated amorphous germanium. However, both hydrogenated amorphous germanium (a-Ge:H) and lithium diffused amorphous germanium (a-Ge:Li) are not photoconducting and can not be doped efficiently. The temperature dependence of conductivity of a-Ge:Li and a-Ge:H is similar. However the temperature dependence of thermopowers of the two are different. Thermopower of a-Ge:H is negative, whereas the thermopower of a-Ge:Li is positive above $T=300\text{K}$ and tends to a small negative value, which is the same as that of a-Ge at low temperatures. These results can be understood, but not completely, by assuming different combinations of bipolar conduction in the extended and the hopping in the localized states at the Fermi level¹ in the two cases. A clear understanding is not possible without considering the potential fluctuations caused by heterogeneities in the structure and composition². Hydrogenation of a-Si by using different methods (e.g. sputtering and glow-discharge) reduces the density of states to a low enough

level, so that the material is photoconducting. The increase in conductivity and negative thermopower shows that Li acts as interstitial donor in hydrogenated amorphous silicon (a-Si:H)³. An increase in the conductivity of the order of 10^5 can be achieved by thermal diffusion of lithium. Light soaking decreases the conductivity and increases the activation energy in the undoped and lightly Li doped a-Si:H. Light soaking does not have any effect on the conductivity of heavily Li doped samples, but it reduces the magnitude of the thermopower. The temperature dependence of thermopower of heavily doped samples is different in the heat-dried and light soaked states. Here also, among other things, the lack of understanding of heterogeneities, makes it difficult to explain the results quantitatively.

The structure of thin films of a-Ge and a-Si is overconstrained and these films have a network of microscopic voids². The voids have dangling bonds at their internal surfaces. They also give rise to heterogeneities and potential fluctuations which can affect the electronic properties to a large extent². Hydrogen and lithium, although reduce the number of dangling bonds, are not good passivators of other defects in a-Ge. Thus the density of states after hydrogenation or Li diffusion is still quite high in a-Ge, as compared to a-Si:H. One

of the reasons can probably be that Ge-Ge bond is stronger than Ge-H⁴ and Ge-Li⁵ bonds. On the other hand, hydrogen acts as a better passivator of defects in a-Si, than in a-Ge. This may be because Si-H bond is stronger than Si-Si bond⁴. We have also studied ~~the~~ surface photovoltage (SPV) in a-Si. The relation, between the space charge density and the surface potential in a-Si:H shows that the SPV will be zero, if the space-charge density remains constant upon illumination. A non-zero SPV will be observed only if there is a transfer of charge from the surface states, into the space-charge region. In this case the saturated value of SPV may not be equal to the surface potential⁶.

The conductance and SPV measurements in different surface conditions show that SPV in a-Si:H does not give surface potential in agreement with the theoretical arguments. The frequency and temperature dependence of SPV also supports above conclusions.

Although a-Si:H can be doped, dopants increase the compositional defects as a side effect⁷. There are evidences to suggest that light soaking (Staebler-Wronski effect)⁸ also increases defects in a-Si:H⁹. However, the nature of defects created by doping and light soaking is probably different¹⁰. The possible types of defects created by doping and light soaking are discussed by

Adler⁷. According to him, no defects are created by light, but recombination of photogenerated carriers induces excess neutral dangling bonds. These metastable centers are responsible for the increase in the density of spins, change of the Fermi level and most of other experimental results. Experimentally, an increase in density of states has been observed by field effect¹¹, deep level transient spectroscopy¹², sub-band gap absorption¹³ and increase in the spin density by the electron spin resonance¹⁴. Whether, new defects are created or the properties of defects are changed by light soaking, their role in affecting the transport processes is not yet fully understood. Same is true for defects created by doping.

The effect of light soaking (Staebler Wronski effect) on SPV is also studied and is found to depend upon the surface conditions. SPV is positive in the heat dried, light soaked states and in presence of the humidity. Light soaking increases SPV on the non-etched surface and decreases it on the etched surface, but the conductance decreases in both cases. Measurement of SPV, and G on a heat-dried sample exposed to a sequence of light soaking and humidity show that the final value of SPV obtained at the end of the cycle depends on the order in which the two are performed. However, the final value of G is almost the same, regardless of the order in which

the light soaking and moisture exposure are performed¹⁵. It is concluded that light soaking changes the surface as well as the bulk of a-Si:H¹⁶. A recent study on boron doped a-Si:H samples shows that light soaking increases metastable negative charge in the oxide layer at the surface¹⁷, which results in the increase of conductance of these p-type samples. Sometimes these surface effects completely mask the bulk effect¹⁷. It is necessary to separate out the effect of light soaking on surface and bulk, in order to get information about the true bulk or surface properties. Further study with experimental methods which can distinguish between the bulk and surface effects is needed to give more insight in understanding of various properties of a-Si:H films.

REFERENCES

1. W.Beyer and J.Stuke, in: Proc. 5th International Conference on Amorphous and Liquid Semiconductors, Cormisch-Partenkirchen, eds. J.Stuke and W.Brenig (Taylor and Francis, London, 1974) p. 251.
2. H.Fritzsche, in Amorphous and Liquid Semiconductors, edited by J.Tauc, (Plenum Press, New York, 1974).
3. W.Beyer and R.Fischer; Appl. Phys. Lett. 31, 850 (1977).
4. W.Paul, in Fundamental Physics of Amorphous Semiconductors, edited by F.Yonezawa (Springer-Verlag, New York, 1981).
5. C.A.Coulson; Valence (The English Language Book Society and Oxford University Press, 1961).
6. D.R.Frankl and E.A.Ulmer, Surface Sci., 6, 115 (1966).
7. D.Adler, Solar Cells, 9, 133 (1983).
8. D.L.Staebler and C.R.Wronski; Appl. Phys. Lett. 31, 292 (1977).
9. H.Fritzsche, Solar Energy Mater., 3, 447 (1980).
10. D.Hauschildt, W.Fuhs and H.Mell, Phys. Stat. Sol. (b), 111, 171 (1982).
11. M.H.Tanielian, N.B.Goodman and H.Fritzsche, J.Phys. (Paris) 42, Suppl.10, C4-375 (1980).
12. D.V.Lang, J.D.Cohen, J.P.Harbison and A.M.Sergent, Appl. Phys. Lett. 40, 474 (1972).
13. A.Skuminich, N.M.Amer and W.B.Jackson, Bull. Am. Phys. Soc. 27, 146 (1982).
14. H.Dersch, J.Stuke and J. Beichler, J. Appl. Phys. Lett., 38, 456 (1981).
15. M.Tanielian, Philos. Mag. B45, 435 (1982).
16. S.Kumar and S.C.Agarwal, Phil. Mag. (1984), to appear.
17. B.Aker and H.Fritzsche; J. Appl. Phys. (1983), to appear.

87520 .

PHY - 1984 - D - KUM - 1RA